THE INFLUENCE OF INSULATORS ON THE PARTICLE DENSITY DISTRIBUTIONS WITH AND WITHOUT MAGNETIC FIELDS

KLEBER S. MASTERSON, JR.

THE INFLUENCE OF INSULATORS ON THE PARTICLE DENSITY DISTRIBUTIONS WITH AND WITHOUT MAGNETIC FIELDS

* * * * *

Kleber S. Masterson, Jr.

THE INFLUENCE OF INSULATORS ON THE PARTICLE DENSITY DISTRIBUTIONS WITH AND WITHOUT MAGNETIC FIELDS

by

Kleber S. Masterson, Jr.

Lieutenant, United States Navy

Submitted in partial fulfillment of
the requirements for the degree of

MASTER OF SCIENCE

IN

PHYSICS

United States Naval Postgraduate School
Monterey, California

1961

THE INFLUENCE OF INSULATORS ON THE PARTICLE DENSITY DISTRIBUTIONS WITH AND WITHOUT MAGNETIC FIELDS

by

Kleber S. Masterson, Jr.

This work is accepted as fulfilling
the thesis requirements for the degree of
MASTER OF SCIENCE
IN
PHYSICS
from the
United States Naval Postgraduate School

TABLE OF CONTENTS

LIST OF ILLUSTRATIONS

MAGNETIC FIELD END EFFECTS

COORDINATE SYSTEMS

SPHEROIDAL WAVE FUNCTIONS

LIST OF TABLES

ABSTRACT

This thesis presents some general equations describing the particle density distributions within a plasma. Solutions to these equations are discussed for various geometries, with particular emphasis given to the effects of diffusion losses at probes of dimensions comparable to or greater than the mean free path and to magnetic field end effects. For many of the geometries discussed, including one probe geometry, the effects of a superimposed magnetic field is discussed.

I

INTRODUCTION

One of the complex problems in the field of plasma physics is that of predicting the effects of surfaces with which the plasma is in contact upon the particle density distribution functions and related phenomena. No plasma is infinite, and consequently a plasma must be confined by walls, which may be either conductors or insulators. Further, in order to make measurements within a plasma, probes may be inserted. What is their effect on the particle density distribution and related phenomena such as potential distribution and energy dissipation? What are the particle currents to various surfaces? The latter are particularly important because they determine the heat liberated at the surface, which in turn is an energy loss which may cause very high temperatures, increased local ionization, and melting of materials in extreme cases. This thesis discusses these effects when the surfaces are insulators.

In this thesis some general equations describing a plasma are presented with their corresponding restrictions. Solutions to these equations are discussed for various geometries, with particular emphasis given to the effects of probes and to magnetic field end effects on the steady-state density distributions and on the energy losses at the surfaces involved. For many of the geometries discussed, including one probe geometry, the effects of a superimposed magnetic field is studied.

II

GENERAL RELATIONS

In this section, general equations describing a plasma are developed and discussed.

A. Conservation Equations

The Boltzmann Transport Equation

$$\frac{\partial}{\partial t}(nX) - \vec{\nabla}_r \cdot (n\overline{\vec{v}X}) - n\overline{(\vec{a}\cdot\vec{\nabla}_v)X} - n\overline{(\vec{\omega}_b \times \vec{v})\cdot\vec{\nabla}_v X} = \iiint (X'-X) F(v) f(v) \rho \, d^3\Omega \, V d^3 v \qquad (2\text{-}1)$$

is used as the starting point for the development of the macroscopic relations governing the plasma. By ascribing appropriate values to X and X' [1] [2], we obtain the continuity equation:

$$\frac{\partial n}{\partial t} + \vec{\nabla}\cdot(n\vec{v}_d) = n(\bar{\nu}_i - \bar{\nu}_a) \qquad (2\text{-}2)$$

(in which $\bar{\nu}_i$ is the mean ionizing frequency and $\bar{\nu}_a$ the mean recombination frequency), and the equation for conservation or momentum:

$$\frac{\partial}{\partial t}(n\vec{v}_d) + \frac{\vec{\nabla}\cdot\vec{\vec{p}}}{m} - n(\vec{a} + \vec{\omega}_b \times \vec{v}_d) = -n\bar{\nu}_c \vec{v}_d, \qquad (2\text{-}3)$$

in which the right hand term is really a definition of the mean collision frequency, $\bar{\nu}_c$, the pressure $\vec{\vec{p}}$ is a symmetric tensor

$$p_{ij} = nm\overline{v_i v_j}, \qquad (2\text{-}3a)$$

and in which

$$\vec{a} = \frac{q}{m}\vec{E} \qquad (2\text{-}3b)$$

and

$$\vec{\omega}_b = -\frac{q}{m}\vec{B}. \qquad (2\text{-}3c)$$

$\vec{E}$, $\vec{B}$, q, m, and v_d are, respectively, the electric field intensity, the magnetic field intensity, particle charge, particle mass, and drift velocity.

The continuity equation (2-2) can be further simplified. We shall consider a two component system of electrons and singly-charged ions in which volume ionization by electrons is essential. Recombination takes place predominately at the walls, with volume recombination being negligible. We have, then,

$$\frac{\partial n_\pm}{\partial t} + \vec{\nabla}\cdot\vec{\Gamma}_\pm = \nu n_-, \tag{2-4}$$

where ν is the net ionizing frequency and the particle current density is

$$\vec{\Gamma}_\pm = n_\pm \vec{v}_{d\pm}. \tag{2-4a}$$

In the above equations, and in the remainder of this thesis, the subscript "+" refers to singly-charged positive ions, and the subscript "-" refers to electrons. Under those conditions for which the rates of decay of ions and electrons are essentially equal, so that

$$\frac{\partial n_+}{\partial t} \approx \frac{\partial n_-}{\partial t} = \frac{\partial n}{\partial t}, \tag{2-5}$$

we obtain for the continuity equation

$$\vec{\nabla}\cdot\vec{\Gamma}_+ \approx \vec{\nabla}\cdot\vec{\Gamma}_- = \nu n_- - \frac{\partial n}{\partial t} \tag{2-6}$$

In the momentum equation (2-3), the pressure term is generally a difficult one to evaluate because $\vec{p}$ is not known, and the dependence on its divergence makes good approximations difficult. However, for the simple case in which the distribution of random velocities is essentially isotropic, so that

$$\overline{v_i v_j} \approx 0 \quad i \neq j, \tag{2-7a}$$

and

$$\overline{v_1^2} \approx \overline{v_2^2} \approx \overline{v_3^2}, \tag{2-7b}$$

3

the pressure tensor reduces to

$$p \approx \frac{nm\overline{v^2}}{3} = nkT = \frac{neD}{\mu}, \tag{2-8}$$

where D and μ are the diffusion and mobility coefficients respectively. The last term is derived from the preceeding ones by the use of Einstein's relation:

$$\frac{D}{\mu} = \frac{kT}{e} = \frac{m\overline{v^2}}{3e}. \tag{2-9}$$

This generalization (equation (2-8)) is valid only for a plasma which is characterized by a small drift velocity,

$$|\vec{v}_d| \ll |\overline{\vec{v}}|. \tag{2-10}$$

The last term in equation (2-3) is frequently written

$$-n\overline{\nu_c}\vec{v}_d = -\frac{e}{m\mu}\vec{\Gamma}, \tag{2-11}$$

which defines the mobility, μ. In the case of ion-neutral particle interactions, ν_c is a constant because the forces are inverse fifth power polarization forces. In all other cases we must introduce an appropriate average value, $\overline{\nu}$, which we will consider independent of $\vec{v}_d$.

One important consequence of the above assumptions is that the ion and electron mobilities and diffusion coefficients are scalar constants.

Substitution of equations (2-8) and (2-11) into the momentum equation (2-3), and rearranging terms, yields, for the positive ions of mass M:

$$\frac{M\mu_+}{e}\frac{\partial\vec{\Gamma}_+}{\partial t} + \vec{\nabla}(D_+n_+) - n_+\mu_+\vec{E} - \mu_+\vec{\Gamma}_+ \times \vec{B} = -\vec{\Gamma}_+, \tag{2-12}$$

and for the electrons (mass m):

$$\frac{m\mu_-}{e}\frac{\partial\vec{\Gamma}_-}{\partial t} + \vec{\nabla}(D_-n_-) + n_-\mu_-\vec{E} + \mu_-\vec{\Gamma}_- \times \vec{B} = -\vec{\Gamma}_-. \tag{2-13}$$

For stationary (steady-state) situations in the plasma, we find that these equations reduce to

$$\vec{\Gamma}_{\pm} \mp \mu_{\pm}\vec{\Gamma}_{\pm} \times \vec{B} = \mp\mu_{\pm} n_{\pm}\vec{E} - D_{\pm}\vec{\nabla} n_{\pm}. \tag{2-14}$$

B. Current Density, Field and Potential Equations

From Poisson's equation we have

$$\vec{\nabla}\cdot\vec{E} = \frac{\rho}{\varepsilon_0} = \frac{(n_+ - n_-)e}{\varepsilon_0}, \tag{2-15}$$

and from Maxwell's equations for the stationary case:

$$\vec{\nabla}\times\vec{E} = 0, \tag{2-16}$$

$$\vec{\nabla}\times\frac{\vec{B}}{\mu} = e(\vec{\Gamma}_+ - \vec{\Gamma}_-). \tag{2-17}$$

These three equations, with the continuity equation (2-6) and the simplified momentum conservation equation (2-14) express the governing conditions for a plasma which complies with the assumptions ennumerated to date. These will be solved for current equations and for general field and potential relations.

From equation (2-6) it is readily deduced that

$$\vec{\Gamma}_+ = \vec{\Gamma}_- + (\vec{\nabla}\times\vec{F}), \tag{2-18}$$

in which ($\vec{\nabla}$ x $\vec{F}$) is a vector which we shall now determine Let us define three orthogonal directions in the plasma, one parallel to the magnetic field, designated by the subscript "$\parallel$", one perpendicular to the field and to any surfaces parallel to the field, "$\perp$", and the third transverse to the field and to the perpendicular

direction "T". In cylindrical coordinates, with a field parallel to the z-axis and cylindrical boundaries parallel to the field these would be the z-, r-, and φ- directions respectively. The ion and electron particle currents at the sheath edge are equal at all points for a steady-state plasma because they must arrive in equal numbers to recombine. For a geometry in which the insulator surfaces coicide with coordinate surfaces (the only geometries for which we will be able to obtain exact solutions for the particle density distributions),

$$\Gamma_{+\perp} = \Gamma_{-\perp} = \Gamma_{\perp} \tag{2-19a}$$

and

$$\Gamma_{+\parallel} = \Gamma_{-\parallel} = \Gamma_{\parallel} \tag{2-19b}$$

at the sheath edges. We now impose the condition that

$$\nabla_T n_+ = \nabla_T n_- = E_T = 0. \tag{2-20}$$

This requirement is met either by a plasma which has a rotational axis of symmetry parallel to the magnetic field or one in which the field lines coincide with one set of orthogonal coordinate lines and in which the resulting distribution is a function of only one coordinate. The latter condition would be met in the vicinity of a plane surface parallel to the magnetic field lines in an "infinite" plasma. Here, for a y-z plane and a field parallel to the z-axis, the perpendicular direction would be the x-direction and the transverse direction the y-direction. If these symmetry conditions are imposed, it is readily deduced that equations (2-19) apply throughout the plasma if the walls are insulators. If, however, the end surfaces are conductors (i.e., electrodes), equation (2-19b) does not apply. The parallel

current is then a conduction current, not a diffusion current, and is not treated by the developments to follow. This current does not affect the perpendicular currents, however, and such a plasma will be treated as an infinite plasma in the longitudinal direction, with

$$\nabla_{\parallel} n = 0. \tag{2-21}$$

From equation (2-14) and the symmetry conditions (2-20), it is immediately seen that the transverse component equation is:

$$\Gamma_{\pm T} = \mp \mu_{\pm} \Gamma_{\perp} B. \tag{2-22}$$

From this equation, and equations (2-19), we can see that $(\vec{\nabla} \times \vec{F})$ of equation (2-18) has only a transverse component:

$$(\vec{\nabla} \times \vec{F}) = (\vec{\nabla} \times \vec{F})_T = -\left(1 + \frac{\mu_+}{\mu_-}\right) \Gamma_{-T}. \tag{2-23}$$

The parallel and perpendicular component equations derived from equation (2-14) are

$$\Gamma_{\pm \parallel} = \pm \mu_{\pm} n_{\pm} E_{\parallel} - D_{\pm} \nabla_{\parallel} n_{\pm}, \tag{2-24}$$

and

$$\Gamma_{\pm \perp} \mp \mu_{\pm} \Gamma_{\pm T} B = \pm \mu_{\pm} n_{\pm} E_{\perp} - D_{\pm} \nabla_{\perp} n_{\pm}. \tag{2-25}$$

A simple solution is possible if the assumption of proportionality holds:

$$\frac{\nabla n_+}{n_+} \approx \frac{\nabla n_-}{n_-} = \frac{\nabla n}{n}. \tag{2-26}$$

By eliminating $E_{\parallel}$ from equation (2-24), we obtain

$$\Gamma_{\parallel} = -D_s \nabla_{\parallel} n_- = -D_{m_{\parallel}} \nabla_{\parallel} n_- \tag{2-27}$$

where $Dm_{\parallel}$ is a quasi-ambipolar diffusion coefficient for diffusion

parallel to a magnetic field and Ds is the ambipolar diffusion coefficient which is commonly developed for a plasma when B = 0 by infering congruence,

$$\vec{\Gamma}_+ = \vec{\Gamma}_- = \vec{\Gamma} \tag{2-28}$$

from the current density divergence equality equation (2-6) and from the proportionality condition (2-26) [2] [3] . D_S is related to Schottky's ambipolar diffusion coefficient,

$$D_a = \frac{D_+\mu_- + D_-\mu_+}{\mu_+ + \mu_-} \tag{2-29}$$

by the equations

$$D_S = D_a \frac{(\mu_+ + \mu_-)n_+}{(\mu_+ n_+ + \mu_- n_-)} \tag{2-30}$$

$$= D_a\left(1 + \frac{\mu_- \rho}{\sigma}\right). \tag{2-30a}$$

In equation (2-30a) we have employed the following relations for charge density and conductivity

$$\rho = (n_+ - n_-)e \tag{2-31a}$$

and

$$\sigma = (\mu_+ n_+ + \mu_- n_-)e. \tag{2-31b}$$

By substituting equation (2-22) into equation (2-25), we obtain

$$\Gamma_{\pm\perp} + \mu_\pm B^2 \Gamma_{\pm\perp} = \pm\mu_\pm n_\pm E_\perp - D_\pm \nabla_\perp n_\pm . \tag{2-32}$$

By the use of equation (2-19a), $E_\perp$ may be eliminated from the electron equation, to yield

$$\frac{\mu_- n_- + \mu_+ n_+ + (\mu_+^2 \mu_- n_- + \mu_-^2 \mu_+ n_+) B^2}{\mu_+ \mu_- n_+ n_-} \Gamma_\perp = -\frac{D_+\mu_- + D_-\mu_+}{\mu_+ \mu_- n_-} \nabla_\perp n_- \tag{2-33}$$

By simplifying and solving for $\Gamma_\perp$, we obtain

$$\Gamma_\perp = \frac{-D_s \nabla_\perp n_-}{1+\left[1+\frac{\rho(\mu_- - \mu_+)}{\sigma}\right]\mu_+\mu_- B^2} = -D_{m_\perp} \nabla_\perp n_- , \qquad (2\text{-}34)$$

where $D_{m_\perp}$ is a quasi-ambipolar diffusion coefficient for diffusion perpendicular to a magnetic field. Thus diffusion perpendicular to the magnetic field is reduced by an inverse dependence on the square of the magnetic field intensity.

If there is no superimposed electric field, so that $\vec{E} = \vec{E}_s$, where $\vec{E}_s$ is the space-charge field, $E_{s_\perp}$ may be obtained by substituting equation (2-34) into (2-32):

$$E_{s_\perp} = \frac{(1-\mu_-^2 B^2) D_{m_\perp} - D_-}{\mu_-} \frac{\nabla_\perp n}{n} . \qquad (2\text{-}35)$$

Similarly,

$$E_{s_\parallel} = \frac{D_{m_\parallel} - D_-}{\mu_-} \frac{\nabla_\parallel n}{n} = \frac{D_s - D_-}{\mu_-} \frac{\nabla_\parallel n}{n} \qquad (2\text{-}36)$$

The transverse space charge field is zero as a consequence of our assumptions that there is no transverse density gradient.

For a quasi-neutral plasma, in which

$$n_+ \approx n_- = n , \qquad (2\text{-}37)$$

it follows from equation (2-30) that $D_s = D_a$, and that

$$E_{s_\parallel} \xrightarrow[n_+ \approx n_-]{} \frac{D_+ - D_-}{\mu_+ + \mu_-} \frac{\nabla_\parallel n}{n} . \qquad (2\text{-}38)$$

In the absence of a magnetic field, equation (2-35) when simplified and added to equation (2-36), yields the single equation for the space-charge field

$$\vec{E}_s = \frac{D_s - D_-}{\mu_-} \frac{\vec{\nabla} n}{n} \xrightarrow[n_+ \approx n_-]{} \frac{D_+ - D_-}{\mu_+ + \mu_-} \frac{\vec{\nabla} n}{n} . \qquad (2\text{-}39)$$

From the field equations, we obtain the following equation for the space charge potential for a plasma with only a perpendicular density gradient:

$$V_\perp = \frac{D_- - (1+\mu_-^2 B^2) D_{m_\perp}}{\mu_-} \ln\left(\frac{n_-}{n_{-o}}\right), \tag{2-40}$$

In the absence of a magnetic field, equation (2-39) yields

$$V = \frac{D_- - D_s}{\mu_-} \ln\left(\frac{n_-}{n_{-o}}\right) \xrightarrow{n_+ \approx n_-} \frac{D_- - D_+}{\mu_+ + \mu_-} \ln\left(\frac{n}{n_o}\right) \tag{2-41}$$

The zero for potential in both of these equations is taken as the "center" of the plasma: that point (or region) where the density gradient is zero.

C. The Diffusion Tensor

The current density equations (2-22), (2-27) and (2-34) can be combined into one equation

$$\vec{\Gamma}_\pm = -\vec{\vec{D}}_{m_\pm} \nabla n_-, \tag{2-42}$$

which, in rectangular coordinates, is

$$\begin{pmatrix} \Gamma_{\pm x} \\ \Gamma_{\pm y} \\ \Gamma_{\pm z} \end{pmatrix} = -\begin{pmatrix} D_{m_\perp} & D_{m_{\pm T}} & 0 \\ D_{m_{\pm T}} & D_{m_\perp} & 0 \\ 0 & 0 & D_{m_\parallel} \end{pmatrix} \begin{pmatrix} \nabla_x n_- \\ \nabla_y n_- \\ \nabla_z n_- \end{pmatrix}, \tag{2-43}$$

and in cylindrical coordinates is

$$\begin{pmatrix} \Gamma_{\pm r} \\ \Gamma_{\pm \phi} \\ \Gamma_{\pm z} \end{pmatrix} = -\begin{pmatrix} D_{m_\perp} & D_{m_{\pm T}} & 0 \\ D_{m_{\pm T}} & D_{m_\perp} & 0 \\ 0 & 0 & D_{m_\parallel} \end{pmatrix} \begin{pmatrix} \nabla_r n_- \\ 0 \\ \nabla_z n_- \end{pmatrix}. \tag{2-44}$$

The components of the diffusion tensor are

$$Dm_{\parallel} = D_s, \tag{2-45a}$$

$$Dm_{\perp} = \frac{D_s}{1+\left[1 + \frac{\rho(\mu_- - \mu_+)}{\sigma}\right]\mu_+\mu_- B^2}, \tag{2-45b}$$

$$Dm_{+T} = \mu_+ B\, Dm_{\perp}, \tag{2-45c}$$

$$Dm_{-T} = -\mu_- B\, Dm_{\perp}. \tag{2-45d}$$

We shall now examine each of these components. Equation (2-45a) reflects the fact that the magnetic field does not affect diffusion in the direction parallel to itself. Further, we have shown that

$$Dm_{\parallel} = D_s \xrightarrow[\text{or } n_+ \approx n_-]{\rho \to 0} D_a. \tag{2-46a}$$

Allis [2] has also shown that

$$D_s \xrightarrow[\sigma_0 \to \infty]{} D_-, \tag{2-46b}$$

where σ_0 is the conductivity at the center of the plasma. The quasi-neutral limit (3-46a) is applicable to a plasma in which the mobilities (and consequently the conductivity) are so great that negligible space charge can develop. The above limits are the low and high limits for the ambipolar diffusion coefficient.

The perpendicular component is more complex. First, as the magnetic field approaches zero,

$$Dm_{\perp} \xrightarrow[B \to 0]{} D_s. \tag{2-47a}$$

As B becomes very large, $Dm_\perp$ approaches zero as $\frac{1}{B^2}$

$$Dm_\perp \xrightarrow[B\to\infty]{} \frac{D_s}{\mu_+\mu_- B^2} \xrightarrow[B\to\infty]{} 0. \tag{2-47b}$$

From equation (2-46a) it is seen that

$$Dm_\perp \xrightarrow[\substack{\rho\to 0 \\ n_+\approx n_-}]{} \frac{D_a}{1+\mu_+\mu_- B^2}, \tag{2-47c}$$

and from (2-60a) that

$$Dm_\perp \xrightarrow[\sigma_c\to 0]{} \frac{D_-\sigma_0}{\rho_0(\mu_- - \mu_+)\mu_+\mu_- B^2}, \tag{2-47d}$$

which can be non-zero only if $\rho_0 = 0$. As shown in equation (2-55), for a long, narrow plasma this can be true only if

$$Dm_\perp \xrightarrow[\sigma_0\to 0]{} \frac{D_-}{1-\mu_-^2 B^2}. \tag{2-47e}$$

From these equations it is apparent that for the parallel and perpendicular diffusion tensor components in a magnetic field the high and low limits are the corresponding electron diffusion values or the quasi-neutral ambipolar values respectively.

For the transverse components, we obtain

$$Dm_{\pm T} = \frac{\mp\mu_\pm D_s B}{1+\left[1+\frac{\rho(\mu_- - \mu_+)}{\sigma_0}\right]\mu_+\mu_- B^2}, \tag{2-48a}$$

$$\xrightarrow[\substack{\rho\to 0 \\ n_+\approx n_-}]{} \frac{\mp\mu_\pm D_a B}{1+\mu_+\mu_- B^2}, \tag{2-48b}$$

$$\xrightarrow[B\to\infty]{} \frac{\mp D_s}{\mu_\mp B} \xrightarrow[B\to\infty]{} 0, \tag{2-48c}$$

$$\xrightarrow[B\to 0]{} \mp\mu_\pm D_s B \xrightarrow[B\to 0]{} 0. \tag{2-48d}$$

The maximum transverse internal current will flow when $Dm_{\pm T}$ are a maximum. For the quasi-neutral plasma, equation (2-48b), this occurs when the magnetic field has a magnitude given by

$$B = \frac{1}{\sqrt{\mu_+ \mu_-}} . \tag{2-49}$$

For helium, using data from reference [4], this is approximately 0.12 weber/m^2. The magnitude of the current density resulting from this field can be determined from equation (2-22)

$$\vec{J}_{T_{max}} = e\left(\Gamma_{+T} - \Gamma_{-T}\right)_{max} \hat{e}_T = -\frac{e(\mu_- + \mu_+) D_a \nabla_\perp \chi}{2\sqrt{\mu_+ \mu_-}} \hat{e}_T , \tag{2-50}$$

where $\hat{e}_T$ is a unit vector in the transverse direction. The magnetic field generated by this current will oppose the applied field, and accounts for the observed diamagnetism of the plasma. This is the term which satisfies equation (2-17), and it must be small compared to B to justify neglecting its effects on the other plasma equations.

In the quasi-neutral plasma, with $n_+ \approx n_-$, the diffusion tensor reduces to

$$\overleftrightarrow{D}_{m_\pm} = \begin{pmatrix} \frac{D_a}{1+\mu_+\mu_- B^2} & \frac{\mp \mu_\pm D_a B}{1+\mu_+\mu_- B^2} & 0 \\ \frac{\mp \mu_\pm D_a B}{1+\mu_+\mu_- B^2} & \frac{D_a}{1+\mu_+\mu_- B^2} & 0 \\ 0 & 0 & D_a \end{pmatrix} \tag{2-51}$$

D. The Continuity Equation

By substituting equation (2-42) into the continuity equation (2-6), we obtain

$$\frac{\partial n}{\partial t} - \vec{\nabla} \cdot \left(\overleftrightarrow{D}_{m_\pm} \vec{\nabla} n_-\right) = \nu n_- \tag{2-52}$$

a second order partial differential equation. For the steady state, this reduces to

$$\vec{\nabla}\cdot(\vec{D}_{m_-}\vec{\nabla}n_-) = -\nu n_- \qquad (2\text{-}53)$$

whereas for a decaying plasma (for which $\nu = 0$), it becomes the diffusion equation

$$\frac{\partial n}{\partial t} - \vec{\nabla}\cdot(\vec{D}_{m_\pm}\vec{\nabla}n_-) = 0 \qquad (2\text{-}54)$$

In order to simplify equation (2-54), we must examine its components. The components of the diffusion tensor, equations (2-45), are constants because of our assumptions and consequently the divergence of the diffusion tensor is zero. In the absence of a magnetic field, $\vec{D}_{m\pm}$ is the scalar D_s, and equation (2-52) becomes the familiar continuity equation:

$$D_s\nabla^2 n_- + \nu n_- = \frac{\partial n}{\partial t} \qquad (2\text{-}55)$$

For the steady state, we can further simplify this by employing the assumption of proportionality, equation (2-26), to obtain

$$\frac{\nabla^2 n}{n} = -\frac{\nu}{D_s} \qquad (2\text{-}56)$$

In the presence of a magnetic field, we shall limit ourselves to orthogonal geometries in which equation (2-53) can be separated into

$$D_{m_\perp}\nabla_\perp^2 n_- + D_{m_\parallel}\nabla_\parallel^2 n_- + \nu n_- = 0 \qquad (2\text{-}57)$$

In equation (2-57) we have made explicit use of the requirement that the transverse density gradient be zero. By employing the assumption of proportionality (equation (2-26)) and a theorem from vector analysis, we see that

$$\frac{\nabla_{\parallel}^2 n_-}{n_-} = \frac{\nabla_{\parallel}^2 n}{n} = \vec{\nabla}_{\parallel} \cdot \left(\frac{\vec{\nabla}_{\parallel} n}{n}\right) + \left(\frac{\vec{\nabla}_{\parallel} n}{n}\right)^2, \tag{2-58}$$

with a similar equation for the perpendicular components. Thus we can divide equation (2-57) by n_- and expand it to obtain

$$D m_{\perp} \vec{\nabla}_{\perp} \cdot \left(\frac{\vec{\nabla}_{\perp} n}{n}\right) + D m_{\parallel} \vec{\nabla}_{\parallel} \cdot \left(\frac{\vec{\nabla}_{\parallel} n}{n}\right) + D m_{\perp} \left(\frac{\vec{\nabla}_{\perp} n}{n}\right)^2 + D m_{\parallel} \left(\frac{\vec{\nabla}_{\parallel} n}{n}\right)^2. \tag{2-59}$$

If we then define a vector $\vec{u}$ such that

$$\vec{u} = \vec{u}_{\perp} + \vec{u}_{\parallel} = \frac{\vec{\nabla}_{\perp} n}{n} + \frac{\vec{\nabla}_{\parallel} n}{n} = \frac{\vec{\nabla} n}{n}, \tag{2-60}$$

we obtain

$$D m_{\perp} \vec{\nabla}_{\perp} \cdot \vec{u}_{\perp} + D m_{\parallel} \vec{\nabla}_{\parallel} \cdot \vec{u}_{\parallel} + D m_{\perp} u_{\perp}^2 + D m_{\parallel} u_{\parallel}^2 + \nu = 0 \tag{2-61}$$

which is a first order partial differential equation in u. In the absence of a magnetic field, D_m is a scalar (D_s), and equation (2-56) can be similarly expressed (in any coordinate system) as

$$\vec{\nabla} \cdot \vec{u} + \vec{u}^2 + \frac{\nu}{D_s} = 0. \tag{2-62}$$

The significance of the transformation of this equation from a second order differential equation in particle density, n, to a first order differential equation in u will become apparent in the discussion of boundary conditions in a later section.

E. Boundary Conditions

1. Derivation

We shall now develop an equation for the boundary condition and evaluate it for a few simplified cases. We consider a quasi-neutral stationary plasma in contact with a plane wall. The magnetic field, if any, is parallel to the wall.

There are two conditions which we must fulfill. The first is that the electron and ion currents to the insulator surface must be equal; the other is that the current must be continuous at the limit of the diffusion region, which can be at the edge of the sheath or at the edge of the free-fall zone.

We have to distinguish different sheath theories according to whether $D_{-\perp} > D_{+\perp}$, $D_{-\perp} < D_{+\perp}$ or $D_{-\perp} \approx D_{+\perp}$, where

$$D_\perp = \frac{D}{1-\mu^2 B^2} \tag{2-66}$$

a. The case $D_{-\perp} >> D_{+\perp}$, ion current inertia-limited.

Let us first examine the problem in which $D_{-\perp} >> D_{+\perp}$. In this case a negative wall charge builds up until the electron current is reduced to equality with the positive ion current. The electrons will be treated as having a Maxwellian distribution

$$n_- = n_0 e^{\frac{eV}{kT_-}} \tag{2-67}$$

where the potential V at the sheath edge is taken as zero, -e is the charge of the electron, and the subscript "o" means evaluation at the sheath edge. This notation will be used throughout this section.

We find that two possibilities exist for the ion motion through the sheath: (1) their motion may be inertia-limited, or (2) their motion may be mobility-limited. In the inertia-limited case, the sheath is a free-fall region and the current in the sheath is that given by kinetic theory:

$$\vec{\Gamma}_{+o} = \frac{n_o \vec{V}_{+o}}{4} \tag{2-68}$$

We must next evaluate the diffusion current to the sheath edge, which is

$$\vec{\Gamma}_{+o} = -\frac{D_a}{1+\mu_+\mu_- B^2} \vec{\nabla} n_o . \tag{2-69}$$

If the electrons and ions are in equilibrium within the body of the plasma

$$D_a \approx 2D_+ \approx \tfrac{2}{3}(\lambda_+ \bar{V}_+). \tag{2-69a}$$

In order that the number of particles varried to the sheath by the above diffusion current equal the number carried to the wall as expressed by equation (2-68), the normal component of the diffusion current must equal the sheath current. Therefore, we have the equation

$$\frac{n_o \bar{V}_+}{4} = \frac{-\frac{2}{3}(\lambda_+ \bar{V}_+) \nabla_n n_o}{1+\mu_+\mu_- B^2} . \tag{2-70}$$

From this equation we see that

$$\left(\frac{\nabla_n n}{n}\right)_o = u_n = -\frac{\alpha}{\lambda_+}, \tag{2-71}$$

a result obtained by Ecker [3], where, for this case

$$\alpha = \frac{3}{8}\left(1+\mu_i\mu-B^2\right). \tag{2-70a}$$

It will be seen that the boundary condition can always be expressed in the form (2-71), with the value of α varying with the sheath characteristics. Let us investigate the potential function V for this condition. If there is no magnetic field, we see from the conservation of energy that

$$\frac{Mv_{+o}^2}{2} = \frac{Mv_+^2}{2} + \frac{eV}{kT_+}, \tag{2-72}$$

where M is the ionic mass. From this we can derive the following equation for the ion current density:

$$j_+ = n_+ e v_+ = n_o e v_{+o} = n_+ e v_o \sqrt{1 - \frac{eV}{kT_+}}. \tag{2-73}$$

Let us now employ a coordinate system in which the x-direction is normal to the sheath and positive towards the wall, and whose origin is at the sheath edge. Solving equations (2-67) and (2-73) for n_- and n_+ respectively, and substituting in Poisson's equation (2-15), we find

$$\frac{d^2V}{dx^2} = \frac{e}{\varepsilon_o}(n_- - n_+) = \frac{en_{io}}{\varepsilon_o}\left\{e^{\frac{eV}{kT_-}} - \frac{1}{\sqrt{1-\frac{eV}{kT_+}}}\right\} \tag{2-74}$$

Multiplying by $\frac{dV}{dx}$ and integrating yields:

$$\left(\frac{dV}{dx}\right)^2 = \frac{2n_o kT_-}{e\varepsilon_o}\left\{\left(e^{\frac{eV}{kT_-}} - 1\right) + \frac{2T_+}{T_-}\left(\sqrt{1-\frac{eV}{kT_+}} - 1\right)\right\} + E_o^2, \tag{2-75}$$

where we have set $\left.\frac{dV}{dx}\right|_o = -E_o$ and $V|_o = 0$. This result has been reported by Ecker[5]. For the sheath to be stable, $\frac{dV}{dx} = -E$ must increase with x. Therefore the quantity in the brackets of equation

(2-75) must be positive. Expanding this quantity in series, we find

$$\frac{eV}{kT_-} + \frac{1}{2}\frac{e^2V^2}{k^2T_-^2} + \frac{2T_+}{T_-}\left(-\frac{1}{2}\frac{eV}{kT_+} - \frac{1}{8}\frac{e^2V^2}{k^2T_+^2}\right) \geq 0, \tag{2-76}$$

from which we see that

$$T_+ \geq \frac{1}{2}T_- \tag{2-77}$$

is the condition for the sheath to be stable. Bohm [7] has calculated the function V for two values of T_+ by numerical integration.

If we neglect the electron density in Poisson's equation, and integrate, we obtain the Langmuir relation [8]:

$$V = -\left(\frac{2M}{e}\right)^{\frac{1}{3}}\left(\frac{9}{8}\frac{1^+}{\varepsilon_0}x^2\right)^{2/3}. \tag{2-78}$$

b. The case $D_{-\perp} \gg D_{+\perp}$, ion current mobility-limited

We shall next examine the case in which the ion current through the sheath is mobility limited; i.e., the ions move in the field of the negative wall charge according to their mobility. Now the electron current density striking the wall is obtained from kinetic theory and the electron density relation (2-67):

$$\left.\frac{n_-\bar{V}_-}{4}\right)_d = \frac{n_0\bar{V}_-\, e^{+\frac{eV(d_-)}{kT_-}}}{4}, \tag{2-79}$$

where $V(d_-)$ is evaluated at the edge of the electron free-flight zone (suitably corrected to account for curvature of the electron paths in the magnetic field). Again equating this current with the diffusion current brought to the sheath, we obtain:

$$\frac{n_0\bar{V}_-\, e^{\frac{eV(d_-)}{kT_-}}}{4} = -\frac{\frac{2}{3}(\lambda\bar{V}_+)\nabla_n n}{1+\mu_\perp\mu_- B^2}. \tag{2-80}$$

In order to further simplify this relation for the case in which the electrons and ions are in equilibrium, we use the relation

$$m\bar{v}_-^2 = M\bar{v}_+^2, \tag{2-81}$$

from which we see that

$$\frac{\nabla_n n}{n} = -\frac{3}{8\lambda_+}\sqrt{\frac{M}{m}}\, e^{\frac{eV(d_-)}{kT_-}}\left(1+\mu_+\mu_- B^2\right). \tag{2-82}$$

Thus we obtain for the parameter α :

$$\alpha = \frac{3}{8}\sqrt{\frac{M}{m}}\, e^{\frac{eV(d_-)}{kT_-}}\left(1+\mu_+\mu_- B^2\right). \tag{2-83}$$

In order to evaluate this expression, it is necessary to know the potential function V(x). The ion current density in the sheath (neglecting the magnetic field) is:

$$j_+ = \mu_+ n_0 e E_0 = \mu_{+\perp} n_+ e E_x = -\mu_{+\perp} n_+ e \frac{dV}{dx}, \tag{2-84}$$

where

$$\mu_\perp = \frac{\mu}{1+\mu^2 B^2}. \tag{2-84a}$$

Again employing Poisson's equation, and solving equations (2-84) and (2-67) for n_+ and n_- respectively, we obtain:

$$\frac{d^2V}{dx^2} = \frac{e}{\varepsilon_0}\left\{n_0 e^{\frac{eV}{kT_-}} + \frac{j_+}{\mu_{+\perp} e \frac{dV}{dx}}\right\} \tag{2-85a}$$

$$\frac{en_0}{\varepsilon_0}\left\{e^{\frac{eV}{kT_-}} + \frac{E_0}{\frac{dV}{dx}}\right\}. \tag{2-85b}$$

At the sheath edge (where x = 0, V = 0, and $\frac{dV}{dx} = +E_0$), $\frac{d^2V}{dx^2} = 0$, a result consistent with the assumption of quasi-neutrality at the

sheath boundary. Equation (2-85b) can be integrated once, and yields a first order differential equation for V:

$$\left(\frac{dV}{dx}\right)^2 = \frac{en_o}{\varepsilon_o}\left\{E_o x + \frac{kT_-}{e}\left(e^{\frac{eV}{kT_-}} - 1\right)\right\} + E_o^2. \tag{2-86}$$

Further integration, to obtain V(x), must be performed numerically. However, if we again neglect the electron density, equation (2-86) can be integrated to yield:

$$V = \sqrt{\frac{8}{9}\frac{J_+ x^3}{\varepsilon_o \mu_+}} \tag{2-87}$$

c. <u>The case $D_{-\perp} \approx D_{+\perp}$</u>

An approximation for the case $D_{-\perp} \approx D_{+\perp}$ can be easily obtained for inertia-limited ion current. By neglecting $\mu_+^2 B^2$ as compared to 1 in the equality

$$\frac{D_-}{1+\mu_-^2 B^2} \approx \frac{D_+}{1+\mu_+^2 B^2}, \tag{2-88}$$

we obtain

$$\frac{D_-}{D_+} \approx 1 + \mu_-^2 B^2, \tag{2-89}$$

from which it is seen that

$$\frac{\mu_+}{\mu_-}\left(\frac{D_-}{D_+} - 1\right) = \mu_+ \mu_- B^2. \tag{2-90}$$

Employing this relation in equation (2-70a) yields

$$\alpha \approx \frac{3}{8}\left(1 + \frac{\mu_+}{\mu_-}\frac{D_-}{D_+} - \frac{\mu_+}{\mu_-}\right). \tag{2-91}$$

If we neglect the last term in the parenthesis as compared with one,

and employ Einstein's relation

$$\frac{D_\pm}{\mu_\pm} = \frac{kT_\pm}{e}, \tag{2-92}$$

we obtain

$$\alpha = \frac{3}{8}\left(1 + \frac{T_-}{T_+}\right). \tag{2-93}$$

d. The case $D_{+\perp} \gg D_{-\perp}$

For the plasma in which $D_{+\perp} \gg D_{-\perp}$, a positive wall charge must build up until the ion and electron currents are equal. The ions, assuming Maxwellian distribution, will have a density within the sheath given by

$$n_+ = n_0 e^{-\frac{eV}{kT_+}}, \tag{2-94}$$

where the ionic charge is +e.

The ion current to the wall is obtained from kinetic theory as

$$\left.\frac{n_+ \bar{V}_+}{4}\right)_{d_+} = \frac{n_0 \bar{V}_+ e^{-\frac{eV(d_+)}{kT_+}}}{4}, \tag{2-95}$$

where the evaluation of $V(d_+)$ is at an ionic mean-free path, d_+, which has been adjusted to include the effects of the magnetic field. Equating this to the diffusion current to the sheath yields the boundary condition (2-71) in which

$$\alpha = \frac{3}{8} e^{-\frac{eV(d_+)}{kT_+}} \left(1 + \mu_+ \mu_- B^2\right). \tag{2-96}$$

In order to evaluate the function V, it is necessary to employ the equation for the electron current (neglecting the effects of the magnetic field):

$$j_- = -\mu_{-\perp} n_0 e E_0 = -\mu_{\perp} n_- e E = \mu_{-\perp} n_- e \frac{dV}{dx}. \qquad (2\text{-}97)$$

By the same procedure used for the mobility-limited ions when $D_{-\perp} >> D_{+\perp}$, we obtain

$$\left(\frac{dV}{dx}\right)^2 = \frac{e n_0}{\varepsilon_0}\left\{-E_0 x + \frac{kT_+}{e}\left(e^{-\frac{eV}{kT_+}} - 1\right)\right\} + E_0^2. \qquad (2\text{-}98)$$

2. Evaluation of α

The over-all problem of evaluating α of the boundary condition equation (2-71) is a much more complicated problem than indicated by the derivations of the previous section. The influence of the transition region, the effect of non-planar geometries, deviation from thermal equilibrium within the plasma proper (and in the transition region), and secondary emission are just a few of the factors which can affect this quantity. The transition region, which joins in a continuous fashion the sheath and the main body of the plasma, presents particularly difficult problems which are beyond the scope of this thesis. In the computation of α for a surface whose dimensions are comparable to or less than the mean free path, it is especially important to compute the fraction of particles brought to the sheath edge which would miss the surface in their flight through the sheath and would pass back into the plasma. Thus, for the limit where the surface is very much smaller than the mean free path, as for a Langmuir probe, α can become vanishingly small.

3. Discussion

An understanding of the processes occuring within the sheath has been shown to be necessary for the evaluation of the boundary

condition equation (2-71). We have seen that the requirement that the current be continuous results in this condition which must be met at the surface of the ion free-fall zone (the region within one ionic mean free path, λ_+, of the wall) or at the surface of the sheath, whichever is farther from the wall. As the sheath thickness and λ_+ become very much smaller than other dimensions, equation (2-71) may be replaced by its limit for vanishing λ_+:

$$n\big)_{wall} = 0. \tag{2-99}$$

This is the generally-used boundary condition, but for small values of α and large λ_+, the error in (2-99) can be appreciable. From (2-71) we obtain:

$$n\big)_{wall} \approx n_{\lambda_+} + \lambda_+ \nabla_n n \approx n_{\lambda_+}(1-\alpha) \tag{2-100}$$

where the subscript λ_+ refers to evaluation at a distance λ_+ from the wall.

The importance of equation (2-71) and of the transformation of the continuity equations to the forms (2-61) and (2-62) is now readily seen. The normal component of the vector $\vec{u}$ defined by equation (2-60) must have a constant magnitude, $-\frac{\alpha}{\lambda_+}$, along the sheath edge. If there is more than one wall, and the walls involved are orthogonal, the density gradients established to satisfy this condition at each sheath edge will not interfere with each other. Parallel surfaces, on the other hand, create an eigenvalue problem because $\vec{u}$ must satisfy the boundary condition at one sheath edge, must change

as prescribed by the continuity equation (2-61) as we move across the plasma, and must again satisfy uniquely the boundary condition at the other surface. If the walls are neither orthogonal nor parallel, the density gradients established to meet the boundary condition for one surface will have along the other surface normal components which are not constant, and vice versa. This will result in a violation of equation (2-71). Consequently, for non-orthogonal geometries we are unable to predict the steady state distributions with the equations developed in this thesis except by an approximate method to be discussed in a later section.

F. Heat Losses

The only source of heat loss considered in this thesis is that which occurs at an insulated surface as a consequence of the particles impinging on the surface and giving up their energy. This energy can come from several sources: (1) the recombination energy, eV_i, from each electron-ion recombination, (2) the kinetic energy of the particles, and (3) excitation energy of excited ions which return to their stable state upon colliding with a wall. All of these are proportional to the particle current density to the surfaces. As a simplification for illustrative purposes in later calculations we shall limit ourselves to plasmas whose temperatures are sufficiently low (below about 10^5 degrees) that only the recombination and electron kinetic energies are appreciable. The heat liberated at a surface is then

$$E_{wall} = \Gamma_n \left(eV_i + \frac{kT_-}{e}\right), \qquad (2\text{-}101)$$

where the subscript "n" means normal to the surface and E_{wall} is expressed in electron volts.

III

SOLUTIONS OF THE CONTINUITY EQUATION

A. General Solutions

This section discusses a procedure to obtain particle distribution functions in several coordinate systems, and presents some of the general features of the solutions. The following sections develop many solutions for specific geometries.

1. Exact Solutions

a. General Development:

With no magnetic field, we have exact solutions in the eleven orthogonal coordinate systems in which the wave equation is separable when the boundary surfaces coincide with coordinate planes. The procedure we shall describe applies to the non-steady state plasma for which we repeat the general continuity equation (2-55)

$$D_s \nabla^2 n_- + \mu n_- = \frac{\partial n}{\partial t}, \tag{3-1}$$

which becomes a wave equation for the steady-state

$$\frac{\nabla^2 n}{n} = -\frac{\nu}{D_s}; \tag{3-1a}$$

for a decaying plasma with no ionization it is

$$D_s \nabla^2 n_- = \frac{\partial n}{\partial t}, \tag{3-1b}$$

with a steady-state counterpart (Laplace's equation)

$$\nabla^2 n_- = 0. \tag{3-1c}$$

In the presence of a magnetic field, we further require that the

coordinate system be one in which the continuity equation may be expanded as

$$D m_{\parallel} \nabla_{\parallel}^2 n_- + D m_{\perp} \nabla_{\perp}^2 n_- + \nu n_- = \frac{\partial n}{\partial t} \tag{3-2}$$

(see equation (2-57).

Equations (3-1) and (3-2) are separable in the geometrical coordinates and time, and the general solution for a generalized coordinate systems u, v, w, may be expressed as

$$n(u,v,w,t) = N(u,v,w,)T(t). \tag{3-3}$$

Substitution of equation (3-3) in equation (3-2), and division by NT yields

$$\frac{D m_{\parallel} \nabla_{\parallel}^2 N}{N} + \frac{D m_{\perp} \nabla_{\perp}^2 N}{N} + \nu = \frac{T'}{T} = -k_t, \tag{3-4}$$

where $-k_t$ is a separation constant. The time solution is

$$T = C_1 e^{-k_t t} \tag{3-5}$$

and then

$$\frac{D m_{\parallel} \nabla_{\parallel}^2 N}{N} + \frac{D m_{\perp} \nabla_{\perp}^2 N}{N} = -(k_t + \nu). \tag{3-6}$$

In the absence of a magnetic field, equation (3-6) reduces to

$$\frac{\nabla^2 N}{N} = -k^2, \tag{3-7}$$

in which

$$k^2 = \frac{k_t + \nu}{D_s}, \tag{3-7a}$$

and, for the steady state ($k_t = 0$)

$$k^2 = \frac{\nu}{D_s}. \tag{3-7b}$$

Our approach to the solution of equations (3-6) and (3-7) is to employ the technique of separation of variables. Thus we assume that the solution is of the form

$$N(u,v,w) = f_1(u)f_2(v)f_3(w), \tag{3-8}$$

and, by substitution into equation (3-6) or (3-7) (as appropriate), we obtain three differential equations, one in terms of each of the coordinate variables, which the functions f_1, f_2, and f_3 must separately satisfy. Magnus and Oberhettinger [9] have summarized the results for eight coordinate systems. Because the separated equations are of the second order, there will be two linearly independent sets of eigenfunctions for each coordinate, $F^{(1)}(k_\ell,u)$ and $F^{(2)}(k_\ell,u)$, $G^{(1)}(k_m,v)$ and $G^{(2)}(k_m,v)$, and $H^{(1)}(k_n,w)$ and $H^{(2)}(k_n,w)$, which satisfy the differential equation in the corresponding variable. We shall call the functions with the superscript (1) functions of the first kind and the others functions of the second kind. The most general solution to these equations will then be a sum of the products of all such linearly independent solutions of the form

$$N_{\ell mn}(u,v,w) = \left[C_{2\ell}F^{(1)}(k_\ell,u) + C_{3\ell}F^{(2)}(k_\ell,u)\right]\left[C_{4m}G^{(1)}(k_m,v) + C_{5m}G^{(2)}(k_m,v)\right]\times \left[C_{6n}H^{(1)}(k_n,w) + C_{7n}H^{(2)}(k_n,w)\right]. \tag{3-9}$$

The complete solution for the particle density distribution is then

$$n(u,v,w,t) = \sum_{\ell,m,n} N_{\ell mn}(u,v,w)T(t) \tag{3-10}$$

$$= \sum_{\ell,m,n} N_{\ell mn}(u,v,w)\,e^{-k_i t}. \tag{3-10a}$$

The summation is over all possible values of ℓ, m, and n. k_ℓ, k_m, and k_n are eigenvalues or spearation constants (depending on the coordinate system chosen) corresponding to ℓ, m, and n respectively. We can sum over only those eigenfunctions which belong to a degenerated eigenvalue (as determined by the boundary conditions). It should be noted that the time-dependent solutions to be developed herein are for those problems for which the boundary condition (2-71) or (2-99) is still applicable. A plasma decaying from a steady-state distribution upon cessation of ionization is considered to be such a plasma.

b. Cartesian Coordinates

An example of the above method of solution is the solution in cartesian coordinates in which the functions of the first and second kinds may all be cosines and sines respectively, or in which one or two pairs of the functions may be exponentials. For example:

$$N(x,y,z) = \sum_{\ell,m,n} \left[C_{2\ell}\cos(k_\ell x) + C_{3\ell}\sin(k_\ell x)\right]\left[C_{4m}\cos(k_m y) + C_{5m}\sin(k_m y)\right] \times \left[C_{6n}\cos(k_n z) + C_{7n}\sin(k_n z)\right]. \tag{3-11}$$

By substitution of this solution in equation (3-7), we see that k^2 of equations (3-7a) and (3-7b) is given by

$$k^2 = \sum_{\ell,m,n} \left(k_\ell^2 + k_m^2 + k_n^2\right), \tag{3-11a}$$

and consequently that the time solution (equation (3-5)) is

$$T_{\ell mn} = C_{10_{mn}} e^{-k_i t} = C_{10_{mn}} e^{-\left[D_0\left(k_\ell^2 + k_m^2 + k_n^2\right) - \nu\right]t}. \tag{3-11b}$$

Obviously, when

$$k^2 = (k_\ell^2 + k_m^2 + k_n^2) = \frac{\nu}{D_s}, \tag{3-12}$$

the time dependence vanishes, and the plasma is "stationary."

Another possible solution, involving exponentials, is

$$N(x,y,z) = \sum_{\ell,m,n} \left[C_{2\ell} e^{k_\ell x} + C_{3\ell} e^{-k_\ell x}\right]\left[C_{4m} e^{k_m y} + C_{5m} e^{-k_m y}\right]\left[C_{6n}\cos(k_n z) + C_{7n}\sin(k_n z)\right], \tag{3-13}$$

where k^2 is given by

$$k^2 = \sum_{\ell,m,n} (k_n^2 - k_\ell^2 - k_m^2). \tag{3-13a}$$

c. Cylindrical Coordinates

There is an independent eigenvalue, k_i, for each set of functions only in cartesian coordinates. For any other coordinate system u,v,w, defined by a transformation equation of the form

$$\begin{aligned} x &= x(u,v,w) \\ y &= y(u,v,w) \\ z &= z(u,v,w), \end{aligned} \tag{3-14}$$

those eigenfunctions of the variables u,v,w which appear together in any of equations (3-14) will be connected through a separation variable which is required to reduce equation (3-4) or (3-7) to separate equations in each of the coordinates. Each such separation variable required for the above purpose reduces the number of eigenvalues available for the satisfaction of the boundary conditions. For example, for cylindrical coordinates, where

$$\begin{aligned} x &= r\cos\varphi \\ y &= r\sin\varphi \\ z &= z, \end{aligned} \tag{3-15}$$

the eigenfunctions in r and φ are related by the separation constant, m, as indicated in the well-known solution

$$N(r,\varphi,z) = \sum_{l,m,n} R(r)\,\Phi(\varphi)\,Z(z), \tag{3-16}$$

where

$$\begin{aligned} R(r) &= C_{2lm} J_m(k_l r) + C_{3lm} N_m(k_l r) && k_l \neq 0 \\ &= C_2 r^m + C_3 r^{-m} && k_l = 0 \\ &= C_2' \ln r + C_3' && k_l = k_n = m = 0 \\ \Phi(\varphi) &= C_{4m}\cos(m\varphi) + C_{5m}\sin(m\varphi) && m \neq 0 \\ &= C_4\varphi + C_5 && m = 0 \\ Z(z) &= C_{6n}\cos(k_n z) + C_{7n}\sin(k_n z) && k_n \neq 0 \\ &= C_6 z + C_7, && k_n = 0, \end{aligned} \tag{3-16a}$$

and

$$k^2 = \sum_{l,n} (k_l^2 + k_n^2), \tag{3-16b}$$

An alternative Z(z) solution is

$$Z(z) = C_{6n} e^{k_n z} + C_{7n} e^{-k_n z} \qquad k_n \neq 0 \tag{3-16c}$$

with

$$k^2 = \sum_{l,n} k_l^2 - k_n^2, \tag{3-16d}$$

$J_m(k\,r)$ and $N_m(k\,r)$ are Bessel functions of order m of the first and second kinds respectively (Bessel and Neumann functions).

c. Spherical, Prolate and Oblate Ellipsoidal Coordinates

In the other coordinate systems to be discussed, the general solutions of (3-7) are:

Spherical:

$$N(r,\theta,\varphi) = \sum_{l,m,n} R(r)\,\Theta(\theta)\,\Phi(\varphi), \tag{3-17}$$

where

$$\begin{aligned} R(r) &= C_{2ln} j_n(k_l r) + C_{3ln} n_n(k_l r) && k_l \neq 0 \\ &= C_{2n} r^n + C_{3n} r^{-n} && k_l = 0 \\ \Theta(\theta) &= C_{4n} P_n^m(\cos\theta) + C_{5n} Q_n^m(\cos\theta) \\ \Phi(\varphi) &= C_{6m}\cos(m\varphi) + C_{7m}\sin(m\varphi) && m \neq 0 \\ &= C_6\varphi + C_7 && m = 0, \end{aligned} \tag{3-17a}$$

and

$$k^2 = \sum_l k_l^2, \tag{3-17b}$$

and in which $P_n^m(\cos\theta)$ and $Q_n^m(\cos\theta)$ are Legendre Polynomials of the first and second kinds respectively and $j_n(k\,r)$ and $n_n(k\,r)$ are spherical Bessel functions of order n of the first and second kinds respectively. The latter are defined by the equations

$$\begin{aligned} j_n(k_l r) &= \sqrt{\frac{\pi}{2k_l r}}\, J_{n+\frac{1}{2}}(k_l r) \\ n_n(k_l r) &= \sqrt{\frac{\pi}{2k_l r}}\, N_{n+\frac{1}{2}}(k_l r). \end{aligned} \tag{3-17c}$$

Prolate Ellipsoidal (See Appendix I for diagram and transformation equations; notation employed is that of Flammer [6] with slight modification):

$$\begin{aligned} N_{lmn}(\eta,\xi,\varphi) = &\left[C_{2lmn} S_{mn}^{(1)}(c_l,\eta) + C_{3lmn} S_{mn}^{(2)}(c_l,\eta)\right] \times \\ &\times \left[C_{4lmn} R_{mn}^{(1)}(c_l,\xi) + C_{5lmn} R_{mn}^{(2)}(c_l,\xi)\right]\left[C_{6m}\cos(m\varphi) + C_{7m}\sin(m\varphi)\right], \end{aligned} \tag{3-18}$$

where

$$k = \frac{2}{d} c_l, \tag{3-18a}$$

and d is the interfocal distance. $S_{mn}^{(1)}(c_l,\eta)$ and $S_{mn}^{(2)}(c_l,\eta)$ are spheroidal

angle functions of the first and second kinds and $R_{mn}^{(1)}(c_l, \xi)$ and $R_{mn}^{(2)}(c_l, \xi)$ are spheroidal radial functions. See Appendix II for tables and graphs of these functions.

Oblate Ellipsoidal functions may be obtained from the prolate functions by the substitution of $-ic_l$ for c_l where appearing in equation (3-18). Equation (3-18a) is unchanged by the transformation.

Similar equations are obtained in parabolic cylinder coordinates (where the functions include Weber-Hermite functions), parabolic coordinates (Whittaker functions), and elliptic cylinder coordinates (Mathieu functions). These are not developed further in this thesis because their geometries are not useful in the problems with which we shall deal.

d. Solutions in the Presence of a Magnetic Field

In the presence of a magnetic field, $\overleftrightarrow{Dm}$ is a tensor, and equation (3-6) must be employed. In order to make a separation of the form (3-6), we are limited to cartesian coordinates or cylindrical coordinates for the problems which we shall treat. Parabolic cylinder and elliptic cylinder coordinates are also suitable, but we shall not need them for the geometries with which we shall be concerned. Further, if we consider the assumptions under which $\overleftrightarrow{D_m}$ was developed, we may immediately limit the treatment to the case where m and C are zero, since no gradients in the φ direction can exist.

In the coordinate systems selected, equation (3-6) can be reduced by separation of variables, by assuming

$$N = N_{\parallel} N_{\perp}, \tag{3-19}$$

and thus obtaining two equations

$$\frac{\nabla_\perp^2 N_\perp}{N_\perp} = -\frac{k_\perp^2}{D_{m_\perp}} = -k_\perp'^2, \tag{3-20a}$$

and

$$\frac{\nabla_{||}^2 N_{||}}{N_{||}} = -\frac{k_{||}^2}{D_{m_{||}}} = -k_{||}'^2, \tag{3-20b}$$

where

$$D_{m_{||}} k_{||}'^2 + D_{m_\perp} k_\perp'^2 = k^2 = k_\perp + V. \tag{3-20c}$$

The solution to the above equations is the same as in the absence of a field, except that equations (3-12) and (3-16d) become (for a field in the z-direction):

$$k^2 = k_\perp + V = \sum_{\ell,m,n} \left\{ D_{m_\perp} (k_\ell^2 + k_m^2) + D_{m_{||}} k_n^2 \right\}, \tag{3-12'}$$

and

$$k^2 = k_\perp + V = \sum_{\ell,n} \left\{ D_{m_\perp} k_\ell^2 + D_{m_{||}} k_n^2 \right\}. \tag{3-16d'}$$

e. Further Simplification of Previous Solutions

The equations developed so far can be simplified considerably by considering some of the restrictions upon the solutions. The requirement of a single-valuedness limits ℓ, m, and n to be integers, and it is possible to further limit them to positive values without loss of generality. Further, if the plasma possesses rotational symmetry (which it must in the presence of a magnetic field under our assumptions), then n and C_6 are both zero in the equations for N(u,v,w)

(with the exception of rectangular coordinates). The requirement that the density be non-negative everywhere within a given region will further limit the solutions. Because all the functions discussed (except the exponential function) are periodic, this latter requirement usually limits the steady-state solutions for bounded regions to the first positive segment of the applicable function, and values of k_l, k_m, and/or k_n are thus determined by the dimensions of the plasma container. From the boundary condition (2-71), the physical reason for this effect is apparent. $\vec{u} = \frac{\vec{\nabla} n}{n}$ has a definite value at the edge of the sheath. Equation (3-7) can be transformed into an equation in $\vec{u}$ in the same manner as in the derivation of equation (2-62), yielding

$$\vec{\nabla} \cdot \vec{u} + \vec{u}^2 = -k^2 \tag{3-21}$$

It is the value of k^2 in this equation that determines the "trajectory" of the vector $\vec{u}$ across the plasma to the sheath on the "opposite" side where $\vec{u}$ must again satisfy the boundary condition (2-71). Because equation (3-22) is a first order equation in $\vec{u}$, the problem is completely stated (except for a condition to determine an arbitrary normalization constant), and only one value of k^2 is possible.

Further, and obvious, simplification can be accomplished for many of the solutions stated herein if they must describe a plasma in a region in which some of the eigenfunctions are singular. In particular, the following functions have singularities for the values indicated: $N_m(0)$, $n_n(0)$, $Q_n^m(\pm 1)$, $S_{mn}^{(2)}(c, \pm 1)$, $S_{mn}^{(2)}(-ic, \pm 1)$.

2. Approximate Solutions

There are a limited number of geometries for which a stable ambipolar solution may be obtained by the separation procedure described herein. It is, however, possible to obtain an approximate solution for the particle density distribution if the geometry is not too radically different from a geometry for which an exact solution is obtainable.

In the discussion of the boundary conditions (Section II-E-3), it was shown that the conditions at the sheath edge control the density distribution in the vicinity of a surface. If there are two or more surfaces bounding the plasma in such a manner that it is not possible to obtain an exact solution for the particle density distribution, then we divide the plasma into "zones of influence" about each of these surfaces. We then calculate the density distribution for each zone as determined by the boundary conditions at the insulator surfaces belonging to that zone. In the region near such surfaces we expect our solution to be very nearly correct. There will be a transition region between the zones of influence in which we expect the greatest difference between the model and the actual plasma. In this region there is either a departure from the ambipolar diffusion or a time dependence (non-stationary plasma), or both. However, we expect that processes in this transition region do not affect the total solutions significantly in many problems. A measure of the importance

of these processes is the degree to which the solutions for the different zones conflict in the transition region. When the discontinuity across the transition region is small, we expect that our solution correctly describes the plasma in the immediate vicinity of the insulator walls and describes it approximately (within an order of magnitude) even in the transition region.

In order to discuss this approximation more quantitatively, let us consider two walls, W_1 and W_2, bounding a partly-ionized gas, and assume that the configurations are such that the model described in this thesis can be applied to each wall in the absence of the other. Thus, two distribution functions, $n_1(q_i)$ and $n_2(q_i)$, are obtained (with q_i being the coordinates). If, through adjustment of the spearation variables of equations (3-6) and (3-7) and of the normalization constants, it is possible to make

$$n_1 = n_2 \tag{3-24a}$$

and

$$\vec{\nabla} n_1 = \vec{\nabla} n_2 \tag{3-24b}$$

everywhere, then the solution is the exact solution. If this cannot be done, then we must find a surface, S, which separates the zones of influence of the walls W_1 and W_2. The separate solutions for these zones, joined at S, form the zero-order approximation of our solution.

There are three general procedures by which we might develop a criterion for determining the position of the surface S. We shall briefly discuss all three in the following paragraphs, but shall not attempt a rigorous proof.

One procedure is to employ a perturbation theory in which we define

$$n_{\pm} = n_0 + \mu n_{\pm}' + \ldots \tag{3-25}$$

and

$$\vec{E} = \vec{E}_0 + \mu \vec{E}' + \ldots \tag{3-26}$$

where μ is a parameter defined by the equation

$$n_{00} \vec{\nabla} \cdot \vec{E} = \frac{1}{\mu} (n_+ - n_-) \tag{3-27}$$

in which n_{00} is defined as the maximum density in the plasma. From equation (3-27) and Poisson's equation it is apparent that

$$\mu = \frac{\epsilon_0}{e n_{00}} \tag{3-28}$$

For our zero approximation, we impose the conditions:

$$\vec{\nabla} \cdot \vec{\Gamma}_0 - \nu n_0 = 0 \tag{3-29}$$

and

$$\vec{\Gamma}_{+0} = \vec{\Gamma}_{-0} = \vec{\Gamma}_0 \tag{3-30}$$

in each zone of influence.

In order to determine a criterion for positioning the surface between the zones of influence, S, (i.e., in order to find an adapted zero-order approximation), we must look at the first order terms. Neglecting quadratic terms in μ, we obtain

$$\Gamma_+' = \mu_+ (\vec{E}_0 n_+' + n_0 \vec{E}') - D_+ \vec{\nabla} n_+' \tag{3-31a}$$

and

$$\Gamma_-' = -\mu_- (\vec{E}_0 n_-' + n_0 \vec{E}') - D_- \vec{\nabla} n_-' \tag{3-31b}$$

If we further assume that either there is no time dependence or that the time dependence can be accounted for by replacing all quantities in the following equations by their time-averages, we obtain the following from the continuity equation:

$$\vec{\nabla}\cdot\vec{\Gamma}_{+}' + \nu n_{+}' + \frac{1}{\mu}\delta(\vec{r}-\vec{r}_S)\hat{n}\cdot(\vec{\Gamma}_{01_S} - \vec{\Gamma}_{02_S}) + \delta(\vec{r}-\vec{r}_S)(\vec{\Gamma}_{+1_S}' - \vec{\Gamma}_{+2_S}') \qquad (3\text{-}32a)$$

and

$$\vec{\nabla}\cdot\vec{\Gamma}_{-}' + \nu n_{-}' + \frac{1}{\mu}\delta(\vec{r}-\vec{r}_S)\hat{n}\cdot(\vec{\Gamma}_{01_S} - \vec{\Gamma}_{02_S}) + \delta(\vec{r}-\vec{r}_S)(\vec{\Gamma}_{-1_S}' - \vec{\Gamma}_{-2_S}') \qquad (3\text{-}32b)$$

where the subscript "S" means evaluation at the surface S, $\delta(\vec{r}-\vec{r}_S)$ is the Dirac delta function, and n is the unit normal to the surface S. The last two terms in the above equations represent particles which would have to be created or absorbed at the imaginary surface S in order to supply the currents indicated. The first order density terms can be either positive or negative. It is apparent from (3-32) that at the surface S,

$$\frac{1}{\mu}(\vec{\Gamma}_{01_S} - \vec{\Gamma}_{02_S}) = -(\vec{\Gamma}_{+1_S}' - \vec{\Gamma}_{+2_S}') = -(\vec{\Gamma}_{-1_S}' - \vec{\Gamma}_{-2_S}') \qquad (3\text{-}33a)$$

If the terms of equation (3-33) are identically zero, then the first order solution can be the trivial solution

$$n_{\pm}' = 0 \qquad (3\text{-}34)$$

Any deviation of the first order solution from equation (3-34) is obviously a function of the magnitude of the first term in equation (3-33). The surface S is thus the surface at which this term is a minimum. If there were a surface along which

$$(\vec{\overleftrightarrow{D}}_m\cdot\vec{\nabla}n_{01})\cdot\hat{n} = (\vec{\overleftrightarrow{D}}_m\cdot\vec{\nabla}n_{02})\cdot\hat{n} \qquad (3\text{-}35)$$

everywhere, subject to the condition that the density solutions were also equal at the surface, then the $\frac{1}{\mu}(\vec{\Gamma}_{01_S} - \vec{\Gamma}_{02_S})$ terms would vanish. This is not possible generally, however, and a least-mean-square procedure should be applied. Because this is not feasible for many problems, the following criterion for determining the position of S, applicable at a given point in which we are interested, is employed to obtain our adjusted zero-order approximation:

$$|\vec{D}_m \cdot \vec{\nabla} n_{01} \cos\gamma_1| = |\vec{D}_m \cdot \vec{\nabla} n_{02} \cos\gamma_2| \tag{3-36}$$

where γ_1 is the angle between $\vec{\nabla} n_{01}$ and the surface normal and γ_2 between $\vec{\nabla} n_{02}$ and the surface normal. Further, if

$$n_{01} = C_1 f_1(q_i) \tag{3-37a}$$

and

$$n_{02} = C_2 f_2(q_i) \tag{3-37b}$$

then at the surface S

$$n_{01_S} = n_{02_S} = C_1 f_1(q_i)_S = C_2 f_2(q_i)_S \tag{3-38}$$

Solving for C_2, substituting the result in equation (3-36), and dividing both sides by $C_1 f_1(q_i)_S$ yields

$$\left| \vec{D}_m \cdot \frac{\vec{\nabla} f_1(q_i)_S}{f_1(q_i)_S} \cos\gamma_1 \right| = \left| \vec{D}_m \cdot \frac{\vec{\nabla} f_2(q_i)_S}{f_2(q_i)_S} \cos\gamma_2 \right| \tag{3-39}$$

Because only order of magnitude results will be obtainable from this approximation, it is reasonable to assume as a first approximation that

$$\cos\gamma_1 \simeq \cos\gamma_2 \tag{3-40}$$

By employing equations (3-37), we obtain the following conditions defining the surface of separation

$$\left| \overleftrightarrow{D}_m \frac{\vec{\nabla} n_{01}}{n_{01}} \right| = \left| \overleftrightarrow{D}_m \cdot \frac{\vec{\nabla} n_{02}}{n_{02}} \right| \qquad (3\text{-}41)$$

The second procedure to derive equation (3-41) is to consider the relative influence of each boundary at all points within the plasma, and define the surface S as that surface at which the influences of the two boundaries are equal. Some measure of this influence must first be found. If we have in the neighborhood of a boundary a solution for the particle density which has a maximum, then certainly beyond that maximum the plasma is not influenced appreciably by that boundary. For the region between the surface and the maximum, the measure of a boundary's influence could be the current created in response to its presence. This procedure leads to equation (3-41) with an added restriction that if there are two points at which this equation is satisfied, we must select the one within the zones defined by the walls and the first maxima of their respective solutions whenever possible.

The third procedure to determine the position of the surface S would be to calculate the probability that a particle at a certain position would go to the one wall or the other. The surface S dividing the two zones would be the surface along which particles would have equal probabilities of reaching all the walls in question. This might be calculated by stochastic methods or from the diffusion equations. We did not attempt the former. The latter method is

to find the surface from which the mathematical solution indicates that as many of the particles produced within a differential volume straddling the surface would go to the one zone as to the other. This procedure also leads to equation (3-41) as the criterion.

B. Specific Solutions of the Continuity Equations.

1. General Conditions

In order to obtain an estimate of the magnitude of certain quantities in the equations to follow, we shall use the following sample data, some of which is taken from Brown [4] :

gas: Helium

$p = 1$ mm Hg.

$T = 700^{\circ}K$

$T = 50{,}000^{\circ}K \approx 4.3$ eV.

$\mu_+ \approx 10^4$ cm^2/volt-sec $= 1$ m^2/volt-sec

$\mu_- \approx 7.6 \times 10^5$ cm^2/volt-sec $= 76$ m^2/volt-sec (3-50)

$D_+ \approx \frac{kT_+}{e}\mu_+ \approx .06$ m^2/sec

$D_- \approx \frac{kT_-}{e}\mu_- \approx 340$ m^2/sec

$D_s \approx D_a = \frac{D_+\mu_- + D_-\mu_+}{\mu_+ + \mu_-} = 4.4$ m^2/sec

$\frac{D_- - D_+}{\mu_+ + \mu_-} \approx 4.4$ volts

$eV_i \approx 24.58$ eV

$eV_i + \frac{kT_-}{e} \approx 29$ eV

$E = 300$ volts/m

$n_{+o} \approx n_{-o} = n_o = 10^{12}$ cm^{-3} $= 10^{18}$m^{-3}

where "n_o" is the density in the center of the plasma or in an undisturbed, constant-density region.

For the calculations of this section we assume that the mean free paths of the ions and electrons are both sufficiently smaller than any boundary dimensions involved, so that boundary condition (2-99),

$$n_{wall} = 0,$$

is applicable. The more general boundary condition (2-71) will be employed in the discussion of cylindrical probes in the next chapter, and the method of employment of that boundary condition will be discussed then.

A quantity often quoted and employed in the literature is the diffusion length, Λ, which is defined by the equation

$$\frac{1}{\Lambda^2} = \frac{1}{\Lambda_\perp^2} + \frac{1}{\Lambda_\parallel^2} = -\frac{\nabla_\perp^2 n}{n} - \frac{\nabla_\parallel^2 n}{n} = -\frac{\nabla^2 n}{n}. \qquad (3\text{-}51)$$

We shall compute this quantity for the various geometries in this section.

Finally, we shall calculate the "zone of influence" of many of the surfaces to be discussed. This we define as that region in which the particle density is less than 50% or less than 90% (as indicated) of the density at the center or undisturbed region of the plasma.

2. Plane and Rectangular Configurations

a. Rectangular cavity

Because it is the most complex geometry we can treat in rectangular coordinates, we begin with a discussion of a rectangular cavity of dimensions x_o, y_o, and z_o. The limitations of the development of the diffusion tensor prevent the application of the following solutions to magnetic fields, and thus the scalar coefficient D_s will be used. Of the possible variations of the solution (such as equations (3-11) and (3-13)), we can immediately rule out those containing the exponentials because of the requirement of zero density at the walls. The boundary conditions also limit the solution to the first positive segments of the sine functions (and exclude the

cosine functions) if the origin is taken at one corner of the cavity. If the origin were selected at the center of the cavity, the cosine functions would be used and the sine functions excluded. With the origin at one corner, and the sides along the positive coordinate axes, we obtain the following solution for the steady state ($k_t = 0$) plasma;

$$n(x,y,z) = n_0 \sin\left(\frac{\pi}{x_0}x\right) \sin\left(\frac{\pi}{y_0}y\right) \sin\left(\frac{\pi}{z_0}z\right) \qquad (3\text{-}52)$$

with the diffusion length given by

$$\frac{1}{\Lambda^2} = -\frac{\nabla^2 n}{n} = \frac{\nu}{D_s} = \left(\frac{\pi}{x}\right)^2 + \left(\frac{\pi}{y_0}\right)^2 + \left(\frac{\pi}{z_0}\right)^2 \qquad (3\text{-}52a)$$

The three components of the particle current density at any point are easily obtained, using equations (2-42)

$$\Gamma_x = -n_0 D_s \frac{\pi}{x_0} \cos\left(\frac{\pi}{x_0}x\right) \sin\left(\frac{\pi}{y_0}y\right) \sin\left(\frac{\pi}{z_0}z\right) \qquad (3\text{-}53)$$

with similar equations for the other components. From these equations it is seen that the particle current density is zero at the center of the cavity, is directed outward from the center to the walls, and is a maximum at the walls where, for the data of (3-50) and a 5 centimeter wall-to-wall separation, the magnitude of the current density at the center of a wall would be approximately 2.7×10^{16} particles/cm^2-sec. It is of interest to note that the steady-state particle current densities at the walls decrease in inverse proportion to a linear increase in cavity dimensions. This decrease is a consequence of the decrease in the gradient of the current density. From equation (3-52a) one can see that the rate of ionization, ν, necessary to replace the particle losses to the walls is inversely proportional to the square of the dimensions (and, incidentally, is primarily determined by the smallest dimension of

the cavity as a consequence). The explanation for the inverse dependence of the rate of ionization per unit volume is easily seen by equating the number of particles destroyed at the walls to the total number created within the cavity. The latter is proportional to the volume and to ν. The number of particles carried to the walls however, is proportional to the surface of the walls and to the current density. The latter is inversely proportional to the linear dimension, as previously mentioned, and consequently the number of particles drawn off is proportional only to the first power of the linear dimension of the cavity. Consequently, the inverse dependent of on the linear dimensions is expected. The fact that the number of particles destroyed at the walls is directly proportional to the linear dimensions of the cavity (and therefore, so are the energy losses) is also worth noting.

The space charge field, according to equation (2-38) is

$$\vec{E}_s = -\left(\frac{D_- - D_+}{\mu_+ + \mu_-}\right)\left[\frac{\pi}{x_0}\cot\left(\frac{\pi}{x_0}x\right)\hat{\imath} + \frac{\pi}{y_0}\cot\left(\frac{\pi}{y_0}y\right)\hat{\jmath} + \frac{\pi}{z_0}\cot\left(\frac{\pi}{z_0}z\right)\hat{k}\right], \qquad (3\text{-}54)$$

or, again using the data from (3-50), is approximately -270 volts/m (directed away from the center of the cavity) at the point ($.25x_0$, $.5y_0$, $.5z_0$). The cavity dimensions are assumed to be 5cm. Again, an inverse relationship to the wall-to-wall separation exists. The space charge potential (equation (2-41)) is

$$V = \frac{D_- - D_+}{\mu_+ + \mu_-}\ln\left\{\sin\left(\frac{\pi}{x_0}x\right)\sin\left(\frac{\pi}{y_0}y\right)\sin\left(\frac{\pi}{z_0}z\right)\right\}, \qquad (3\text{-}54a)$$

or approximately -1.53 volts at the point ($.25x_0$, $.5y_0$, $.5z_0$) for a5 cm. cavity. The potential is with respect to the center of the cavity. The potential predicted by equation (3-54) becomes singular

at the walls, and this feature of the solution indicates a limitation of these equations: they are not applicable beyond the sheath edge.

Using the current equations (3-53) we can compute the energy lost at the walls. From equation (2-101) we obtain

$$E_{wall} = 2n_o D_s\left(eV_i + \frac{kT_-}{e}\right)\left\{\frac{\pi}{z_o}\int_0^{x_o}\int_0^{y_o} \sin\left(\frac{\pi}{x_o}x\right)\sin\left(\frac{\pi}{y_o}y\right)dx\,dy + \right.$$
$$\left. + \frac{\pi}{y_o}\int_0^{x_o}\int_0^{z_o} \sin\left(\frac{\pi}{x_o}x\right)\sin\left(\frac{\pi}{z_o}z\right)dx\,dz + \frac{\pi}{x_o}\int_0^{y_o}\int_0^{z_o} \sin\left(\frac{\pi}{y_o}y\right)\sin\left(\frac{\pi}{z_o}z\right)dy\,dz\right\}, \quad (3\text{-}55)$$

where the factor 2 takes into account the surfaces adjoining the corner opposite the origin. This equation reduces to

$$E_{wall} = \frac{8n_o D_s\left(eV_i + \frac{kT_-}{e}\right)}{\pi}\left[\frac{y_o z_o}{x_o} + \frac{x_o z_o}{y_o} + \frac{x_o y_o}{z_o}\right]$$
$$= \frac{8n_o D_s\left(eV_i + \frac{kT_-}{e}\right)}{\pi}\left[\frac{y_o^2 z_o^2 + x_o^2 z_o^2 + x_o^2 y_o^2}{x_o y_o z_o}\right]. \quad (3\text{-}55a)$$

The heat liberated per unit area is obtained by dividing each integral in (3-55) by the appropriate area, obtaining for the three sides of the cavity:

$$\frac{E_{wall}}{\text{unit area}} = \frac{4n_o D_s\left(eV_i + \frac{kT_-}{e}\right)}{\pi x_o}, \quad \frac{4n_o D_s\left(eV_i + \frac{kT_-}{e}\right)}{\pi y_o}, \quad \frac{4n_o D_s\left(eV_i + \frac{kT_-}{e}\right)}{\pi z_o}, \quad (3\text{-}55b)$$

Again using 5 cm. dimensions and the data from (3-50), we see that E_{wall} is approximately 4.86×10^{19} eV/sec $\simeq 7.8$ joules/sec. From equation (3-55a) it is seen again that the total heat lost per secnd is proportional to the linear dimensions, and that doubling the length of all the sides, for instance, will double the rate of heat loss.

One very important fact about plasma characteristics may be seen from the preceeding equations, and in particular from equation (3-52a). That is that the effect of a small dimension on the characteristics is very much greater than that of large dimensions, so that a long, narrow plasma has, in the middle region of the longer dimension,

characteristics that are almost completely dependent on the shorter dimension and are relatively independent of the longer dimension. Thus, a plasma whose z-dimension is very much greater than its dimensions in other directions can often be treated quite properly as "infinite" in the z-direction, with corresponding simplifications of the equations describing the plasma.

The zones of influence of the rectangular surfaces are indicated in Figure 3-1.

If ionization ceases, $\nu = 0$, and the plasma decays exponentially in accordance with equation (3-5), with k_t given by (3-7a), (3-12), and (3-52a) as

$$k_t = \left(\frac{\pi}{x_0}\right)^2 + \left(\frac{\pi}{y_0}\right)^2 + \left(\frac{\pi}{z_0}\right)^2, \tag{3-56}$$

Thus the plasma will decay to 1/e of its initial value in time.

$$\tau = \frac{1}{D_s\left[\left(\frac{\pi}{x_0}\right)^2 + \left(\frac{\pi}{y_0}\right)^2 + \left(\frac{\pi}{z_0}\right)^2\right]} \text{ sec}, \tag{3-57}$$

which, for a cavity of 5 cm dimensions, is about 20 μsec. This decay time is inversely proportional to the square of the linear dimensions.

If the initial distribution is not the steady-state distribution, but instead some function $f(x,y,z)$, then the coefficients of equation (3-11) must be obtained in the normal manner for a Fourier series, and a series of the form (3-10) must be developed. For example, if the initial distribution is a constant density n_0 throughout (except discontinuously zero at the surfaces), the particle distribution function will be

$$n(x,y,z,t) = \sum_{l,m,n=0}^{\infty} \left\{ \left[\frac{1}{2l+1}\sin\frac{(2l+1)\pi x}{x_0}\right]\left[\frac{1}{2m+1}\sin\frac{(2m+1)\pi y}{y_0}\right]\left[\frac{1}{2n+1}\sin\frac{2n+1\,\pi z}{z_0}\right] e^{-(k_t)_{lmn} D_s t} \right\} \tag{3-58}$$

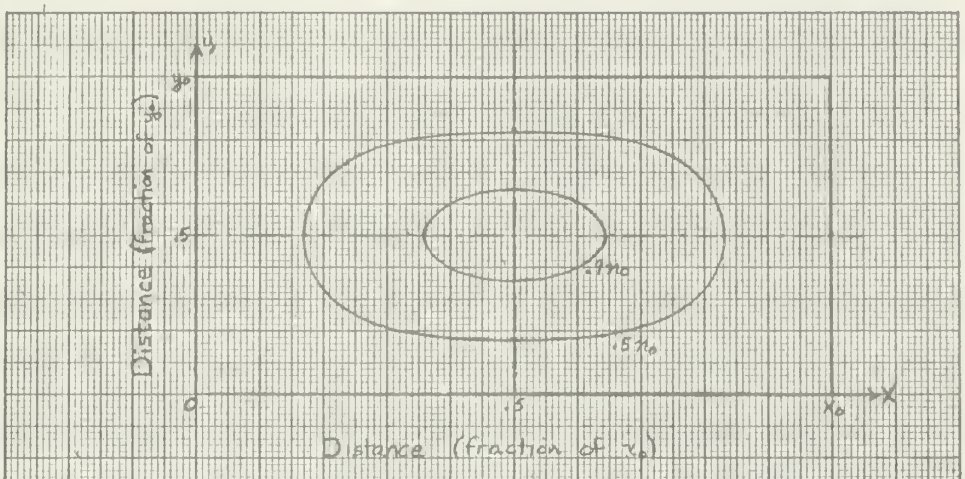

Figure 3-1 Zones of Influence for Rectangular Cavity
Cross-section through center of cavity

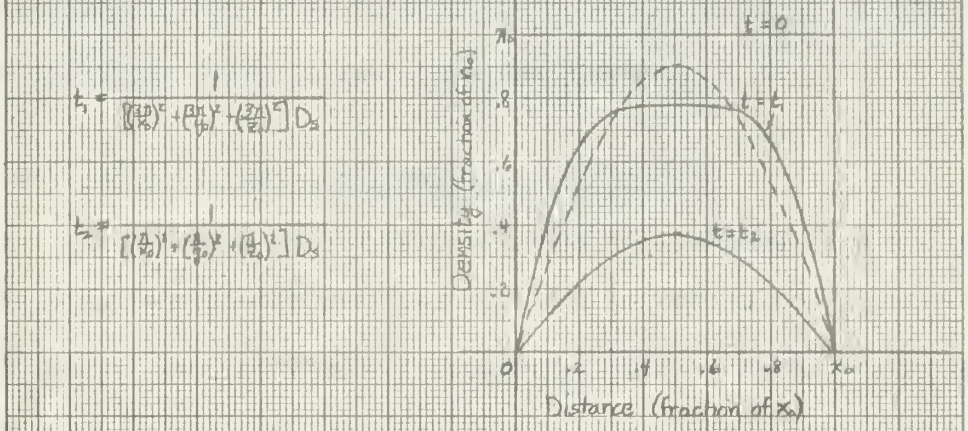

Figure 3-2 Decaying Plasma in Rectangular Cavity
Density along axis through center of cavity and parallel to the x-axis. (Dotted curve is Bessel distribution corresponding to time $t=\tau_a$)

with

$$(k_t)_{lmn} = \left[\frac{2l+1\,\pi}{x_0}\right]^2 + \left[\frac{(2m+1)\pi}{y_0}\right]^2 + \left[\frac{(2n+1)\pi}{z_0}\right]^2 . \qquad (3\text{-}58a)$$

It is to be noted that the higher order terms decay at a faster rate, so that the plasma approaches the steady-state distribution as it decays. Figure 3-2 shows the decay of such a plasma at three different times. Other features of this solution are that the rate of decay is inversely proportional to the square of the linear dimensions so that a plasma in a large cavity decays more slowly than one in a small one. Further, we again see that the shortest dimensions control the decay rate, so that dimensions which are very much larger than the smallest dimension may again be treated as infinite. For instance, for a length which is ten times that of the others, the error in ignoring it in equation (3-57) is less than one percent.

b. Infinite tube, rectangular cross-section

By allowing z_0 to go to infinity and setting $z = z_0/2$ in the equations of the previous section, we obtain the equations for an infinitely long rectangular geometry. Thus we have for the steady state

$$n(x,y) = n_0 \sin\left(\frac{\pi}{x_0}x\right)\sin\left(\frac{\pi}{y_0}y\right), \qquad (3\text{-}59)$$

with

$$\frac{1}{\Lambda^2} = k^2 = \frac{\nu}{D_s} = \left(\frac{\pi}{x_0}\right)^2 + \left(\frac{\pi}{y_0}\right)^2 . \qquad (3\text{-}59a)$$

The current density, potential and other equations are similarly obtained and will not be stated here.

c. Infinite Plane.

By again allowing one dimension to become infinite, for example, y_o, and by replacing y by $y_o/2$, we obtain the equations for the simplest geometry, two parallel planes separated by a distance x_o, or a single plane in contact with an infinite plasma in which

$$x_o = \pi\sqrt{\frac{Dm_\perp}{\nu}}, \tag{3-60}$$

where we know the rate of ionization from other considerations, or where $x_o/2$ is the distanceto the undisturbed region of the plasma. The restriction that there be no magnetic field can now be dropped if the only density gradient is along the coordinate lines perpendicular to the planes and if the field is parallel to these planes. If the field is perpendicular to the plane (so that it does not affect diffusion perpendicular to the plane), or if there is no field, then $Dm_\perp$ in equation (3-60) and in the equations to follow can be replaced by its no-field limit, Ds.

The particle density distribution for the steady state is

$$n = n_o \sin\left(\frac{\pi}{x_o}x\right), \tag{3-61}$$

with

$$\frac{1}{\Lambda^2} = k^2 = \frac{\nu}{Dm_\perp} = \left(\frac{\pi}{x_o}\right)^2. \tag{3-61a}$$

The other equations are derived from those describing the rectangular cavity by replacing y and z by $y_o/2$ and $z_o/2$ respectively, by letting y_o and z_o become infinite, and by replacing Ds by $Dm_\perp$.

3. Cylindrical Configurations

a. Finite Cylinder, interior

For a cylinder of radius R and length z_o, we can immediately simplify Equation (3-16) for the steady state by considering the

functions and the boundary conditions. The Neumann functions are singular at the origin, and so their coefficients, $C_{3\ell n}$, must be zero. Further, if the origin is taken at the center of the base of the cylinder, the coefficients of the cosine functions, C_{7n}, must be zero also, because the density is zero at $z = 0$ (using boundary condition (2-99)). Then, as in the case of the rectangular configurations, the requirements that n always be positive (or zero) and the boundary condition at $z = z_0$ requires us to set all the sine coefficients to zero except $C_{6\ell}$, and k_ℓ becomes $\frac{\pi}{z_0}$. Because we have discussed no forces which would tend to establish an assymetric angular distribution, and indeed in the case of the derivation of the diffusion tensor in a magnetic field have specified that no such assymetry exist, we set $m = 0$. Thus we are limited to the zero order Bessel function, and because of the boundary conditions must select the first positive segment of that function. Thus we obtain the well-known distribution function

$$n(r,z) = n_0 J_0\left(\frac{2.4}{R} r\right) \cos\left(\frac{\pi}{z_0} z\right), \tag{3-62}$$

where

$$\frac{1}{\Lambda^2} = \frac{1}{\Lambda_\perp^2} + \frac{1}{\Lambda_{11}^2} = \left(\frac{2.4}{R}\right)^2 + \left(\frac{\pi}{z_0}\right)^2, \tag{3-62a}$$

and

$$\nu = \left(\frac{2.4}{R}\right)^2 D_{m_\perp} + \left(\frac{\pi}{z_0}\right)^2 D_{m_{11}}. \tag{3-62b}$$

The magnetic field, if any, is parallel to the cylinder axis.

The ion current density components are obtained by using Equation (2-42):

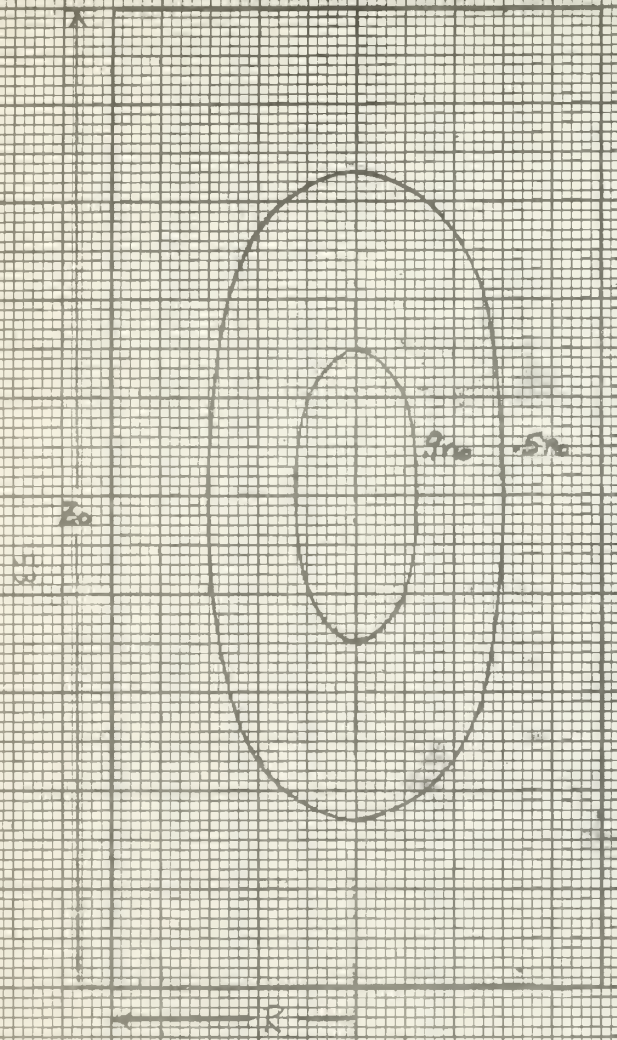

Figure 3-3 Cylinder Zones of Influence

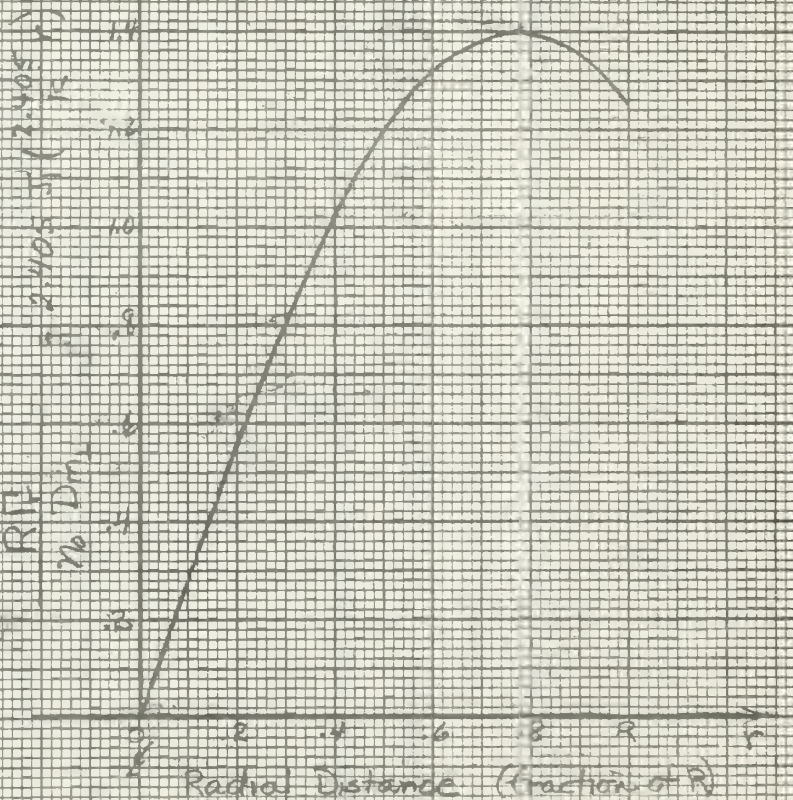

Figure 3-4 Radial Current Density vs Radial Distance from Center (Cylinder)

(3-63)

Thus, at the center of the cylinder ($r = 0$, $z = \frac{1}{2} z_0$), the current density is zero, and within the remainder of the cylinder Γ_r' and Γ_z' are both directed from the center to the walls. Γ_z' is a maximum at the ends of the cylinder, but Γ_r' reaches a maximum (see Figure 3-4) when

$$\frac{2.4}{R} r = 1.2$$

i.e., at $r = 0.75R$. This maximum occurs at a radius less than R because the additional current supplied by ionization beyond $r = 0.75R$ is not sufficient to counteract the effect of the increasing cylindrical volume into which the current is flowing. As for the rectangular cavity, an increase in cylinder size is accompanied by a decrease in ionization rate and current densities in the steady state.

The space charge field, as obtained from (2-35) and (2-36) is:

$$E_r = E_\perp = -\frac{(1+\mu^2 B^2) D_{m_\perp} - D_-}{\mu_-} \frac{2.4}{R} \frac{J_1\left(\frac{2.4}{R} r\right)}{J_0\left(\frac{2.4}{R} r\right)}$$

$$E_z = E_\parallel = \frac{D_{m_\parallel} - D_-}{\mu_-} \frac{\pi}{z_0} \cos\left(\frac{\pi}{z_0} z\right). \qquad (3\text{-}64)$$

The zones of influence of the cylinder surface are indicated in Figure 3-3.

One of the characteristics of this plasma which is of interest is the fact that the shape of the steady state configuration of ion density is dependent only upon the cylinder dimensions if the strength of the magnetic field is less than that at which the "pinch" effect

begins to appear. However, the ion current density in the radial direction (perpendicular to the field) is proportional to the inverse square of the magnetic field (at high B) through its dependence on $Dm_{\perp}$.

If the steady state plasma begins to decay, the distribution is given by the equation:

$$n(r,z,t) = n_0 \sin\left(\frac{\pi}{z_0} z\right) J_0\left(\frac{2.4}{R} r\right) e^{-\left[\left(\frac{\pi}{z_0}\right)^2 Dm_{\parallel} + \left(\frac{2.4}{R}\right)^2 Dm_{\perp}\right] t} \qquad (3\text{-}65)$$

If, however, a decaying plasma with initial distribution $F(r, \varphi, z)$ is to be described, it is necessary to develop a series from Equation (3-16) in the same manner as used to develop a Fourier series, obtaining equations similar to (3-58).

b. Infinite Cylinder, interior

In a manner similar to that of the rectangular problem it is possible to treat a very long cylinder as if it were effectively of infinite length. Employing identical procedures, we obtain for the particle density distribution function of a "long" cylinder of radius R:

$$n(r) = n_0 J_0\left(\frac{2.4}{R} r\right), \qquad (3\text{-}66)$$

where

$$\frac{1}{\Lambda^2} = \left(\frac{2.4}{R}\right)^2 \quad \text{and} \quad \nu = \left(\frac{2.4}{R}\right)^2 Dm_{\perp}. \qquad (3\text{-}66a)$$

The particle current density is given by

$$\Gamma_r = + \frac{2.4}{R} Dm_{\perp} n_0 J_1\left(\frac{2.4}{R} r\right), \quad \Gamma_{\varphi} = \Gamma_z = 0, \qquad (3\text{-}67)$$

the field by

$$E_r = \frac{\left[(1 - \mu_-^2 B^2)\right] Dm_{\perp} - D_-}{\mu_-} \frac{2.4}{R} \frac{J_1\left(\frac{2.4}{R} r\right)}{J_0\left(\frac{2.4}{R} r\right)}, \quad E_{\varphi} = E_z = 0, \qquad (3\text{-}68)$$

the space charge potential by

$$V = \frac{D_- - (1-\mu_-^2 B^2) D m_\perp}{\mu_-} \ln\left[J_0\left(\frac{2.4}{R} r\right)\right] \tag{3-69}$$

and the heat liberated at the walls per unit cylinder length by

$$\begin{aligned} E_{wall}/_{unit\ length} &= 2\pi R\left(eV_i + \frac{kT_-}{e}\right) n_0 \frac{2.4}{R} \cdot J_1(2.4)\, D m_\perp \\ &\simeq 7.85\, n_0 D m_\perp \left(eV_i + \frac{kT_-}{e}\right) \end{aligned} \tag{3-70}$$

It should be noted that the latter is independent of the cylinder dimensions, and using the data of (3-50), is approximately 1.32×10^{19} B^{-2} eV/m-sec = 2.11 B^{-2} joule/m-sec (with B in webers/m^2).

The decay problem is treated in the same manner as for the finite cylinder, and we obtain for decay from the steady state

$$n(r,t) = n_0 J_0\left(\frac{2.4}{R}\right) e^{-\left(\frac{2.4}{R}\right)^2 D m_\perp t} \tag{3-71}$$

Figure 3-4 is a plot of the radial current density as a function of radial position for a steady plasma. Figure 3-5 is a graph of the space charge potential versus radial position for an infinite cylinder. The fact that the space charge field and potential become infinite at the wall is a consequence of the assumption that $n_{wall} = 0$. As in the rectangular case, these equations are not valid within the sheath.

c. Infinite Cylinder in Infinite Plasma

Using our techniques, there is no exact steady-state solution to the continuity equation (3-1) or (3-2) for a plasma exterior to a cylinder of finite length because we cannot combine the solutions (3-16) in a manner such as to meet the boundary conditions at the ends of the cylinder. However, for the infinite cylinder of radius R it is possible to solve for the distribution function. Again we limit ourselves to those problems in which no assymetric forces are acting

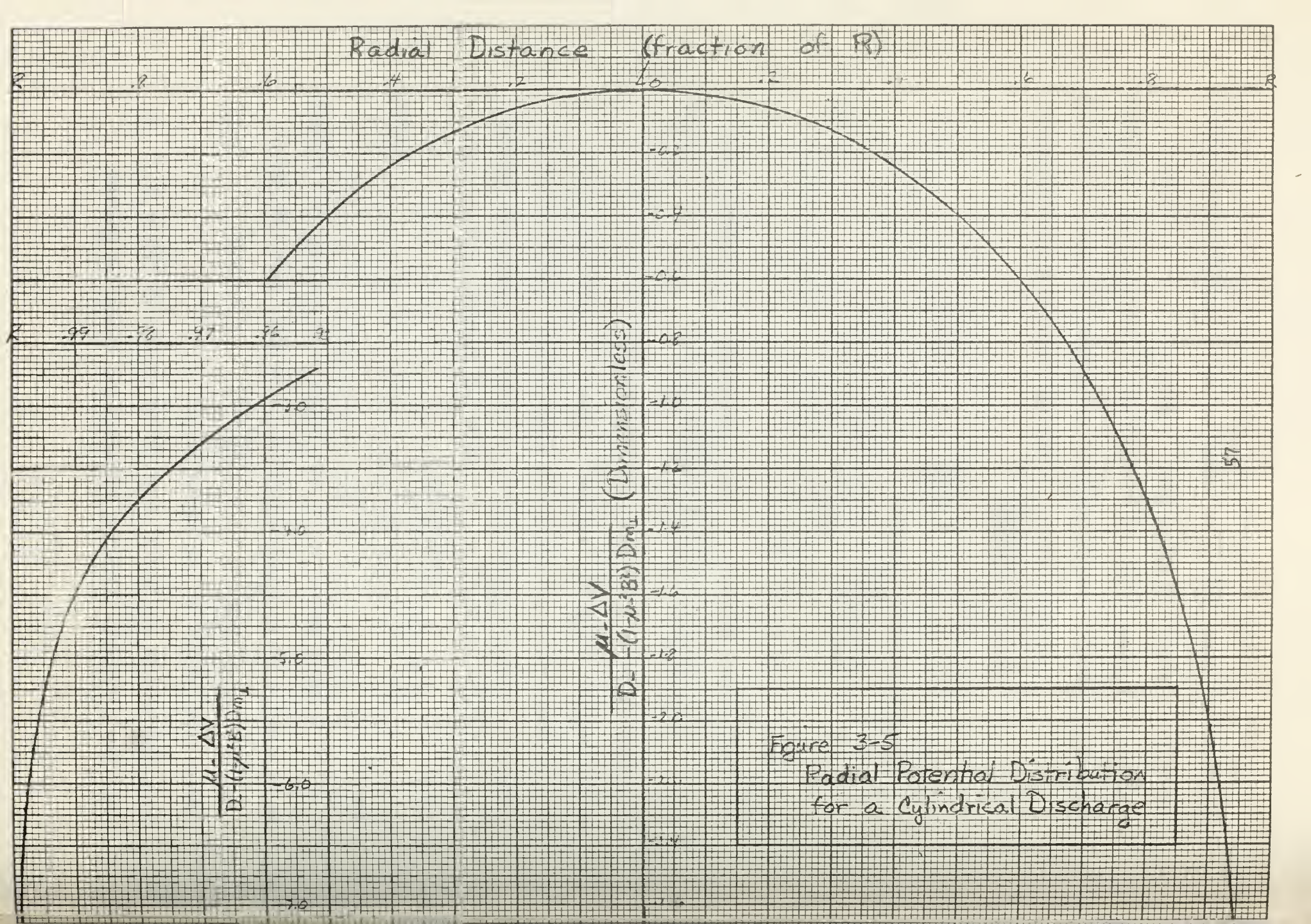

Figure 3-5
Radial Potential Distribution
for a Cylindrical Discharge

(and thus to axially symmetric plasmas), but retain the Neumann functions because the origin is no longer within the limits of r. We obtain from (3-16), for the steady state,

$$n(r) = A\left\{J_0\left(\sqrt{\frac{\nu}{D_{m_\perp}}}\,r\right) + C N_0\left(\sqrt{\frac{\nu}{D_{m_\perp}}}\,r\right)\right\} \qquad R \le r \le R' \tag{3-72}$$

where A is a normalization constant which we shall determine later, R is the cylinder radius, R' is that radius at which n(r) is a maximum, and

$$C = -\frac{J_0\left(\sqrt{\frac{\nu}{D_{m_\perp}}}\,R\right)}{N_0\left(\sqrt{\frac{\nu}{D_{m_\perp}}}\,R\right)} \tag{3-72a}$$

if the boundary condition (2-99) ($n_{wall} = 0$) applies, and is a more complicated function if equation (2-71) applies. The latter function will be developed in the section on probe theory. R'' the radius at which equation (3-72) is a maximum, is found by setting the first derivative to zero; i.e., it is the solution of

$$J_1\left(\sqrt{\frac{\nu}{D_{m_\perp}}}\,R''\right) = C N_1\left(\sqrt{\frac{\nu}{D_{m_\perp}}}\,R''\right) \tag{3-72b}$$

The normalization constant, A, can be determined if the density $n(r_1)$ at a radius r_1 is known. Then

$$A = \frac{n(r_1)}{\left\{J_0\left(\sqrt{\frac{\nu}{D_{m_\perp}}}\,r_1\right) + C N_0\left(\sqrt{\frac{\nu}{D_{m_\perp}}}\,r_1\right)\right\}} . \tag{3-72c}$$

The radial current density is

$$\Gamma_r = D_{m_\perp} A \sqrt{\frac{\nu}{D_{m_\perp}}}\left\{J_1\left(\sqrt{\frac{\nu}{D_{m_\perp}}}\,r\right) + C N_1\left(\sqrt{\frac{\nu}{D_{m_\perp}}}\,r\right)\right\} \tag{3-73}$$

d. Coaxial Cylinders

The equations of the previous section also describe the particle and current density relations which exist between the surfaces of coaxial cylinders of infinite length with inner radius R and outer radius R' . Because of the boundary conditions, ν is no longer an independent variable, but is an eigenvalue in the steady state plasma.

Using the boundary condition of zero density at the walls, the value of $\sqrt{\frac{\nu}{D_{m_\perp}}}$ is seen from equation (3-72) to be that value for which

$$J_0\left(\sqrt{\frac{\nu}{D_{m_\perp}}}R'\right) + CN_0\left(\sqrt{\frac{\nu}{D_{m_\perp}}}R'\right) = 0 \qquad (3\text{-}74)$$

4. Spherical Geometries

Distribution functions for decaying plasmas with arbitrary initial distributions and for steady-state plasmas in spherical geometries can be obtained by series development of equations (3-17). Equations for the spherically symmetric plasma in the steady state (with ionization occuring) are very similar to (3-66) and (3-72) with spherical Bessel functions (equation (3-17c)) replacing the cylindrical Bessel functions in equations describing spherical geometries corresponding to the cylindrical geometries treated. In addition, it is of interest to describe the steady state solution for a steady or very slowly decaying plasma in which there is no ionization occuring, and in which a sphere has been placed. We treat the latter problem first.

a. Sphere in Homogeneous Plasma-no ionization occuring

If we have a spherically symmetric infinite plasma with an undisturbed particle density, n_0, in which $\nu = \frac{\partial n}{\partial t} = 0$, with neither magnetic nor electric fields imposed, we have from equations (3-17)(with $k_\ell = m = 0$) the following density distribution around a sphere of radius R

$$n(r) = n_0 - \frac{n_0 R}{r} \qquad r \geq R \qquad (3\text{-}75)$$

We have employed the boundary conditions that n(r) be zero at the sphere and equal n_o at large distances. The zones of influence for such a sphere are

$$\begin{aligned} 50\% &- r \leq 2R \\ 90\% &- r \leq 10R , \end{aligned} \tag{3-76}$$

and the radial current density is

$$\Gamma_r = - \frac{D_s n_o R}{r^2} . \tag{3-77}$$

This current density is a maximum (of magnitude $\frac{n_o D_s}{R}$) at the surface of the sphere and approaches zero as $1/r^2$ at large r. The current is directed toward the sphere and represents a flow of particles from a source at infinity to a sink at the sphere.

The heat liberated at the surface of the sphere is

$$E_{sphere} = \frac{4}{3}\pi R^2 n_o D_s \left(eV_i + \frac{kT_-}{e}\right). \tag{3-78}$$

It is proportional to the square of the radius of the sphere.

Using the equations thus stated, it should be possible to calculate the particle density distribution which a small spherical surface in a large, slowly-decaying plasma would establish about itself.

b. Spherical Shell-internal plasma

From equations (3-17) it is also possible to obtain easily the steady state relations for a plasma bounded by a sphere of radius R centered within a spherical shell of radius R'. We shall again assume spherical symmetry, thus limiting ourselves to the spherical Bessel functions of zero order. By employing the following relations for these functions

$$\begin{aligned} j_o(kr) &= \frac{\sin(kr)}{kr} \\ n_o(kr) &= -\frac{\cos(kr)}{kr} , \end{aligned} \tag{3-79}$$

and doing some manipulating, we obtain

$$n(r) = C_1 r^{-1} \sin\left[\frac{\pi(r-R)}{R'-r}\right] \qquad R' \geq r \geq R, \tag{3-80}$$

where

$$\frac{\nu}{D_s} = \frac{1}{\Lambda^2} = \left(\frac{\pi}{R'-R}\right)^2, \tag{3-80a}$$

and for which derivation the condition of vanishing density at the surfaces was employed. C_1 is an arbitrary normalization constant which can be determined if the density is known at some radius r_1 within the plasma.

Then,

$$n_1 = C_1 r_1^{-1} \sin\left[\frac{\pi(r_1-R)}{R'-R}\right], \tag{3-80b}$$

and

$$C_1 = n_1 r_1 \csc\left[\frac{\pi(r-R)}{R'-R}\right]. \tag{3-80c}$$

The radius of maximum density, R'', can be found by setting the first derivative of (3-80) to zero, which yields the following equation for R''

$$\frac{\pi}{R''-R} \cos\left[\frac{\pi(R''-R)}{(R'-R)}\right] = \frac{1}{R''} \sin\left[\frac{\pi(R''-R)}{(R'-R)}\right]. \tag{3-81}$$

For a sphere within an infinite plasma in which ionization is occuring, this is the radius at which the effect of the spherical surface becomes zero.

The current density within this plasma is

$$\Gamma_r = -n_1 r_1 D_s \csc\left[\frac{\pi(r_1-R)}{R'-R}\right] \times$$
$$\times \left\{\frac{\pi}{r(R'-R)} \cos\left[\frac{\pi(r-R)}{R'-R}\right] - \frac{1}{r^2} \sin\left[\frac{\pi(r-R)}{R'-R}\right]\right. \tag{3-82}$$

It is to be noted that it has two components. The first is directed toward both surfaces from a radius within the plasma, and the second

is directed radially outward from the center, but is zero at both surfaces.

For a spherical shell of radius R' with no internal sphere, one obtains

$$n(r) = \frac{n_0 R'}{\pi r} \sin\left(\frac{\pi r}{R'}\right), \tag{3-83}$$

with

$$\frac{1}{\Lambda^2} = \frac{\nu}{D_s} = \frac{\pi}{R'} \tag{3-83a}$$

This equation was obtained from equation (3-80) by setting R = 0, and by evaluation of C_1 by L'Hospital's rule

$$\lim_{r\to 0} \frac{C_1 \sin\left(\frac{\pi r}{R'}\right)}{r} = \lim_{r\to 0} \frac{C_1 \frac{\pi}{R'} \cos\left(\frac{\pi r}{R'}\right)}{1} = C_1 \frac{\pi}{R'} = n_0 \tag{3-83b}$$

where n_0 is the density at the center. Figure 3-6 is a graph of this function.

5. Prolate Spheroidal Geometries (the wire or probe)

The influence of a prolate ellipsoid upon a plasma is now considered (see Appendix I for transformation equations and figure). In its limit, when the minor axis is small and the major axis approaches the length d, the effects of such a body can be used as an approximation of the effects of a finite wire or narrow probe of length d.

Flammer [6] shows that the wave equation

$$(\nabla^2 + k^2)\, N = 0, \tag{3-84}$$

equation (3-7), expands in prolate spheroidal coordinates to:

$$\left[\frac{\partial}{\partial\eta}(1-\eta^2)\frac{\partial}{\partial\eta} + \frac{\partial}{\partial\xi}(\xi^2-1)\frac{\partial}{\partial\xi} + \frac{\xi^2-\eta^2}{(\xi^2-1)(1-\eta^2)}\frac{\partial^2}{\partial\varphi^2} + c^2(\xi^2-\eta^2)\right] N = 0, \tag{3-85}$$

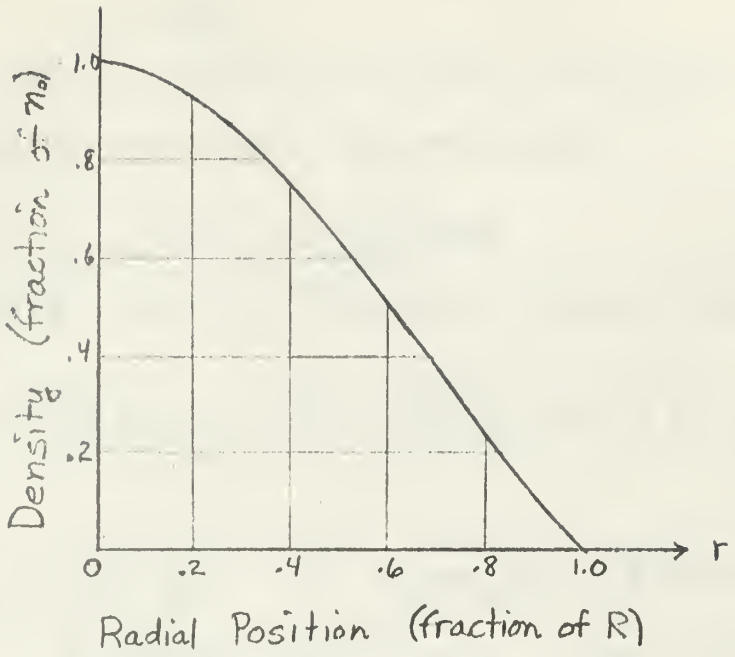

Figure 3-6 Radial Density Distribution for Hollow Sphere

in which we have set

$$c = \tfrac{1}{2} k d, \tag{3-85a}$$

and that, by the method of separation of variables, solutions to (3-85) may be obtained in the form of the Lamé products

$$N_{mn} = S_{mn}(c,\eta)\, R_{mn}(c,\xi) \begin{Bmatrix} \cos \\ \sin \end{Bmatrix} (m\varphi) \tag{3-86}$$

The functions $S_{mn}(c,\eta)$ and $R_{mn}(c,\xi)$ satisfy the ordinary differential

$$\frac{d}{d\eta}\left[(1-\eta^2)\frac{d}{d\eta} S_{mn}(c,\eta)\right] + \left[\lambda_{mn} - c^2\eta^2 - \frac{m^2}{1-\eta^2}\right] S_{mn}(c,\eta) = 0 \tag{3-86a}$$

$$\frac{d}{d\xi}\left[(\xi^2-1)\frac{d}{d\xi} R_{mn}(c,\xi)\right] - \left[\lambda_{mn} - c^2\xi^2 + \frac{m^2}{\xi^2-1}\right] R_{mn}(c,\xi) = 0 \tag{3-86b}$$

in which the separation constants λ_{mn} and m are the same in both equations. It is a combination of such functions (of the first and second kinds) that is given in Equation (3-18) as the general solution to (3-84)

a. Prolate Ellipsoid in stationary infinite plasma

Before proceeding further with the prolate wave functions, one special case, analogous to that of the sphere in the infinite stationary plasma, should be treated. By imposing the boundary condition that at large ξ the density, n, of a stationary, non-ionizing plasma be independent of φ and η (so that $\frac{\partial n}{\partial \eta} = 0$ and $\frac{\partial^2 n}{\partial \varphi^2} = 0$), we can reduce equation (3-85) to

$$\frac{d}{d\xi}\left[(\xi^2-1)\frac{dn}{d\xi}\right] = 0 \tag{3-87}$$

which integrates to:

$$n = n_0\left[1 - \frac{\coth^{-1}(\xi)}{\coth^{-1}(\xi_0)}\right] \qquad 1 < \xi_0 \le \xi < \infty \tag{3-88}$$

where n_o is the uniform density at infinity, and the density at the surface ξ_o is zero. The current density is then:

$$\Gamma_\xi = \frac{n_o D_s}{\coth^{-1}(\xi_o)(\xi^2-1)} \tag{3-89}$$

To investigate the properties of this solution, we shall use the identity

$$\coth^{-1}(\xi) = \tfrac{1}{2}\ln(\xi+1) - \tfrac{1}{2}\ln(\xi-1) \tag{3-90}$$

by which Equation (3-88) becomes:

$$n = n_o\left[1 - \frac{\frac{1}{2}\ln(\xi+1) - \frac{1}{2}\ln(\xi-1)}{\frac{1}{2}\ln(\xi_o+1) - \frac{1}{2}\ln(\xi_o-1)}\right] \tag{3-91}$$

at very large distances (i.e., $\xi >> 1$), $\ln(\xi + 1) - \ln(\xi - 1) \approx \frac{2}{\xi}$ and equation (3-91) can be expanded to

$$n \approx n_o\left(1 - \frac{\xi_o}{\xi}\right) \tag{3-92}$$

which is identical to equation (3-75) for spherical geometry, a result which reflects the fact that the surface "looks like" a sphere at large distances. In the vicinity of the surface, i.e., for $\xi \approx \xi_o$, we let

$$\xi = \xi_o + \epsilon \tag{3-93}$$

(with ϵ such that the mean free path, λ, is much less than ϵ), and expand, obtaining

$$n = n_o\left[1 - \frac{\ln(\xi_o+\epsilon+1) - \ln(\xi_o+\epsilon-1)}{\ln(\xi_o+1) - \ln(\xi_o-1)}\right] \tag{3-94a}$$

$$= n_0\left[1 - \frac{\ln(\xi_0+1) + \ln\left(1+\frac{\epsilon}{\xi_0+1}\right) - \ln(\xi_0-1) - \ln\left(1+\frac{\epsilon}{\xi_0-1}\right)}{\ln(\xi_0+1) - \ln(\xi_0-1)}\right], \tag{3-94b}$$

$$= n_0\left[\frac{\ln\left(1+\frac{\epsilon}{\xi_0+1}\right) - \ln\left(1+\frac{\epsilon}{\xi_0-1}\right)}{\ln(\xi_0+1) - \ln(\xi_0-1)}\right]. \tag{3-94c}$$

By neglecting second order terms in ϵ and using the expansion

$$\ln(x+1) = x + \frac{x^2}{2} + \cdots, \tag{3-95}$$

equation (3-94c) can be reduced to

$$n \approx -n_0\left[\frac{\frac{\epsilon}{\xi_0+1} - \frac{\epsilon}{\xi_0-1}}{\ln\frac{\xi_0+1}{\xi_0-1}}\right] = n_0\left[\frac{2\epsilon}{(\xi_0^2-1)\ln\frac{\xi_0+1}{\xi_0-1}}\right]. \tag{3-96}$$

Thus, for the density at the surface, $\epsilon = 0$ and therefore $n = 0$. Equation (3-96) shows that the density is a linear function of the distance from the surface for short distances.

At large distances, the current density can be seen from Equation (3-92) to be an inverse square function of distance (as it is for a sphere):

$$\Gamma_\xi = -D_s\nabla n = -D_s\sqrt{\frac{\xi^2-1}{\xi^2-\eta^2}}\left(\frac{n_0\xi_0}{\xi^2}\right) \approx -\frac{n_0 D_s \xi_0}{\xi^2} \tag{3-97}$$

At short distances, we obtain from (3-96)

$$\Gamma_\xi = -D_s\sqrt{\frac{\xi^2-1}{\xi^2-\eta^2}}\,\frac{2}{(\xi_0^2-1)\ln\frac{\xi_0+1}{\xi_0-1}} \tag{3-98}$$

which is a minimum at the center of the surface ($\eta = 0$) and approaches infinity at the ends ($\eta = \pm 1$). This occurs because the area at the ends is zero, and thus any current flowing towards them constitutes

an 'infinite' current density.

The current density at the surface is found from (3-98) to be

$$\Gamma_{\xi_0} = \frac{-2 n_0 D_s}{\sqrt{(\xi_0^2 - 1)(\xi_0^2 - \eta^2)}\ \ln \frac{\xi_0 + 1}{\xi_0 - 1}} \tag{3-99}$$

which again becomes infinite at the ends and is a minimum at the center. We can obtain an estimate of the heating at the surface per unit length if we approximate the ellipsoid with a cylinder of radius $r = (\xi_0^2 - 1)^{\frac{1}{2}}$ and approximate the current density with that at the center ($\eta = 0$).

$$E_{\text{surface/unit length}} \approx \frac{4\pi n_0 \left(e V_i + \frac{kT_-}{c}\right)}{\xi_0 \ln \frac{\xi_0 + 1}{\xi_0 - 1}} \tag{3-100}$$

To find the behavior at small radii, we let $\xi_0 = 1 + \epsilon_0$ obtaining:

$$E_{\text{surface/unit length}} \approx \frac{4\pi n_0 \left(e V_i + \frac{kT_-}{c}\right)}{(1+\epsilon_0)\left[\ln(2+\epsilon_0) - \ln(\epsilon_0)\right]} \tag{3-101}$$

$$\approx \frac{-4\pi n_0 \left(e V_i + \frac{kT_-}{c}\right)}{\ln \epsilon_0}$$

which approaches zero as ϵ_0 approaches zero.

b. Prolate Spheroid in steady state plasma - ionization occuring

Given an infinite plasma of homogeneous density n_0 at large distances and a prolate spheroid whose surface is the surface ξ_0, one can simplify equation (3-18) considerably by consideration of boundary conditions. First, the requirement that the wave function be finite at $\eta = \pm 1$ confines the solution to angle functions of the first kind since the angle functions of the second kind are singular at these points. If we look for those solutions for which the density, n, is uniform at large distances for all φ, then N is a function of η and ξ alone, and $m = 0$. Further, the prolate angle functions

reduce to the associated Legendre functions when c vanishes; i.e., as the spheroidal insulator becomes spherical in shape. Therefore, we can determine the subscript "n" in Equation (3-18) by studying the Legendre function, $P_n^0(\eta)$ because our solution must satisfy the limiting case of a hemispherical body. Only $P_0^0(\eta)$ is positive for all η in the range $-1 \leq \eta < 1$. Because n must be positive for all η, the subscript must be 0. Consequently, we obtain for the density distribution

$$n = n_o S_{oo}^{(1)}(c,\eta)\left[R_{oo}^{(1)}(c,\xi) + B R_{oo}^{(2)}(c,\xi)\right], \tag{3-102}$$

where

$$C = \frac{kd}{2} = \frac{d}{2}\sqrt{\frac{\nu}{D_s}}. \tag{3-102a}$$

If we employ boundary condition (2-99) ($n_{wall} = 0$),

$$B = -\frac{R_{oo}^{(1)}(c,\xi_o)}{R_{oo}^{(2)}(c,\xi_o)} \tag{3-102b}$$

It must be remarked that this solution does not satisfy the requirement that the density be independent of η at large distances. However, for small values of c, and therefore for either very small or for nearly spherical bodies the η dependence is negligible. The deviation is only 1% for c = 0.5, but increases to practically 95% for c = 5.0.

c. Prolate spheroid and infinite wall

Let us consider a semi-infinite plasma of uniform density n_o at large distances, bounded only by a single infinite plane which, in prolate spheroidal coordinates, is $\eta = 0$. Further, consider an insulator (probe) whose surface is defined by $\xi = \xi_o$ projecting into the plasma as indicated in Figure (3-7). The solution to the continuity

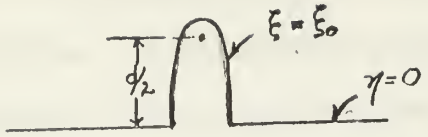

Figure 3-7 Prolate Spheroid and Infinite Wall

equation is developed in the same manner as in the previous section, except that in this instance the appropriate Legendre function is $P_1^0(\eta)$ because it has the property of being positive for all values of in the range 0 to +1 and further of being zero at $\eta = 0$. Thus the density is

$$n = n_o S_{01}^{(1)}(c,\eta)\left[R_{01}^{(1)}(c,\xi) + B R_{01}^{(2)}(c,\xi)\right], \tag{3-103}$$

where, again,

$$C = \frac{kd}{2} = \frac{d}{2}\sqrt{\frac{\nu}{D_s}}, \tag{3-103a}$$

and if $n_{wall} = 0$,

$$B = -\frac{R_{01}^{(1)}(c,\xi_o)}{R_{01}^{(2)}(c,\xi_o)} \tag{3-103b}$$

The field and potential equations along the axis of the probe (i.e., for $\eta = 1$) are:

$$(E_\xi)_{\eta=1} = \frac{2}{d}\frac{D_+ - D_-}{\mu_+ + \mu_-}\frac{\left[R_{01}^{(1)'}(c,\xi) + B R_{01}^{(2)'}(c,\xi)\right]}{\left[R_{01}^{(1)}(c,\xi) + B R_{01}^{(2)}(c,\xi)\right]} \tag{3-104}$$

where the prime indicates the first derivative, and

$$(V_{12})_{\eta=1} = \frac{2}{d}\frac{D_+ - D_-}{\mu_+ + \mu_-}\ln\frac{n_2}{n_1} \tag{3-105}$$

$$= \frac{2}{d}\frac{D_+ - D_-}{\mu_+ + \mu_-}\ln\left\{\frac{R_{01}^{(1)}(c,\xi_2) + B R_{01}^{(2)}(c,\xi_2)}{R_{01}^{(1)}(c,\xi_1) + B R_{01}^{(1)}(c,\xi_1)}\right\}$$

6. Oblate Spheroidal Geometries (circular lamina)

In general, the solutions to the continuity equation in oblate spheroidal coordinates are the same as for the prolate with -ic replacing c and $+i\xi$ replacing ξ in the equations. Consequently these will not be further discussed, except for the problem of the circular lamina in an infinite, stationary, non-ionizing plasma.

a. Lamina in stationary plasma

To study the influence in an infinite plasma of a circular lamina, the effect of an oblate ellipsoid is first discussed and then the limit as the semi-minor axis approaches zero.

Proceeding as for the prolate case, by imposing the condition that at large ξ the plasma density be independent of ψ and η, and by substituting $+i\xi$ for ξ we obtain from equation (3-85)

$$\frac{d}{d\xi}\left[(1+\xi^2)\frac{d\eta}{d\xi}\right] = 0. \tag{3-106}$$

Integrating twice, we obtain

$$\eta = C_1 \tan^{-1}(\xi) + C_2. \tag{3-107}$$

Letting $\lim_{\xi\to\infty} \eta = \eta_0$, we get

$$\eta_0 = C_1 \tan^{-1}(\infty) + C_2 = 1.571\, C_1 + C_2 \tag{3-108}$$

Using as the boundary condition

$$\eta(\xi_0) = 0 = C_1 \tan^{-1}(\xi_0) + C_2 \tag{3-109}$$

and subtracting this from equation (3-108) yields

$$C_1 = \frac{\eta_0}{1.571 - \tan^{-1}(\xi_0)}. \tag{3-110}$$

$$\therefore \quad C_2 = -\frac{\eta_0 \tan^{-1}(\xi_0)}{1.571 - \tan^{-1}(\xi_0)} \tag{3-111}$$

so that, for an oblate ellipsoid in an infinite plasma,

$$\eta = \eta_0 \left\{ \frac{\tan^{-1}(\xi) - \tan^{-1}(\xi_0)}{1.571 - \tan^{-1}(\xi_0)} \right\} \tag{3-112}$$

When the semi-minor axis is zero, $\xi_o = 0$, and the figure is a circular lamina of radius $r_o = c$. Equation (3-125) becomes

$$n = \frac{n_o \tan^{-1}(\xi)}{1.571} \tag{3-113}$$

The zone of influence of this lamina, within which $n \leq \frac{1}{2} n_o$, is given by

$$\tan^{-1}(\xi) \geq \frac{1.571}{2} = 0.785, \tag{3-114}$$

i.e., $$\xi = 1, \tag{3-114a}$$

which is an oblate ellipsoid with semi-major axes $r = \sqrt{2}\, r_o$ and semi-minor axis $z = r_o$.

The current density in this plasma (with $c \approx r_o$) will be:

$$\Gamma_\xi = -D_s n_o \frac{1}{c}\sqrt{\frac{1+\xi^2}{\xi^2+\eta^2}}\frac{dn}{d\xi} = -\frac{D_a n_o}{1.5\, n\, r_o \sqrt{(\xi^2+\eta^2)(\xi^2+1)}} \tag{3-115}$$

This current density is a maximum at the surface of the lamina, decreases as $\frac{1}{\xi^2}$ to zero towards infinity, and because the area of the "side" of the lamina is zero, is infinite at the sides ($\eta = 0$) of the "surface". If we assume the current density at the center of the surface to be an approximation to the surface current density across the entire surface, then the recombination energy liberated per unit surface will be approximately

$$E_{surface} \approx \frac{\pi D_a n_o r_o}{1.571}\left(eV_i + \frac{kT_-}{e}\right) \tag{3-116}$$

which, as for the sphere, is proportional to the radius.

IV

APPROXIMATE SOLUTIONS FOR INSULATED PROBES

When an insulated probe is inserted into a dense plasma--that is, a plasma in which the mean free path is equal to or less than the probe dimensions--Langmuir's probe theory [8] may not be applicable. Particle losses at the probe surfaces may cause appreciable effects on the particle density distribution, and hence on the probe potential. Under these conditions, α of equation (2-71) can be appreciably large and consequently so may the effect of the insulator on the steady-state distribution. The approximation described in Section III-A-2 has been employed to calculate this effect for a floating probe in a partially ionized gas. Two different geometries are considered. The first is a prolate ellipsoid inserted radially into a cylindrical discharge, with the sensing element on its tip. The other is a cylindrical probe aligned parallel to the discharge axis. For the latter, we are able to account for the effects of a longitudinal magnetic field.

A. The Prolate Probe

We do not have an exact solution of the continuity equation (2-55) for a cylindrical or ellipsoidal probe projecting from a cylinder wall into a plasma. However, we have seen that there is a solution for the density distribution in a long, narrow plasma (equation (3-66). In the absence of a magnetic field, it is

$$n = n_0 J_0\left(\sqrt{\frac{\nu}{D_s}}\, r\right), \tag{4-1}$$

in which

$$\sqrt{\frac{\nu}{D_s}} = \frac{2.405}{R}. \tag{4-1a}$$

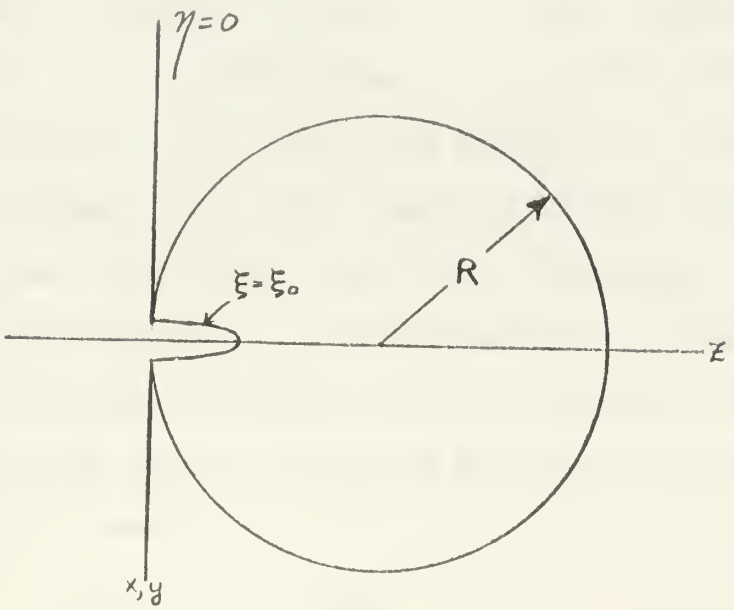

Figure 4-1 Prolate Probe in Cylindrical Discharge

Further, we have obtained a solution for a prolate spheroid attached to an infinite wall (equation (3-102))

$$\eta = \eta_0' \, S_{01}^{(1)}(c,\eta)\left[R_{01}^{(1)}(c,\xi) + B\, R_{01}^{(2)}(c,\xi)\right] \qquad (4\text{-}2)$$

Based on the assumptions outlined in Section III-A-2, we shall approximate the effect of a narrow cylindrical or prolate ellipsoidal probe by joining the two models described above as indicated in Figure 4-1. The infinite wall is tangent to the cylinder, and the z-axis of the probe ($\eta = 1$) lies along the diameter of the cylinder. We assume that the presence of the probe does not significantly alter the ionization or diffusion rates, so that equation (3-103a) becomes

$$C = \frac{d}{2}\sqrt{\frac{\nu}{D_s}} \approx \frac{2.4\ell}{R} \qquad (4\text{-}2a)$$

where $\frac{d}{2} \approx \ell$, the length of the probe (if the minor axis is much shorter than the major axis) and R is the radius of the cylinder. No effort will be made to describe the density throughout the cylinder. We shall merely attempt to predict the density distribution along the $\eta = 1$ axis of the probe (i.e., along the diameter of the cylinder). It is this density distribution which is responsible for the potential distribution sampled by a sensing element at the tip of the probe. In accordance with the procedure outlined in Section III-A-2, we readily obtain the following condition for determining the position along this axis of the dividing surface between the two models

$$\left|\frac{\vec{\nabla} n}{n}\right|_{\text{Probe}} = \left|\frac{\vec{\nabla} n}{n}\right|_{\text{Cylinder}} \qquad (4\text{-}3)$$

Equation (4-3) was solved graphically because sufficient published data on the derivatives of the spheroidal wave functions was not available.

Because of this paucity of information on the spheroidal wave functions, it was also necessary to limit the study of this problem to the limiting case where λ is so small that the boundary condition (2-99) ($n_{wall} = 0$) may be employed. For this problem, B of equation (4-2) is readily obtained:

$$B = - \frac{R_{01}^{(1)}(c, \xi_o)}{R_{01}^{(2)}(c, \xi_o)} \qquad (4-4)$$

The normalization constant, n_o', of equation (4-2) was determined in relation to n_o of equation (4-1) by the graphical solution of equation (4-3).

A study of the solutions, and of the physical properties of our model, reveals that this model can be justified as an approximation to the particle distribution in the vicinity of the probe for probe penetrations varying from zero to about half the cylinder diameter. For short probe lengths, particle losses to the adjacent regions of the infinite wall (which, for the short probe, is a reasonable approximation of the adjacent cylinder wall) is the predominant factor in establishing the particle distribution in the vicinity of the probe. For instance, for a probe length of 0.2R, the parameter c of equations (4-2) is 0.48. From Figure II-1 (Appendix II) we see that the prolate angle function $S_{01}^{(1)}$ is very nearly that for c = 0, which corresponds to zero probe penetration. Consequently, the effect of the short probe is very slight in comparison to the effect of the wall, as we expect from consideration of the surface which would be the cause of most of the particle losses from the region around the probe. However, for deeper penetration, the angle function changes appreciably, indicating that the surface of the probe exerts a more

dominant influence. Again, this is expected since particles in the vicinity of the tip of the probe are more likely to diffuse to some portion of the probe than to succeed in reaching the wall. Thus, even though the infinite wall is no longer a good approximation of the cylinder wall for the deeper penetration, the increased probe surface losses justify using the resulting particle density distribution functions to describe the plasma near the end of the probe. When the probe penetrates more than half-way through the plasma, the influence of the opposite walls of the cylinder on the particle distribution near the end of the probe become increasingly more important, and our model breaks down.

Conversion from prolate coordinates to probe dimensions is accomplished with the following equations.

probe length: $$\ell = \frac{d}{2}\xi_0 \approx \frac{d}{2} \qquad (4\text{-}5)$$

probe radius (= semi-minor axis): $$r_p = \frac{d}{2}\sqrt{\xi_0^2-1} = \frac{\ell}{\xi_0}\sqrt{\xi_0^2-1} \approx \ell\sqrt{\xi_0^2-1} \qquad (4\text{-}6)$$

$\xi = \xi_0$ is the equation of the probe surface.

Flammer [6] was the source of the information on the spheroidal wave functions. Data not calculated or graphed in this reference is presented in Appendix II.

The graphs on the following pages were computed using the procedures outlined in this section and subsidiary equations developed in preceeding sections.

Figure 4-2 is a graph of density versus distance for probes of several radii but equal depths of penetration. Note that the magnitude of the dependence of the probe influence on the probe radius is

relatively small, an order of magnitude change in probe radius causing an increase in the region of influence of only 50%.

Figure 4-3 is a graph of the density distribution for various depths of penetration of a probe of radius $r_p = 0.02R$ (which, for a 2.5 cm discharge, corresponds to a 0.5 mm probe).

Figure 4-4 shows "effective probe length" vs. true probe length for the 0.02R probe. The effective length is based on the intersection of the two models, and is approximately the point of the original particle distribution that the probe samples. The curve marked $\lambda >> 2r_p$ is the effective probe length when the probe does not disturb the plasma, and corresponds to the true probe length. The broken segment of the curve is an estimate for that region in which this model breaks down, as outlined above.

Figure 4-5 is a graph of the potential disturbance associated with various depths of probe penetration. This potential disturbance is defined as the potential drop between the point the plasma samples (the effective probe length) and the sheath edge. A sheath depth of 0.01R was assumed for this calculation. These potentials can be used with the effective length data to analyze experimental results or to predict them from the theory.

Figure 4-6 represents such a potential prediction. It is the prediction of the potential measured by such a probe assuming that it actually measures a difference between the potential at the maximum density region of the plasma (zero potential) and the potential at the sheath edge at the tip of the probe.

A very significant prediction of the above theory is that the use of an insulated probe in a plasma of short mean free path will cause

a definite asymmetry even in an originally symmetric plasma. Although these results are not applicable directly to a plasma in the presence of a magnetic field, some of this effect is still expected.

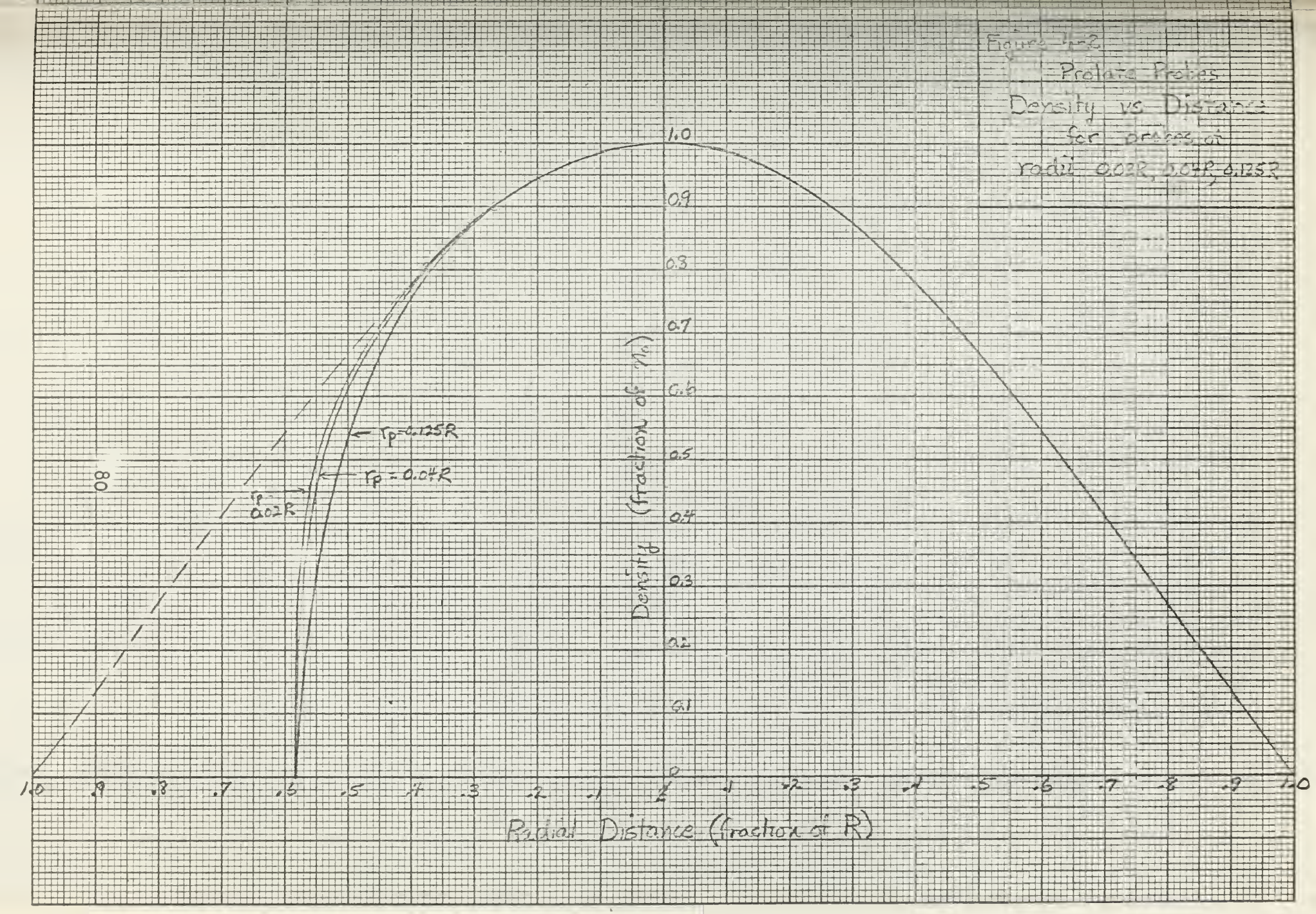
Figure 1-2
Prolate Probes
Density vs Distance
for probes of
radii 0.02R, 0.04R, 0.125R
1.0
0.9
0.8
0.7
0.6
0.5
0.4
0.3
0.2
0.1
0
Density (fraction of n_0)
r_p=0.125R
r_p = 0.04R
r_p 0.02R
1.0 .9 .8 .7 .6 .5 .4 .3 .2 .1 0 .1 .2 .3 .4 .5 .6 .7 .8 .9 1.0
Radial Distance (fraction of R)

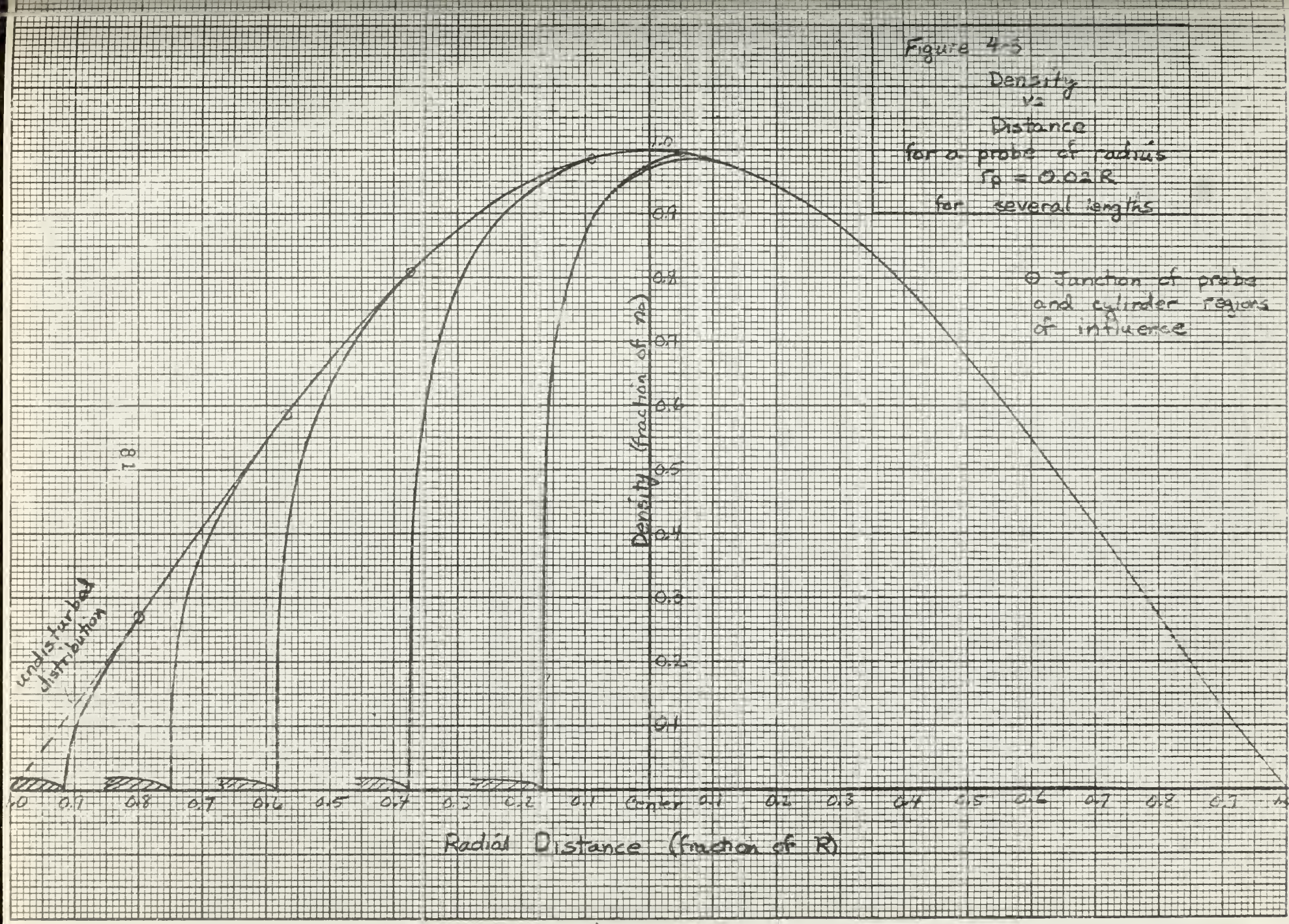
Figure 4-5
Density
vs
Distance
for a probe of radius
$r_p = 0.02 R$
for several lengths
⊖ Junction of probe and cylinder regions of influence
1.0
0.9
0.8
0.7
0.6
0.5
0.4
0.3
0.2
0.1
Density (fraction of n_0)
undisturbed distribution
1.0 0.9 0.8 0.7 0.6 0.5 0.4 0.3 0.2 0.1 Center 0.1 0.2 0.3 0.4 0.5 0.6 0.7 0.8 0.9 1.0
Radial Distance (fraction of R)

Figure 4-4
Effective Probe Length
vs
True Probe Length

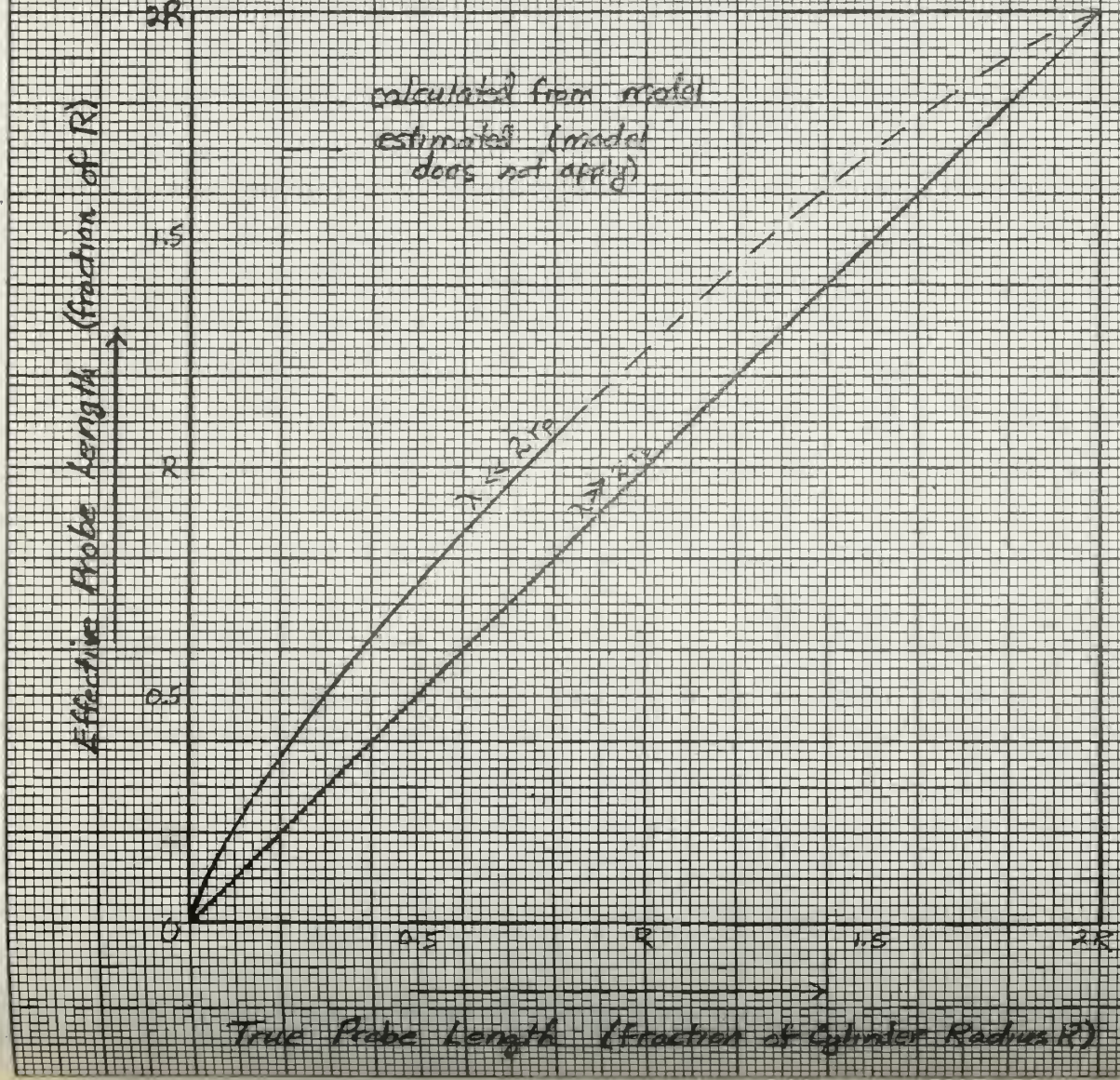

Figure 4-5
Potential Drop to Probe Sheath Edge
vs
Effective Probe Length

Sheath Thickness
≈ 0.01R

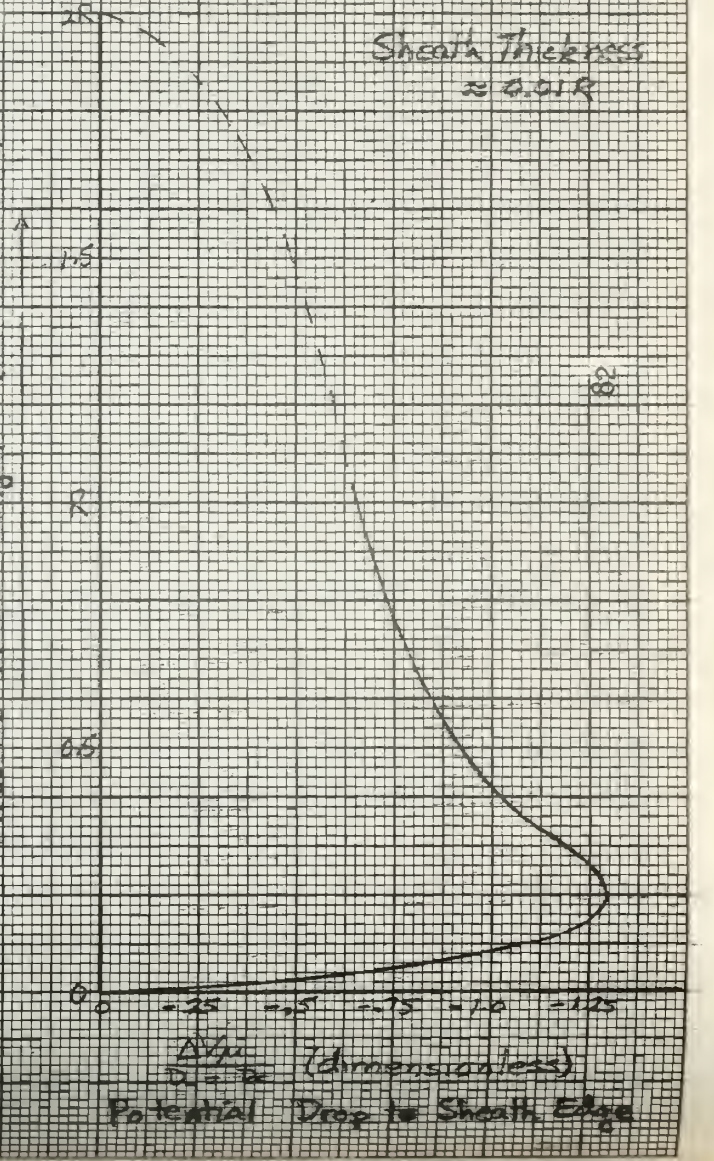

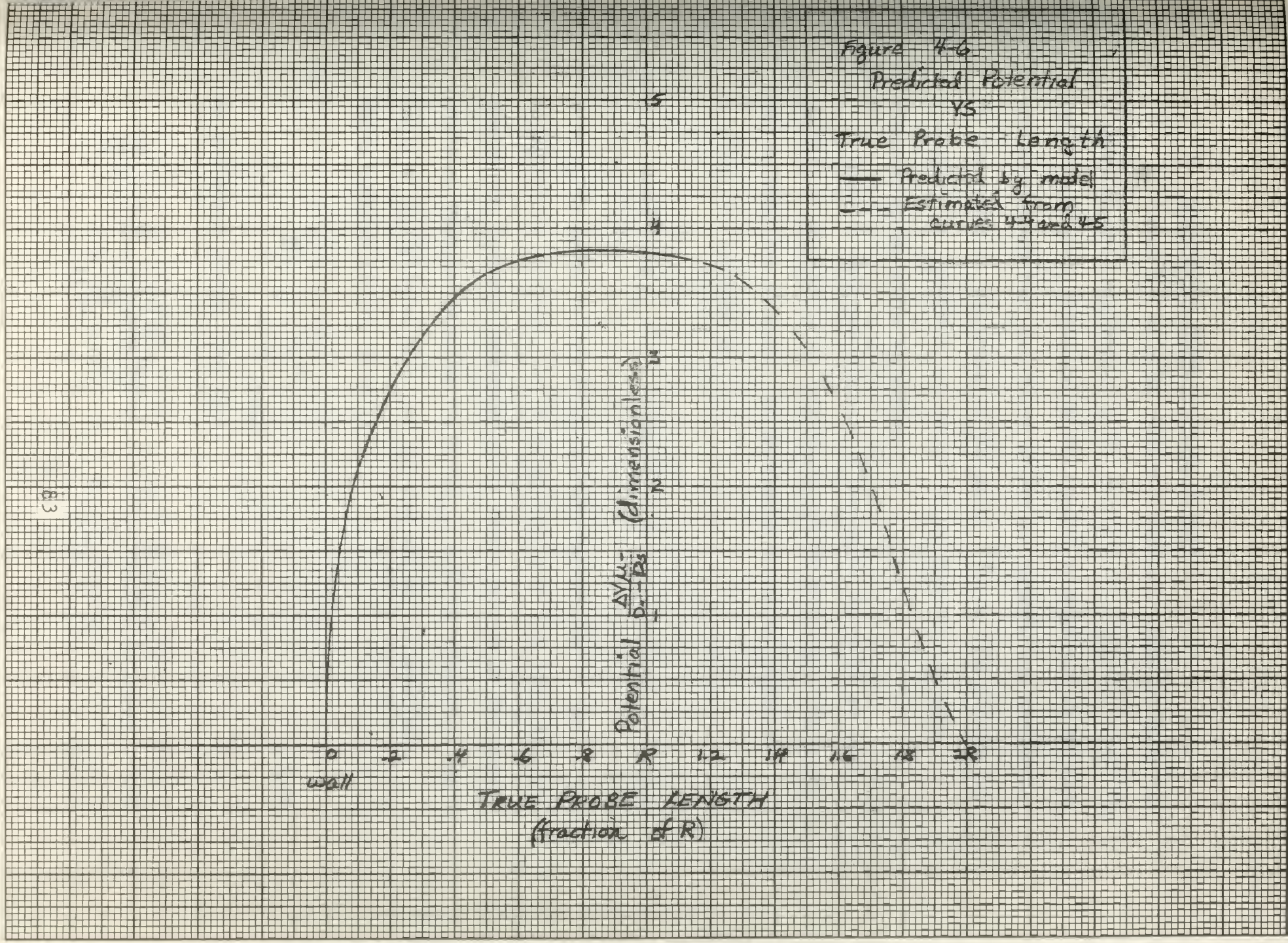
Figure 4-6
Predicted Potential
vs
True Probe Length
Predicted by model
Estimated from curves 4-4 and 4-5
5
4
3
2
1
Potential ΔV/U∞ D_1 (dimensionless)
0
.2
.4
.6
.8
R
1.2
1.4
1.6
1.8
2R
wall
TRUE PROBE LENGTH
(fraction of R)

B. Cylindrical Probe Parallel to Axis

Figure 4-7 is a top view of a possible insulated probe configuration for measurements in the presence of a magnetic field. The cylindrical probe (enlarged in the figure) is supported at its ends and long enough that the effect of the end supports are negligible in the region at the center of the probe. The sensing element (or elements) are located at the center of the probe on the common diameter of the probe and plasma.

There is only one alignment of the probe for which an exact solution of the continuity equation (2-57) is possible: when probe and cylinder are co-axial. As previously developed (equation (3-72)), the solution is

$$n = n'\left\{ J_0\left(\sqrt{\frac{\nu}{D_{m_\perp}}}\, r\right) + C N_0\left(\sqrt{\frac{\nu}{D_{m_\perp}}}\, r\right)\right\} \qquad r_p \le r \le R \qquad (4\text{-}7)$$

with r_p the probe radius, R the cylinder radius, and n' the normalization constant. If λ is not very much less than the probe dimensions, boundary condition (2-71) should be used at the probe surface. However, equation (2-99) ($n_{wall} = 0$) is often still applicable at the cylinder wall, and was used for our calculations. Using equation (2-71), which is

$$\frac{\alpha}{\lambda} = \frac{\nabla_n n}{n}\bigg|_{sheath} \qquad (4\text{-}8)$$

at the sheath yields, from (4-1)

$$\frac{\alpha}{\lambda} = \frac{-\sqrt{\frac{\nu}{D_{m_\perp}}}\left\{ J_1\left[\sqrt{\frac{\nu}{D_{m_\perp}}}(r_p+\lambda)\right] + C N_1\left[\sqrt{\frac{\nu}{D_{m_\perp}}}(r_p+\lambda)\right]\right\}}{J_0\left[\sqrt{\frac{\nu}{D_{m_\perp}}}(r_p+\lambda)\right] + C N_0\left[\sqrt{\frac{\nu}{D_{m_\perp}}}(r_p+\lambda)\right]} \qquad (4\text{-}9)$$

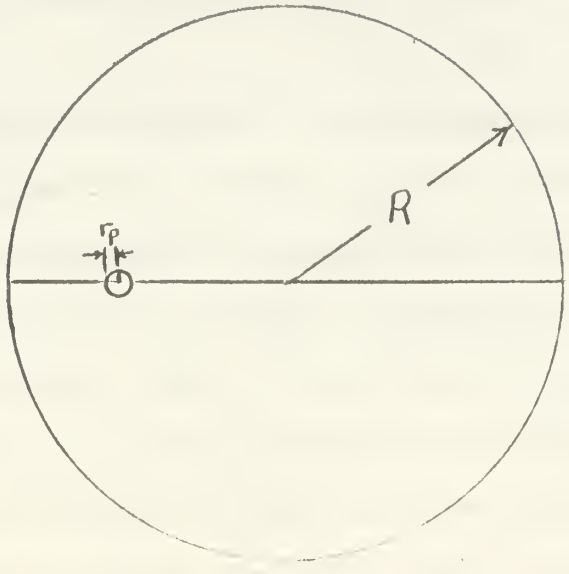

Figure 4-7 Cylindrical Probe Parallel to Cylinder Axis (top view)

from which we obtain

$$C = -\frac{\frac{\alpha}{\lambda} J_0\left[\sqrt{\frac{\nu}{D_{m_\perp}}}(r_p+\lambda)\right] + \sqrt{\frac{\nu}{D_{m_\perp}}} J_1\left[\sqrt{\frac{\nu}{D_{m_\perp}}}(r_p+\lambda)\right]}{\frac{\alpha}{\lambda} N_0\left[\sqrt{\frac{\nu}{D_{m_\perp}}}(r_p+\lambda)\right] + \sqrt{\frac{\nu}{D_{m_\perp}}} N_1\left[\sqrt{\frac{\nu}{D_{m_\perp}}}(r_p+\lambda)\right]} \qquad (4\text{-}10)$$

Next, employing equation (2-99) at the outer cylinder, we obtain

$$J_0\left(\sqrt{\frac{\nu}{D_{m_\perp}}} R\right) = C N_0\left(\sqrt{\frac{\nu}{D_{m_\perp}}} R\right) \qquad (4\text{-}11)$$

Equations (4-10) and (4-11) are sufficient to determine both C and $\sqrt{\nu/D_{m_\perp}}$ and they are most easily solved by successive approximation.

Table 4-1 lists the results for these parameters for various α between zero and one, using the following probe dimensions and mean free path:

$$r_p = 0.02R$$

$$\lambda = 0.02R \qquad (4\text{-}12)$$

(again this corresponds to a 0.5 mm probe in a 2.5 cm cylinder). Even when there is no recombination at the probe ($\alpha = 0$), the rate of ionization for the steady state must be greater than when the probe is not present because the probe still occupies a finite volume in the cylinder.

When the probe is off-axis, it is necessary to employ the approximation described in Section III-A-2. Equation (4-3) is still applicable for determining the separation of the zones along the common diameter (the only location in which we will be interested). In order to evaluate $\sqrt{\nu/D_{m_\perp}}$ in the vicinity of the probe for various probe positions, we interpolate between the calculated value when the probe is coaxial and the value it would have when the probe is at the cylinder wall (and has negligible effect on the eigenvalue because of the low density there). This latter value we assume to be the

familiar 2.405/R. Assuming that this parameter would depend on the density of the plasma in the position in which it is placed, we obtain the following relationship

$$\sqrt{\frac{\nu}{D_{m_\perp}}} = \frac{1}{R}\left[2.405 + \Delta y \ \frac{n(r)}{n(r_o)}\right] \qquad (4\text{-}13)$$

where

$$\Delta y = R\left(\sqrt{\frac{\nu}{D_{m_\perp}}}\right)_{coaxial} - 2.405 \qquad (4\text{-}13a)$$

From the values thus calculated, a mean was calculated for each α (see Table 4-1), and this value was used in the computations of the density distribution in the vicinity of the probe. The use of a more precise value is not justified by the nature of the approximation. For the density distribution in the regions controlled by the cylinder walls, the value of $\sqrt{\nu/D_{m_\perp}}$ for the cylinder alone was used (2.405/R) because the exact effect of the probe on this distribution could not be accurately estimated. The degree of error resulting from these approximations can be inferred from a comparison of the exact solution for the coaxial probe and the approximate solution shown in Figure 4-14. As expected from the approximation model, the maximum error is in the region where the two models are joined (where the positional error is 0.1R and the magnitude of the approximation is 12% greater than that of the exact solution). The magnitude of the error decreases towards either surface, but the percent error remains approximately constant. Consequently, the potential determinations (which are based on a logarithm of a ratio of densities) will be reasonable approximations.

Several distribution curves have been obtained by using the procedure outlined above: (1) Figure 4-8 is a graph of the exact solution for a 0.02R' co-axial cylinder for various α ; (2)Figure 4-9 is a graph of the exact solution for co-axial cylinders of various radii at a given α; (3) Figure 4-10 is the density distribution for various α for a 0.02R probe in an off-axis position; and (4) Figure 4-11 is for a given α and various probe positions for a 0.02R' probe.

Effective Probe Position vs. actual probe position is indicated in Figure 4-12 and potential correction to be applied to probe readings in Figure 4-13; we have assumed the sensing point to be on the side facing the center of the plasma when the actual position is less than $\frac{1}{2}$R from the wall. Potential curves are given in Figures 4-14 and 4-15. The former one is for one contact, oriented as indicated above. The latter is for two contacts, one on either side of the probe along the common diameter. Figure 4-13, the potential correction curve, is just the potential difference between the sheath edge and the point of intersection of the zones of influence for various α and probe positions.

Figure 4-16 is a curve of heat liberated at the probe for various values of probe radius when the probe is aligned with the center of the cylinder, and 4-17 is for various values of α . It is assumed for these calculations that the fraction of particles which diffuse to the sheath reach the surface and recombine, liberating $(eV_i + kT_e/2)$ of energy.

The results of the above theory indicate that the cylindrical probe should have considerably less effect on the particle distribution functions than the prolate probe in a given cross-section of the plasma. This would be expected from the decreased surface

involved for the cylindrical geometry. Consequently, there is less assymetry produced by the probe, and the potential curves, particularly with contacts on both sides of the cylindrical probe, should be more symmetric. However, the effect of measuring a potential at an "effective distance" causes some flattening of the predicted curve. Figure 4-9 indicates that the density distribution in the vicinity of the probe is relatively insensitive to the probe dimensions. Consequently, the potential drop associated with this probe configuration is relatively constant for various probe radii.

TABLE 4-1 CYLINDRICAL PROBE PARAMETERS--EXACT VALUES OF $\sqrt{\nu/D_{m\perp}}$ and C vs. α for probe at center, and mean values vs. α.

α	Probe at Center		Mean Values	
	$\sqrt{\frac{\nu}{D_{m\perp}}}$	C	$\sqrt{\frac{\nu}{D_{m\perp}}}$	C
1	$\frac{2.91}{R}$	.569	$\frac{2.70}{R}$	.554
.5	$\frac{2.84}{R}$	.478	$\frac{2.66}{R}$	.467
.25	$\frac{2.75}{R}$	.365	$\frac{2.61}{R}$	.361
.1	$\frac{2.61}{R}$	.216	$\frac{2.53}{R}$	.215
.05	$\frac{2.53}{R}$	.131	$\frac{2.48}{R}$	.131
.02	$\frac{2.47}{R}$	.064	$\frac{2.44}{R}$	.063
.01	$\frac{2.44}{R}$	.037	$\frac{2.43}{R}$	.036
0	$\frac{2.41}{R}$	.007	$\frac{2.41}{R}$	.007

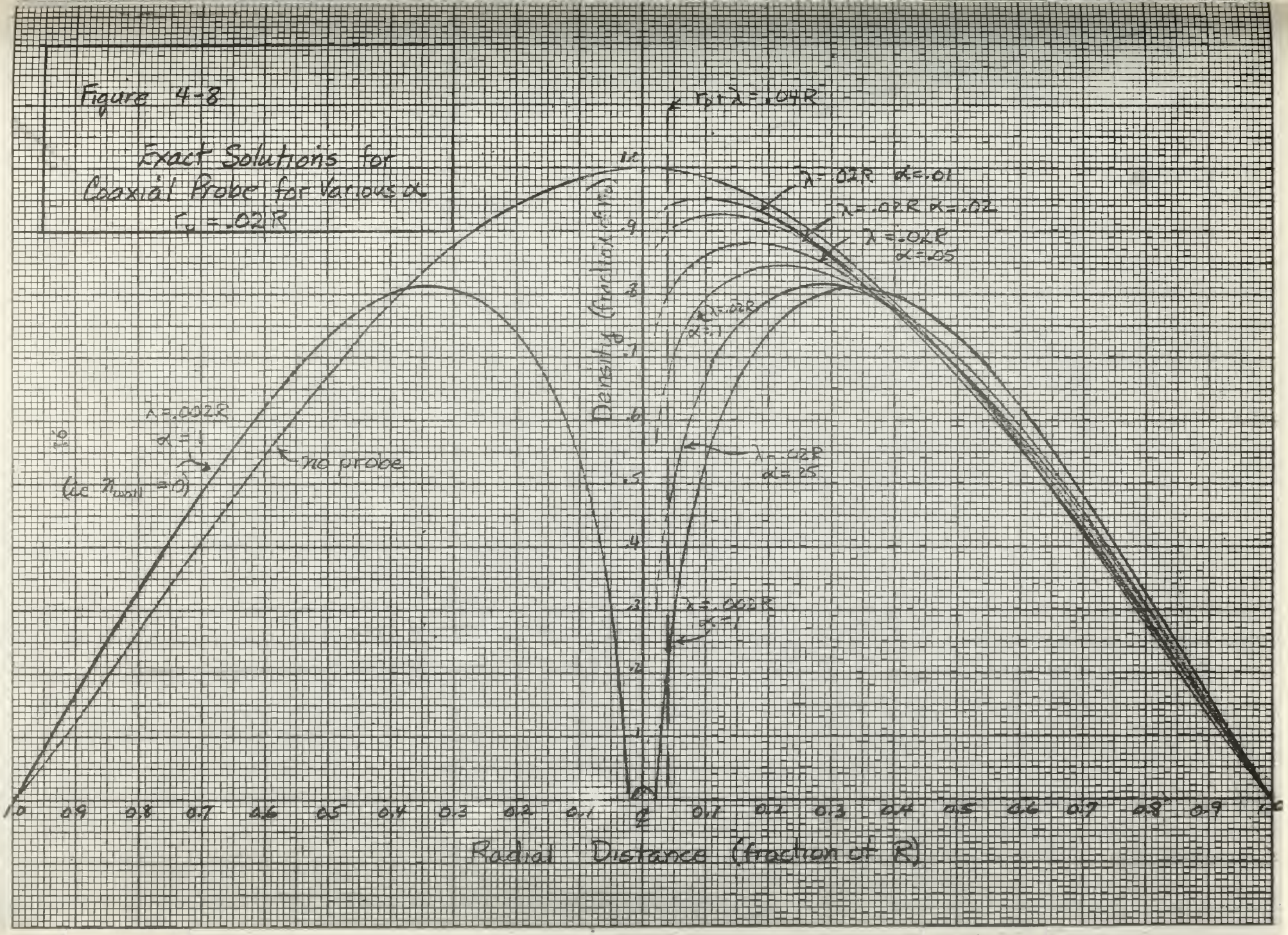
Figure 4-8
Exact Solutions for Coaxial Probe for Various α
$r_0 = .02R$
$r_0 + \lambda = .04R$
$\lambda = .02R$ $\alpha = .01$
$\lambda = .02R$ $\alpha = .02$
$\lambda = .02R$ $\alpha = .05$
$\lambda = .02R$ $\alpha = 1$
$\lambda = .02R$ $\alpha = .25$
$\lambda = .002R$ $\alpha = 1$
$\lambda = .002R$ $\alpha = 1$
(i.e. $r_{wall} = \infty$)
no probe
Density (Fraction of Wall)
1.0
.9
.8
.7
.6
.5
.4
.3
.2
.1
0
1.0 0.9 0.8 0.7 0.6 0.5 0.4 0.3 0.2 0.1 0 0.1 0.2 0.3 0.4 0.5 0.6 0.7 0.8 0.9 1.0
Radial Distance (fraction of R)

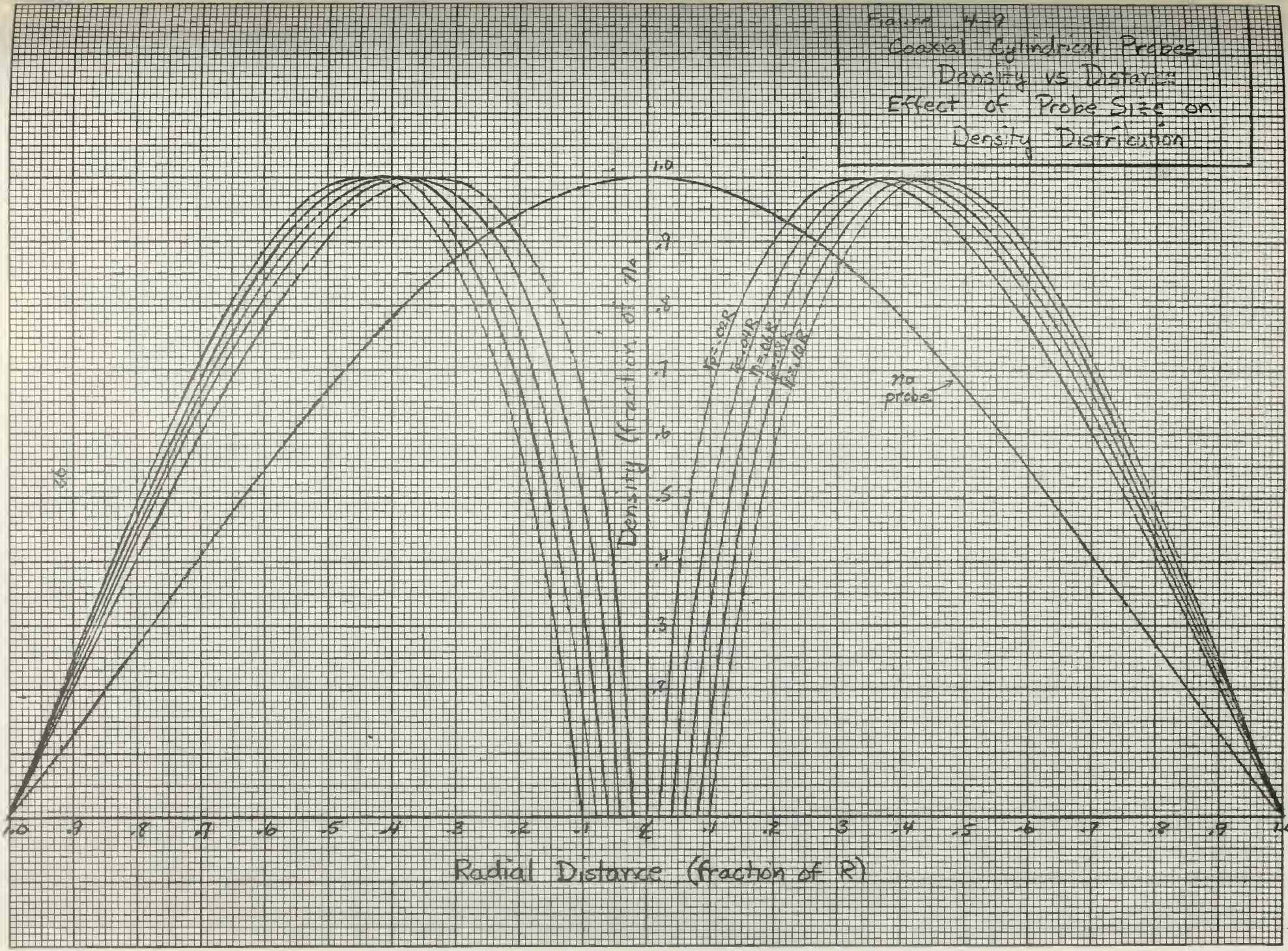
Figure 4-9
Coaxial Cylindrical Probes
Density vs Distance
Effect of Probe Size on
Density Distribution
1.0
.9
.8
.7
.6
.5
.4
.3
.2
.1
Density (fraction of n∞)
R=.05R
R=.025R
R=.01R
no probe
1.0 .9 .8 .7 .6 .5 .4 .3 .2 .1 0 .1 .2 .3 .4 .5 .6 .7 .8 .9 1.0
Radial Distance (fraction of R)

Figure 4-10

Density Distribution for Various α

$r_0 = \lambda = 0.02R$

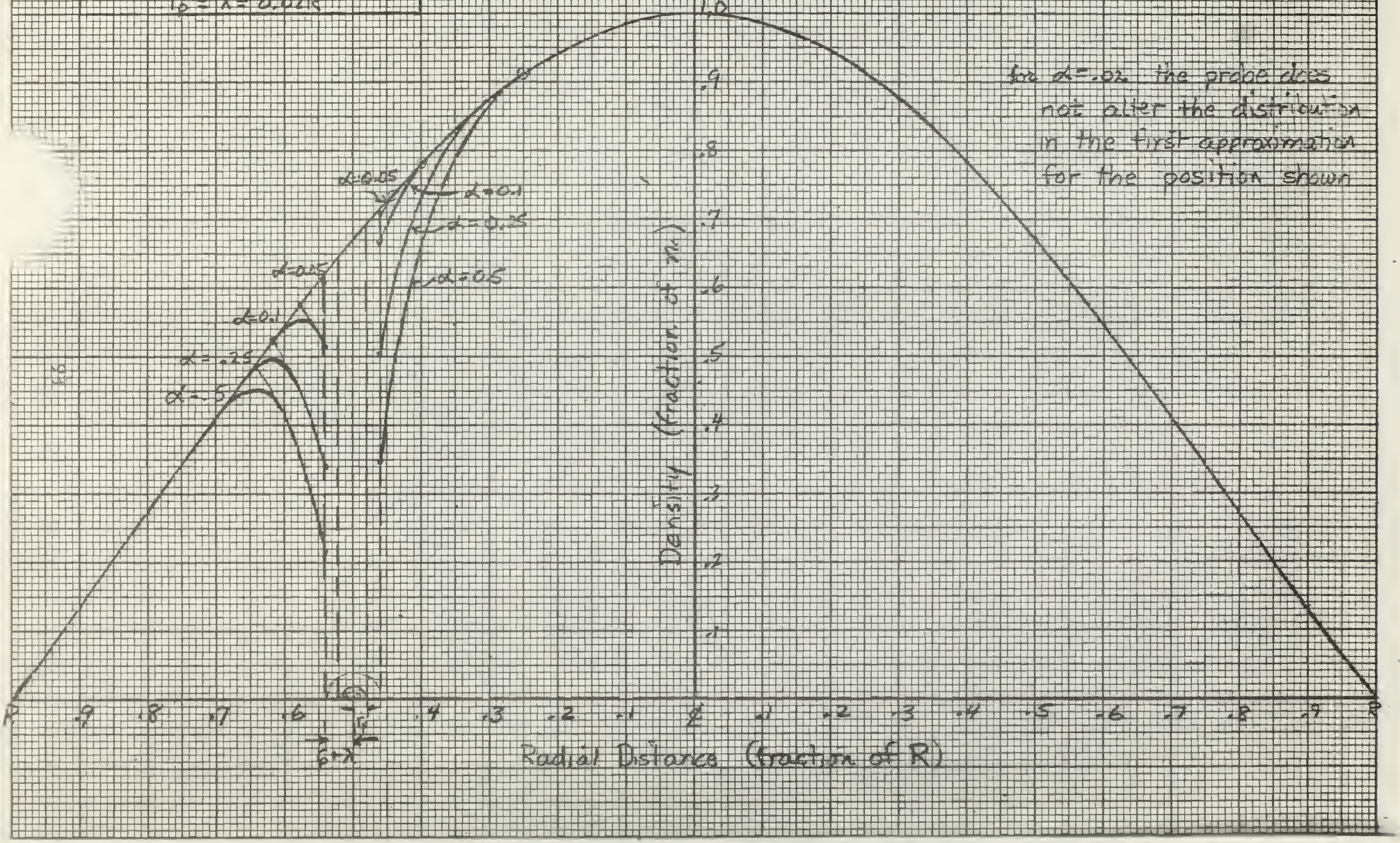

for α=.02 the probe does not alter the distribution in the first approximation for the position shown

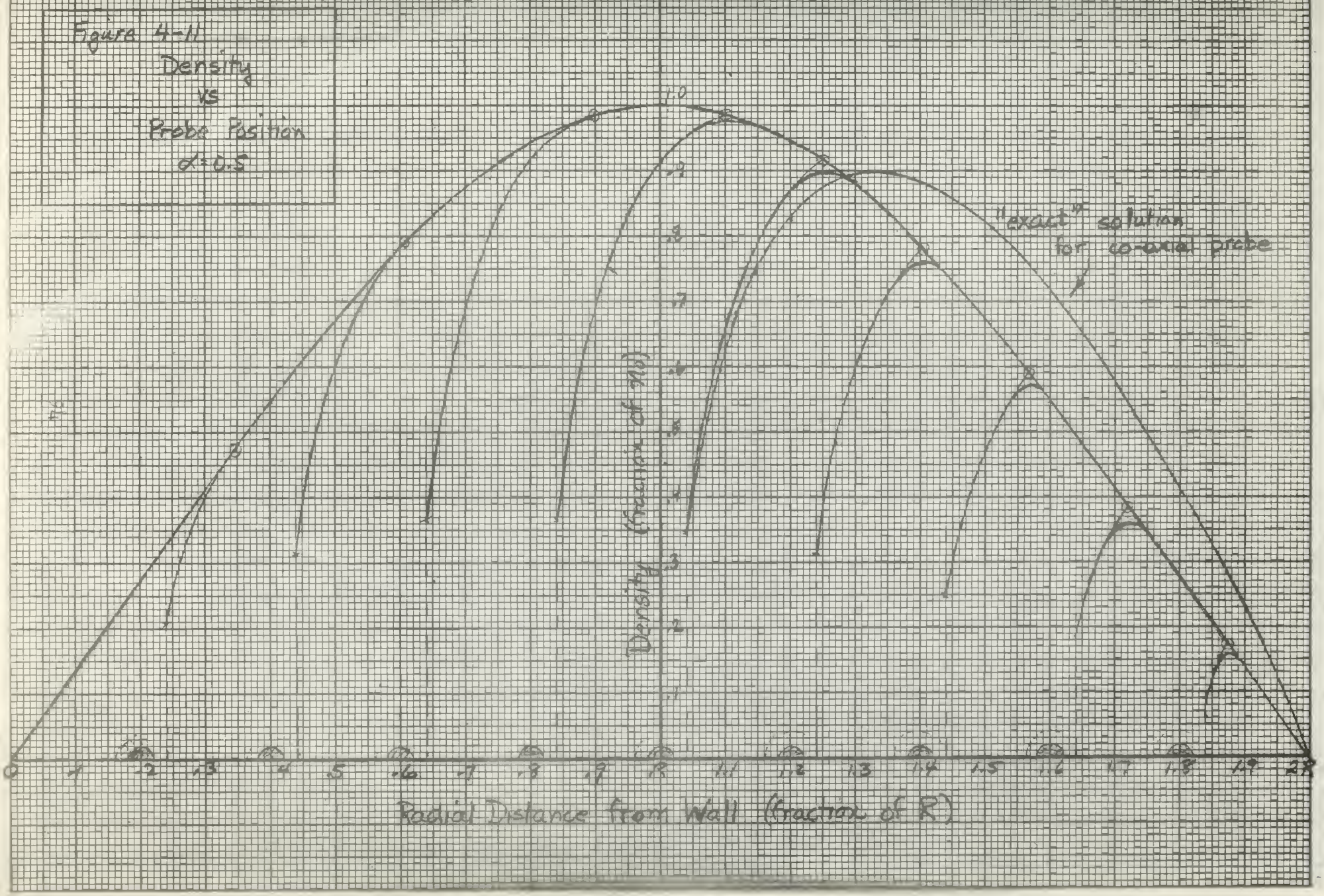
Figure 4-11
Density
vs
Probe Position
α = 0.5
"exact" solution
for co-axial probe
Density (fraction of max)
Radial Distance from Wall (fraction of R)

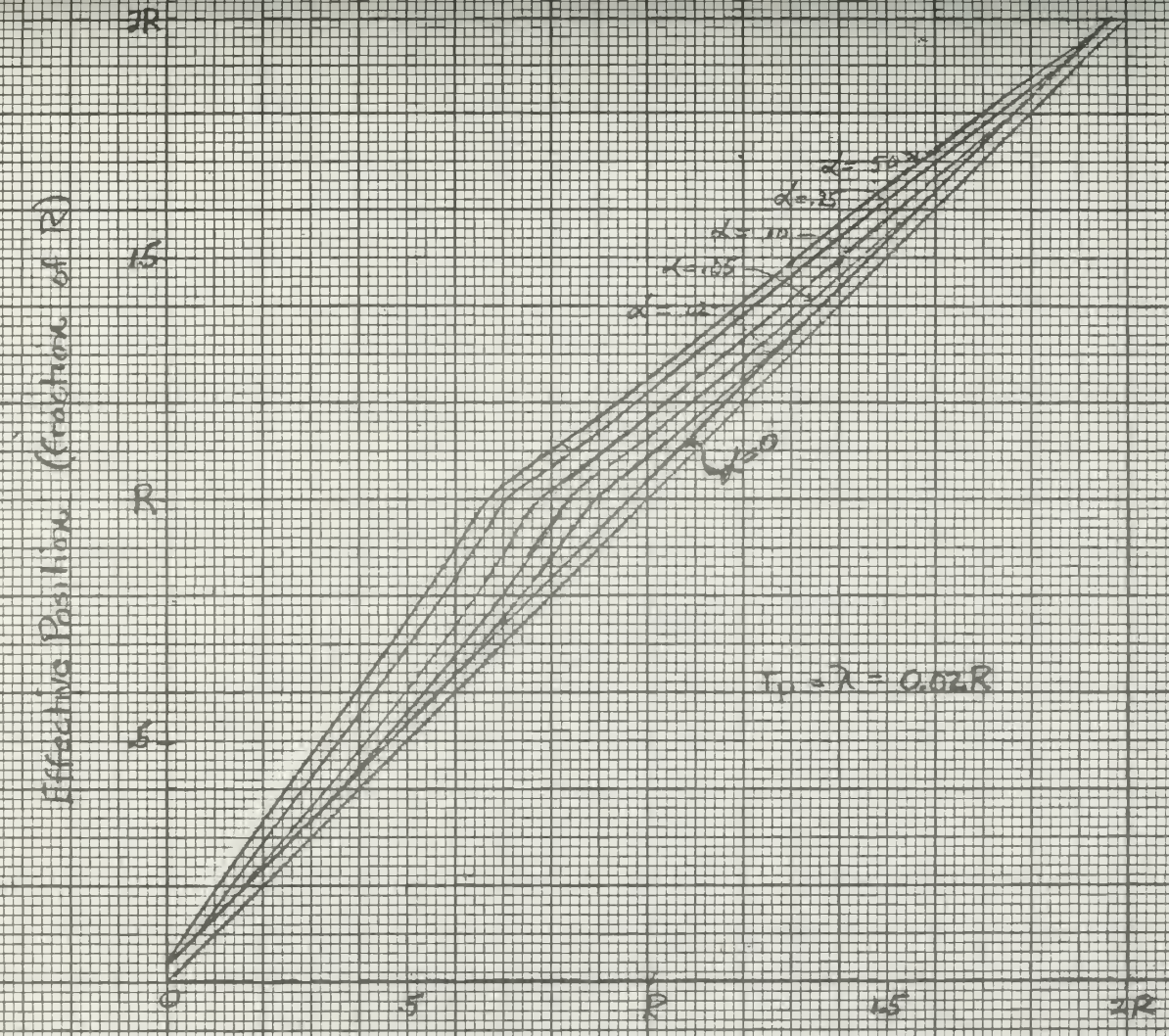

Figure 4-12 Cylindrical Probe
Effective Probe Position vs Actual Position.

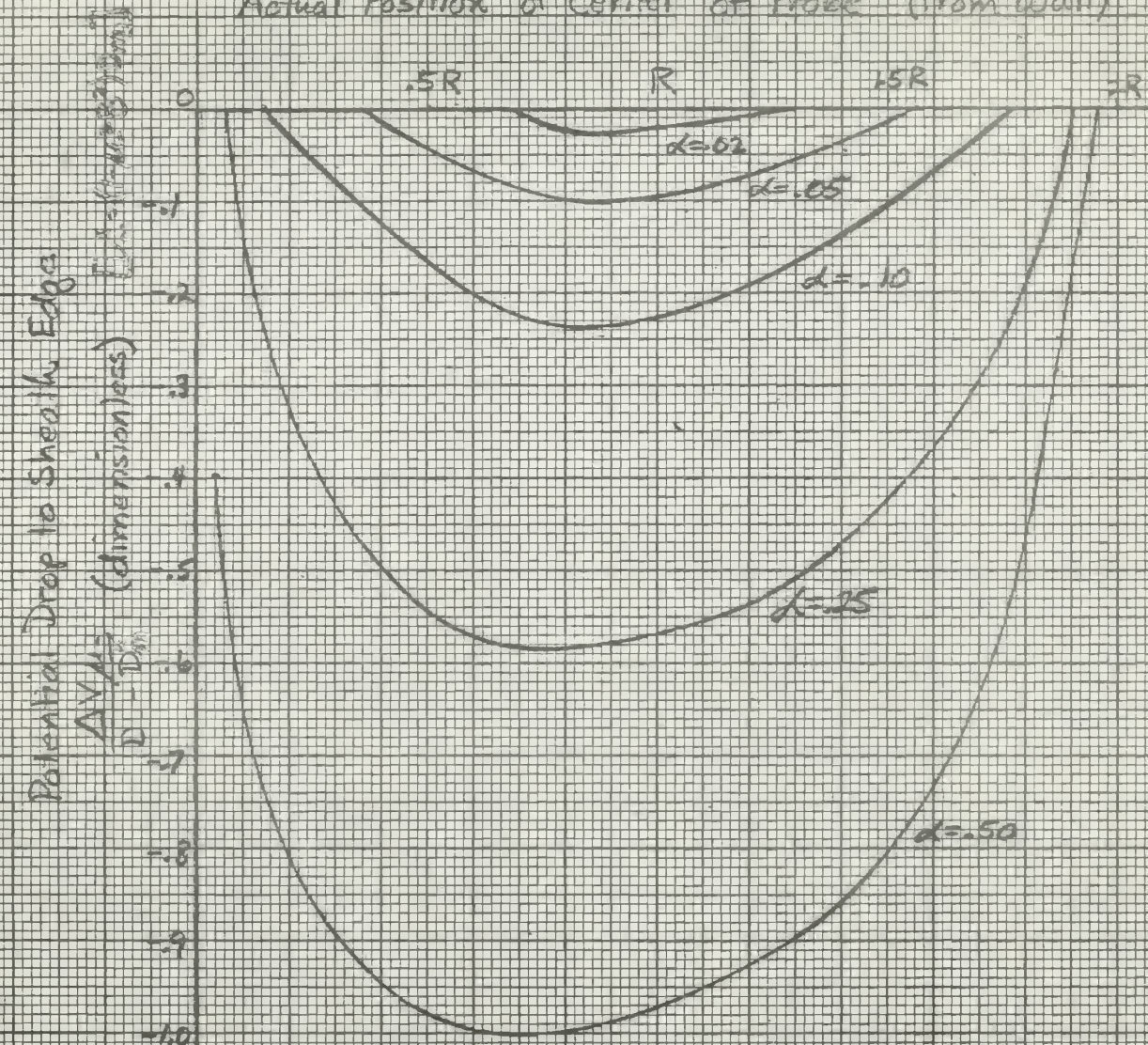

Figure 4-13
Estimated Potential Corrections vs. Probe Position for various α
$r_p = \lambda = 0.022$

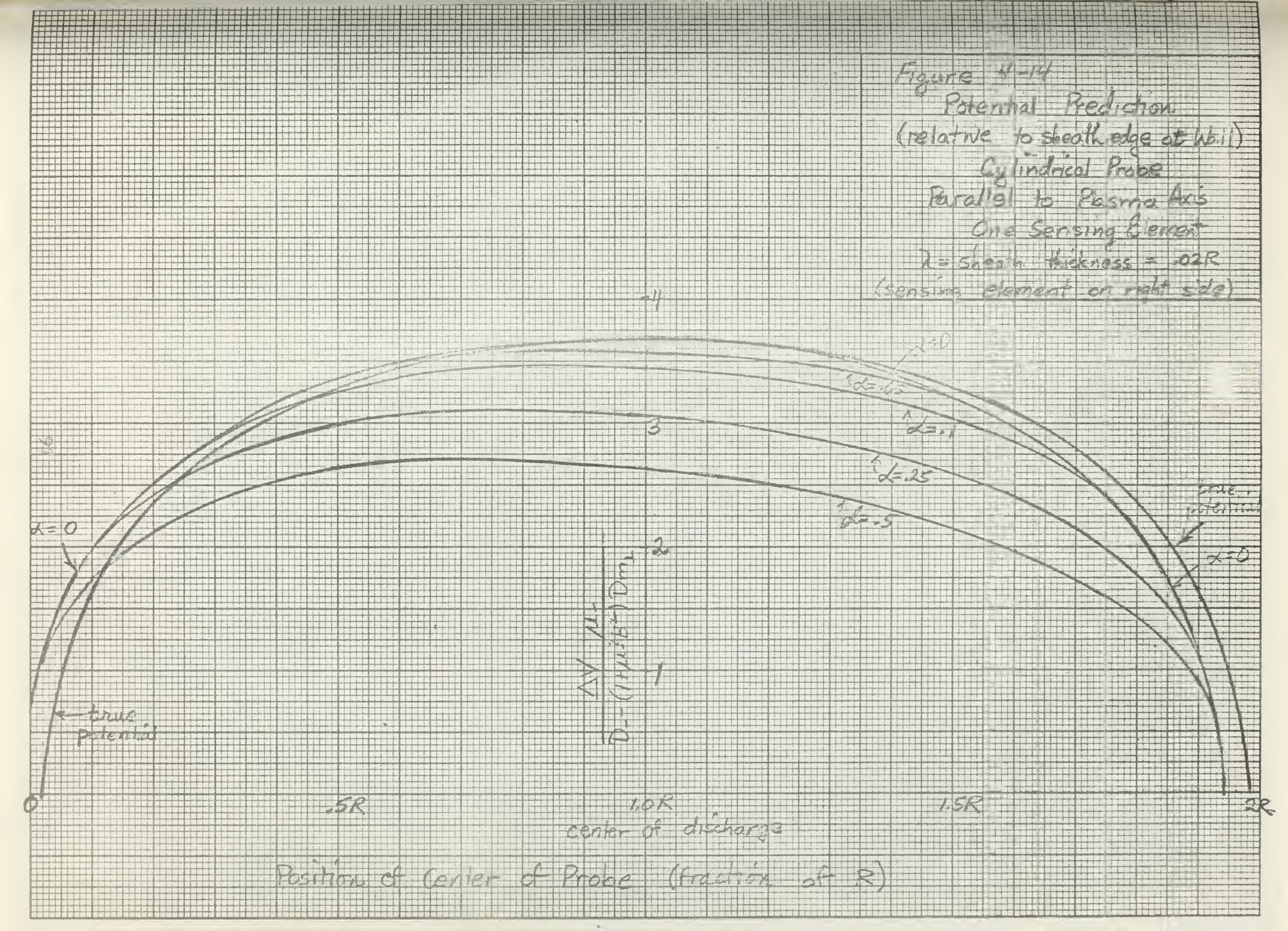
Figure 4-14
Potential Prediction
(relative to sheath edge at Vb.i)
Cylindrical Probe
Parallel to Plasma Axis
One Sensing Element
λ = Sheath thickness = .02R
(sensing element on right side)
-4
3
2
1
0
α=0
α=.05
α=.1
α=.25
α=.5
α=0
true potential
true potential
ΔV (Volts) Dim.
.5R
1.0R
1.5R
2R
center of discharge
Position of Center of Probe (fraction of R)

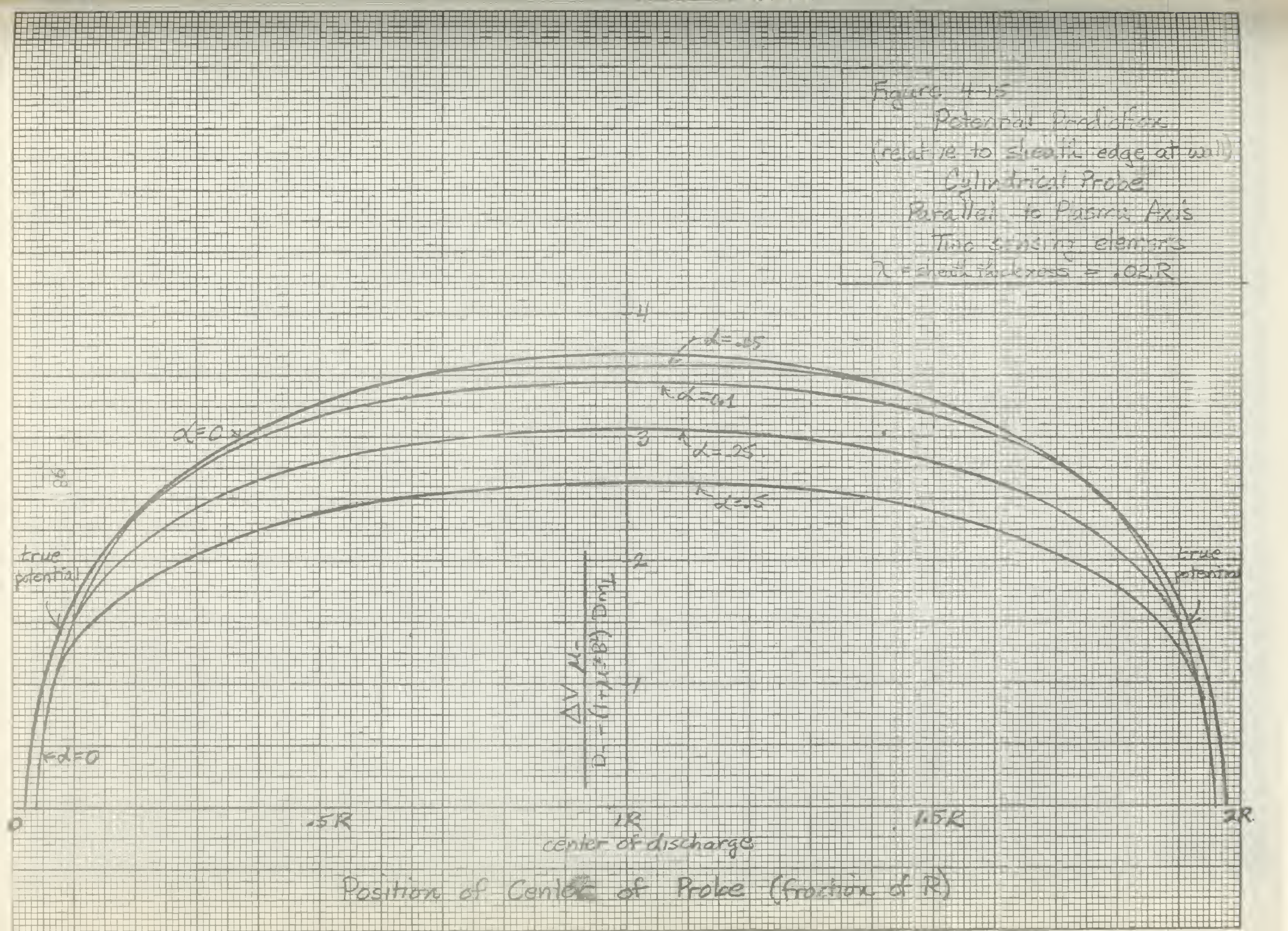
Figure 4-15
Potential Predistortion relative to sheath edge at wall
Cylindrical Probe
Parallel to Plasma Axis
Two sensing elements
λ = sheath thickness ≈ .02R
α=.5
α=0.1
α=.25
α=1
α=0
true potential
true potential
ΔV/Δr
D - (1+λ+B) (Dm)
4
3
2
1
0
.5R
1R
1.5R
2R
center of discharge
Position of Center of Probe (Fraction of R)

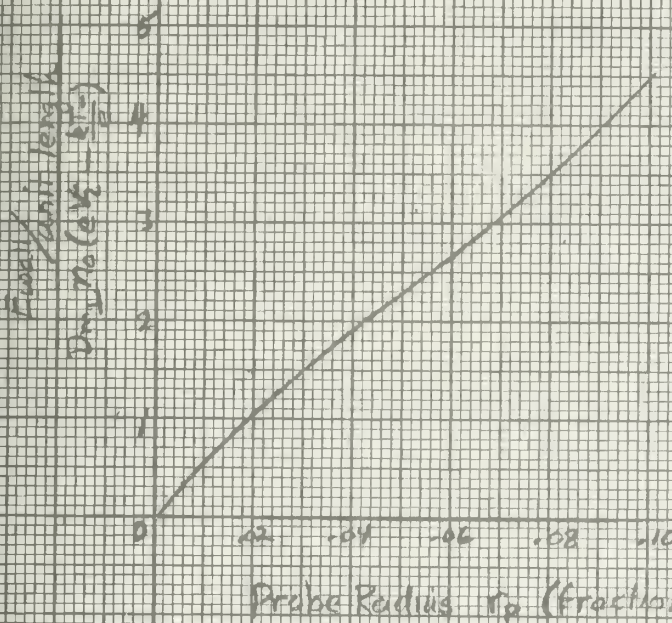

Figure 4-16 Wall loss/unit length at probe vs Probe radius. $\lambda = 0.02R$

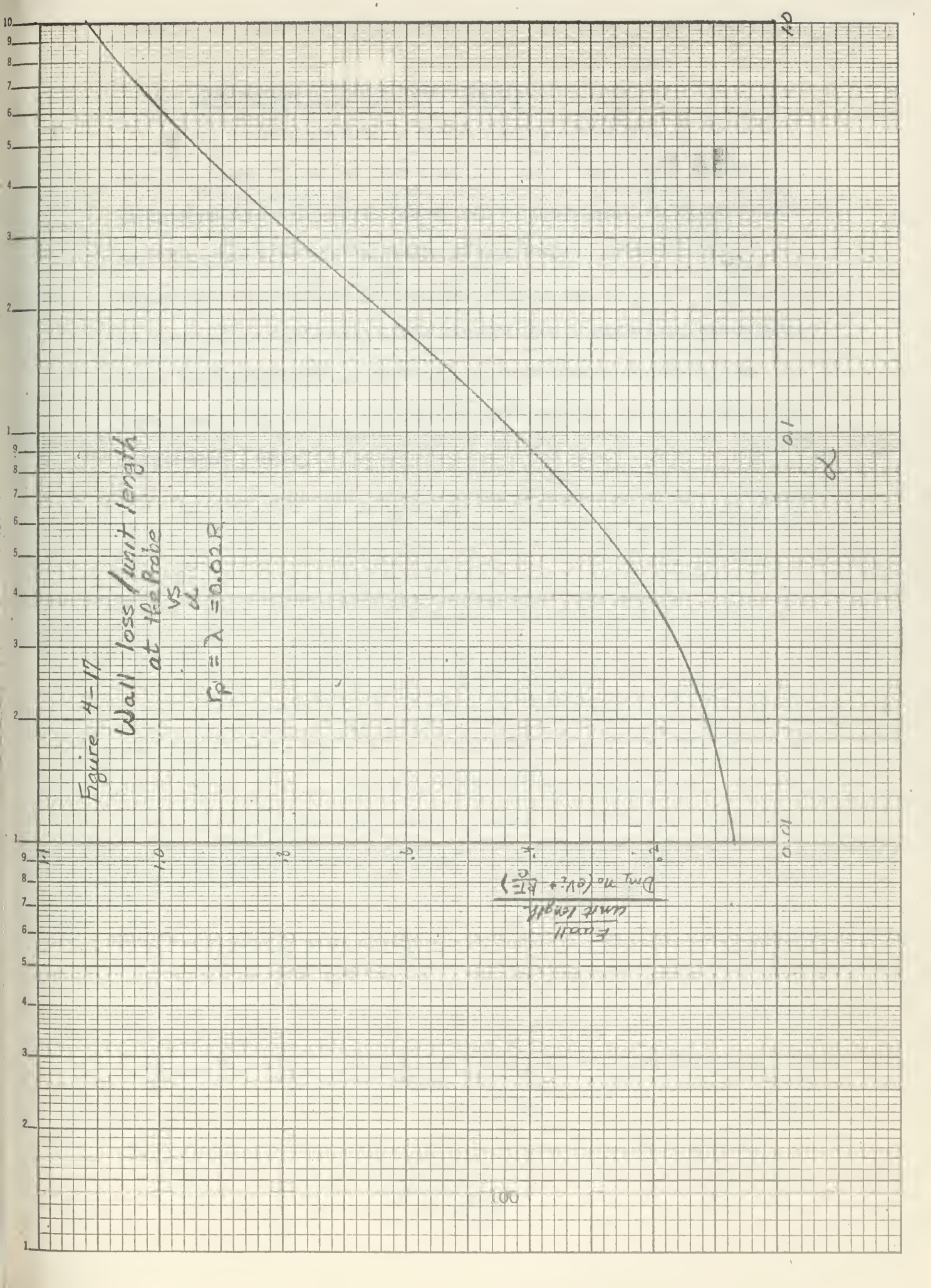
Figure 4-17
Wall loss limit length at the Probe
vs
α
$r_p = \lambda = 0.02R$
α
$\frac{\text{Ecoul. Limit length}}{D_{mi} n_o (qV_c + \frac{RT_e}{e})}$

C. Evaluation of Probe Measurements

In a dense plasma, in which the mean free path is of the order of magnitude of or less than the probe dimensions, strong deviations from Langmuir's theory can be expected. These deviations depend on the size and character of the probe. By using the approximation described in this thesis, one can calculate these effects in terms of an "effective probe length" and a "potential disturbance." These two parameters can then be used to analyze or predict the experimental results in the manner just employed for the prolate and cylindrical probes.

V

MAGNETIC FIELD END EFFECTS

Let us now investigate the effects on the particle density distribution functions of the decrease in magnetic field intensity at the end of a coil with attendent intersection of field lines with the container walls. The effect expected is that diffusion along the field lines, being greater than that perpendicular to the walls (radial diffusion), would cause the density distribution near the ends of the field coil to decrease more with increasing radial distances from the axis than predicted from radial diffusion alone. Particle losses by longitudinal diffusion to the end of the field coil, where some of the field lines intersect the container walls, would be responsible for this effect, which would manifest itself physically as a constriction near the ends of the field coil.

An exact solution of the continuity equation for this configuration (Figure 5-1--note the enlarged radial scale) could not be found, and consequently the approximation described in Section III-A-2 was used. The plasma is divided into zones in which the diffusion would be primarily radial or primarily longitudinal (along field lines). The latter zone, in the vicinity of the intersection of the field lines with the plasma container, is a zone in which the particle distribution is controlled by the loss of particles diffusing along the field lines and recombining at the region of the wall where the lines intersect the wall. The size of the region of parallel diffusion increases, of course, with increasing magnetic field. If we neglect the curvature of the field lines and use the boundary condition

$$n_{wall} = C \qquad (2\text{-}99)$$

we obtain for the density distribution along a field line

$$n(z) = n' \sin\left(\sqrt{\frac{\nu'}{D_{m_\parallel}}}\, z\right) = n' \sin\left(\frac{\pi}{z_0} z\right) \tag{5-1}$$

where n' is a normalizing factor to be determined, the z-axis is the cylinder and magnetic field axis, and the origin is the intersection of the field line and the wall. This solution cannot be rigorously derived, but is justified as an approximation consistent with the accuracy of this calculation. Comparison with the solution for a bounded cylinder in a homogeneous field, equation (3-62), shows the same z-dependence for the density distribution.

A second zone in this plasma is that in the vicinity of the center of the field coils in which wall losses due to radial diffusion to the walls control the density distribution. Here

$$n(r) = n_0 J_0\left(\sqrt{\frac{\nu}{D_{m_\perp}}}\, r\right) = n_0 J_0\left(\frac{2.405}{R} r\right) \tag{5-2}$$

where n_0 is the density in the center of the cylinder.

Then, as a first approximation, we shall assume that the ionization coefficient, ν', in the zone of parallel diffusion will not differ significantly from that of the corresponding stable radial configuration. In higher approximations we would have to calculate the change in this quantity due to induced changes ir electron temperature by the different fields, but we shall assume these to be regligible. Consequently,

$$\nu' \approx \nu \tag{5-3}$$

Therefore, we obtain from equations (5-1) and (5-2)

$$z_0 = \sqrt{\frac{D_{m_\parallel}}{D_{m_\perp}}}\ \frac{2.41}{R} \tag{5-4}$$

The surface separating the two models (equation (3-41)) is that at which

$$\left| D_{m_{\parallel}} \frac{\frac{\pi}{z_c}\cos\left(\frac{\pi}{z_c}z\right)}{\sin\left(\frac{\pi}{z_c}z\right)} \right| = \left| D_{m_{\perp}} \frac{\frac{2.4}{R}J_1\left(\frac{2.4}{R}r\right)}{J_0\left(\frac{2.4}{R}r\right)} \right| \qquad (5\text{-}5)$$

Substitution from equation (5-4) reduces this to

$$\left| \frac{J_1\left(\frac{2.4}{R}r\right)}{J_0\left(\frac{2.4}{R}r\right)} \right| = \left| \sqrt{\frac{D_{m_{\parallel}}}{D_{m_{\perp}}}} \cot\left(\frac{\pi}{z_c}z\right) \right| = \left| a\cot\left(\frac{\pi}{z_c}z\right) \right| \qquad (5\text{-}6)$$

Figure (5-2) is a nomogram from which the z-coordinate of the separation surface, z, can be obtained as a fraction of z_o, using r (as a fraction of cylinder radius R) and

$$a = \sqrt{\frac{D_{m_{\parallel}}}{D_{m_{\perp}}}} = \sqrt{1+\mu_1\mu_2 B^2} \qquad (5\text{-}7)$$

as arguments. From equation (5-7), it is apparent that "a" decreases (with B) along the cylinder axis (indicated on Figure (5-1)) beyond the end of the field coils. Consequently, when using the nomogram to determine z_o, it is necessary to use the value of "a" at the junction of the two models. This requires a trial-and-error procedure.

In order to illustrate this method of approximation, and to estimate these effects, a system with the following dimensions was selected:

Plasma container radius: 2.5 cm.

magnetic coils: width = 15 cm.
spacing = 5 cm.
number = 10
inside diameter = 25 cm.
outside diameter = 50 cm.
overall length = 195 cm.

The axial field of the above array of field coils was computed with a digital computer (figure 5-3), using the thick coil equations from reference [20] . The author states that they agree to within a few percent of measured values, and for the region within the coil array, experimental curves from a very similar array were available and agreed very well. The field was assumed constant through any cross-section of the cylinder, which is a good approximation because of the small radius of the cylinder. Figure 5-1 shows the field lines as computed from the field strength data.

Figure (5-1) also shows the separation of the two zones of diffusion for three different orders of magnitude of B^2, namely,

$$B^2 = \frac{100-1}{\mu_+\mu_-}, \quad a = 10$$

$$B^2 = \frac{1000-1}{\mu_+\mu_-}, \quad a = 31.6$$

$$B^2 = \frac{10,000-1}{\mu_+\mu_-}, \quad a = 100 \qquad (5\text{-}8)$$

It is to be noted that for $B \approx \frac{10}{\mu_+\mu_-}$ (a = 10) the effect of the parallel diffusion is very small, and is centered at the end of the coil array. For $B \approx \frac{100}{\mu_+\mu_-}$ (a = 31.6) the effect is appreciable, and extends more than half-way into the cylinder. Figure (5-4) is a density profile of the resulting particle distribution; Figure (5-5), selected cross-sections from Figure (5-4); and, Figure (5-6) is a plot of constant density curves.

One feature of the density distribution which must be discussed is the question of determining the density distribution of the central zone when it does not extend to the walls but rather terminates at the edge of a longitudinal zone. A longitudinal current (between

electrodes at either end of the cylinder) is responsible for the ionization within the plasma, and this current must be constant through the plasma. Further, we have assumed that the ionization coefficient, ν , is constant. From this it follows that the electron temperature is constant, and therefore the longitudinal electric field must be approximately constant. But if the field and current are approximately constant, then the total number of particles in a cross-section must be constant. Further, the plasma in the radial-diffusion region which is not controlled by the cylinder boundaries because of the intervening region of parallel diffusion is expected to maintain its Bessel distribution (thus satisfying the diffusion equation and not requiring a different ionization coefficient). As a consequence of the constant field and current restrictions, however, the total cross-section particle density (particles per unit length),

$$\int_0^R \pi r^2 n(r)\, dr \qquad (5\text{-}9)$$

is a constant, equal to the total number of particles per unit length at the center of the field coil. Therefore the normalization of the Bessel distribution for the center of the plasma in regions where the distribution at greater radii is controlled by longitudinal diffusion must be so determined that equation (5-9) is satisfied.

One effect which we ignore in the previous formulation is that due to the small radial component of the magnetic field at the end of the coil. This component is strongest at greater radii, and decreases the mobility of the particles in the longitudinal direction. Consequently, it would contribute further to the constriction of the

plasma at this point. We neglect this influence, assuming the curvature of the field lines to be very small (recall that the radial scale of Figure (5-1) is greatly enlarged).

It should be noted that there is a discontinuity in the direction of $\vec{\nabla} n$ along all the dividing surfaces between zones, and a discontinuity in particle density, n, along the a = 31.6 boundary from 90 cm to 130 cm and the a = 100 boundary from the center to 164 cm. The former discontinuity is a consequence of our approximation. The density discontinuity occurs because the dividing surface lies along one of the field lines, and is a result of the fact that the sine distribution for the longitudinal model cannot be made to match the normalized radial distribution along such a line except at the end which is nearer the end of the coil. The transition regions are centered along these dividing surfaces, and are the region of greatest uncertainty. Along those surfaces at which the particle density, n, is discontinuous, this approximation is even more uncertain. Because of this, the a = 100 description, with a discontinuity in both and n along its entire length, must be much too crude to be valid, and further attempts to fit this approximation to the effects of such large fields are not attempted. The description for a = 31.6 is believed to be a valid "order-of-magnitude" approximation.

In Figure (5-7) the heat liberated at the walls by the ions and electrons carried to them is indicated as a function of position along the cylinder. There are three curves; all calculated for a = 31.6: (1) the wall heat loss for normal ambipolar diffusion without a magnetic field, (2) the wall heat loss for radial diffusion with a magnetic field, accounting for the increase in radial diffusion which accompanies the decrease in magnetic field outside the coils, and

(3) the estimated heat loss for the magnetic field, taking into account the longitudinal as well as radial diffusion. This latter curve is a very crude approximation based on the results predicted by this model with adjustments to compensate for the errors introduced by the discontinuities at the separation surfaces. The figure shows that the heating at the wall within the region of parallel diffusion and within the coil array is greatly decreased because the particles are transported to the end of the cylinder instead of directly to the walls. However, outside the coil, where particles from within the coil are carried by the longitudinal diffusion, the effects of such additional heating is masked by the heating due to the increased raidal current which flows because of the lower magnetic field intensity.

The values of magnetic field B for which this effect can be approximately described by this model are those whose order of magnitude corresponds to a ≈ 31.6. Smaller fields ($a \leq 10$) will not cause an appreciable end-effect constriction. Larger fields ($a \geq 100$) are not describable by this model. For a plasma which fits the sample data given in section 3-B-1, this is seen from equation (5-8) to be approximately

$$B \approx \sqrt{\frac{999}{76}} \approx 4 \quad \text{weber/m}^2 \qquad (5\text{-}10)$$

It must be recalled, however, that the above description is based upon the walls being perfect insulators. Electron diffusion, predominately parallel to the field lines because of the small electron Larmor radius, is restrained by the build-up of a negative wall charge in the vicinity of the magnetic field line intersections with the cylinder walls. Similarly, the ion diffusion, which would be predominantly

radial because of the larger Larmor radii, would be opposed by a large positive wall charge within the coil. In this manner, the conditions of equal electron and ion radial current and equal longitudinal current are met. However, it is known that insulators have a surface conductivity which depends on the material and the temperature. The effect of this conductivity is to permit an exchange of carriers along the wall. Consequently, we obtain diffusion which is somewhere between Allis diffusion [15] and our quasi-ambipolar diffusion. The wall charge build-up is avoided by the exchange of ions and electrons between negatively and positively charged zones. This exchange results in recombination along the length of the cylinder and would probably invalidate the conclusions of Figure (5-7) if the currents were appreciable. Further, if this surface conductivity were sufficiently high, the diffusion would approach Allis diffusion, under which condition the ratio of the parallel and perpendicular components of the diffusion tensor would no longer be $1 + \mu_+\mu_- B^2$ but would be $1 + \mu^2 B^2$. Thus the field strength which would produce a constriction describable by this model would be reduced to

$$B \approx \sqrt{\frac{77}{76^2}} \approx 0.4 \text{ weber/m}^2 \qquad (5\text{-}11)$$

The description of the density distributions would not be affected by the change in diffusion process since the only effect on the diffusion is a change in the magnitudes of the components of the diffusion tensor. In practice the diffusion would be somewhere between the extremes of no surface conductivity and perfect conductivity. Therefore, the value of B to which these calculations correspond would intermediate between 0.4 weber/m^2 and 4 weber/m^2, depending upon the surface current conducted by the plasma container walls.

It should be noted that this description predicts negligible end effects for the plasma described for fields below about 0.1 weber/m^2. For particles with higher mobilities, however, this effect could occur in smaller magnetic fields.

Figure 5-1 Magnetic Field End Effects
Zones of Influence

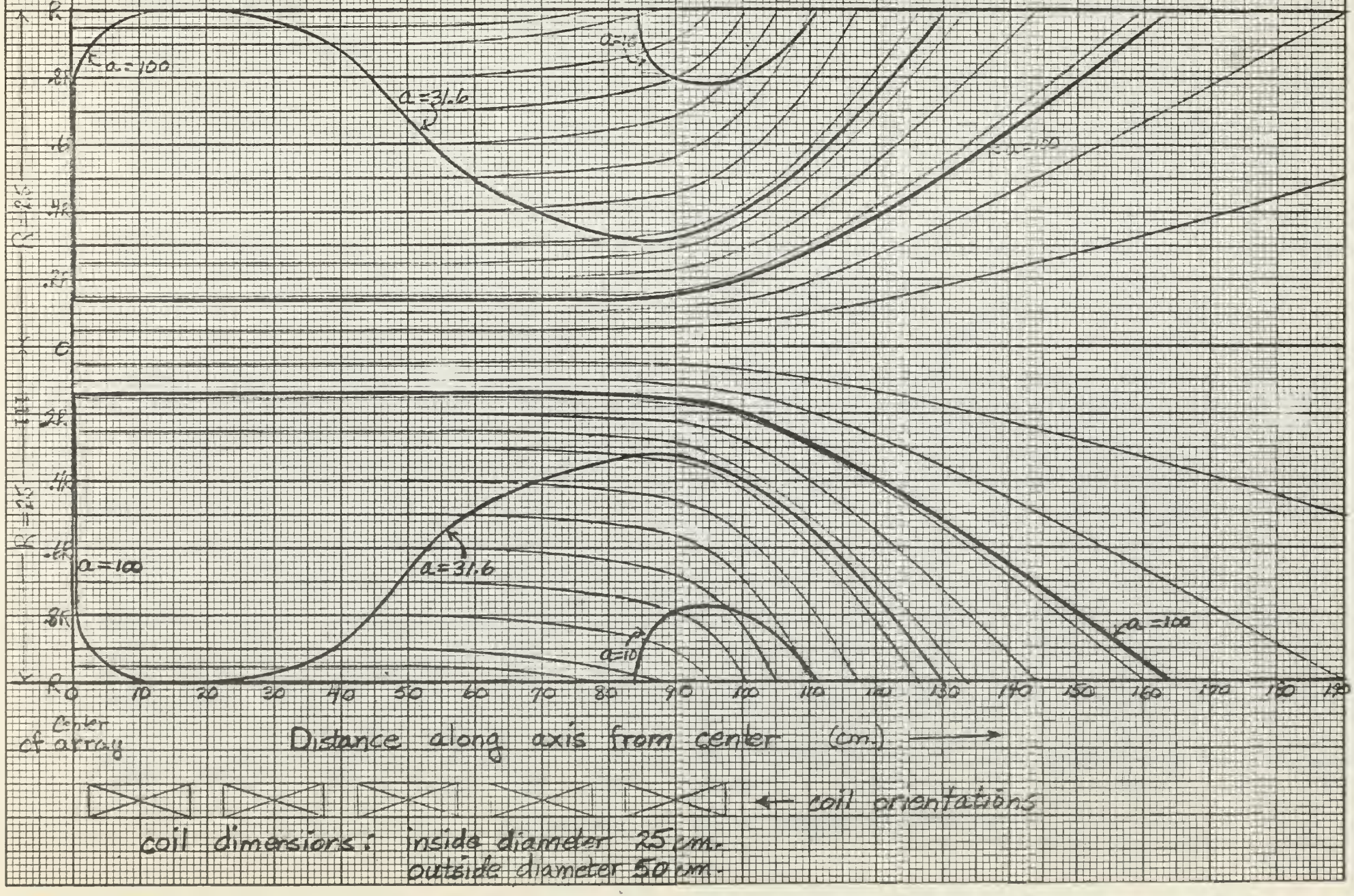

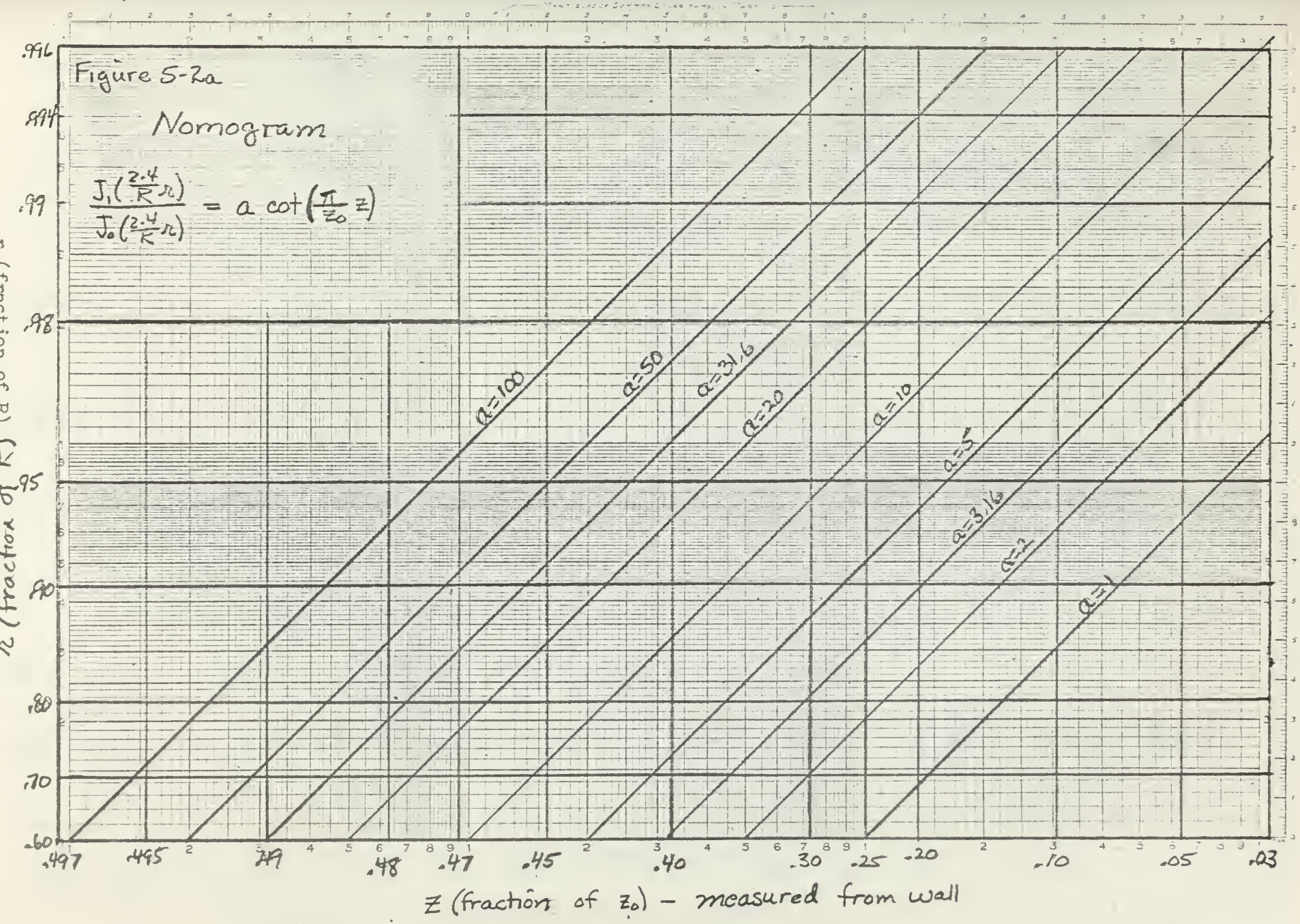
Figure 5-2a
Nomogram
$\frac{J_1(\frac{2.4}{R}r)}{J_0(\frac{2.4}{R}r)} = a \cot(\frac{\pi}{2_0}z)$
a=100
a=50
a=31.6
a=20
a=10
a=5
a=3.16
a=2
a=1
.996
.994
.99
.98
.95
.90
.80
.70
.60
.497
.495
.49
.48
.47
.45
.40
.30
.25
.20
.10
.05
.03
r (fraction of R)
z (fraction of z_0) – measured from wall

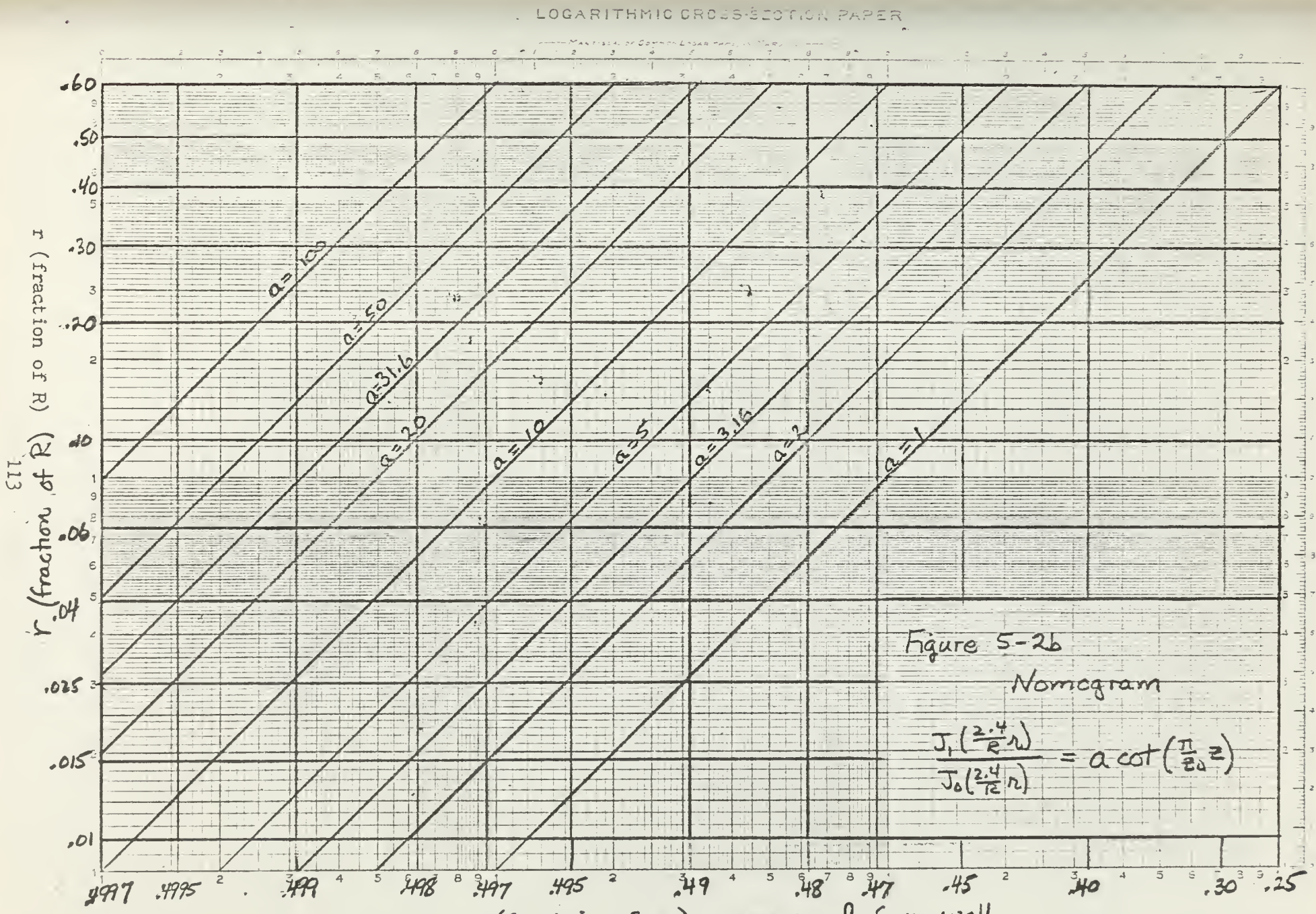
LOGARITHMIC CROSS-SECTION PAPER
r (fraction of R)
.60
.50
.40
.30
.20
.10
.06
.04
.025
.015
.01
a=100
a=50
a=31.6
a=20
a=10
a=5
a=3.16
a=2
a=1
.4997
.4995
.499
.498
.497
.495
.49
.48
.47
.45
.40
.30
.25
z (fraction of z₀) — measured from wall
Figure 5-2b
Nomogram
$\frac{J_1\left(\frac{2.4}{R}r\right)}{J_0\left(\frac{2.4}{R}r\right)} = a\cot\left(\frac{\pi}{2_0}z\right)$

Figure 5-2b

Figure 5-3

Magnetic Field Intensity for Coil Assembly of Chapter V

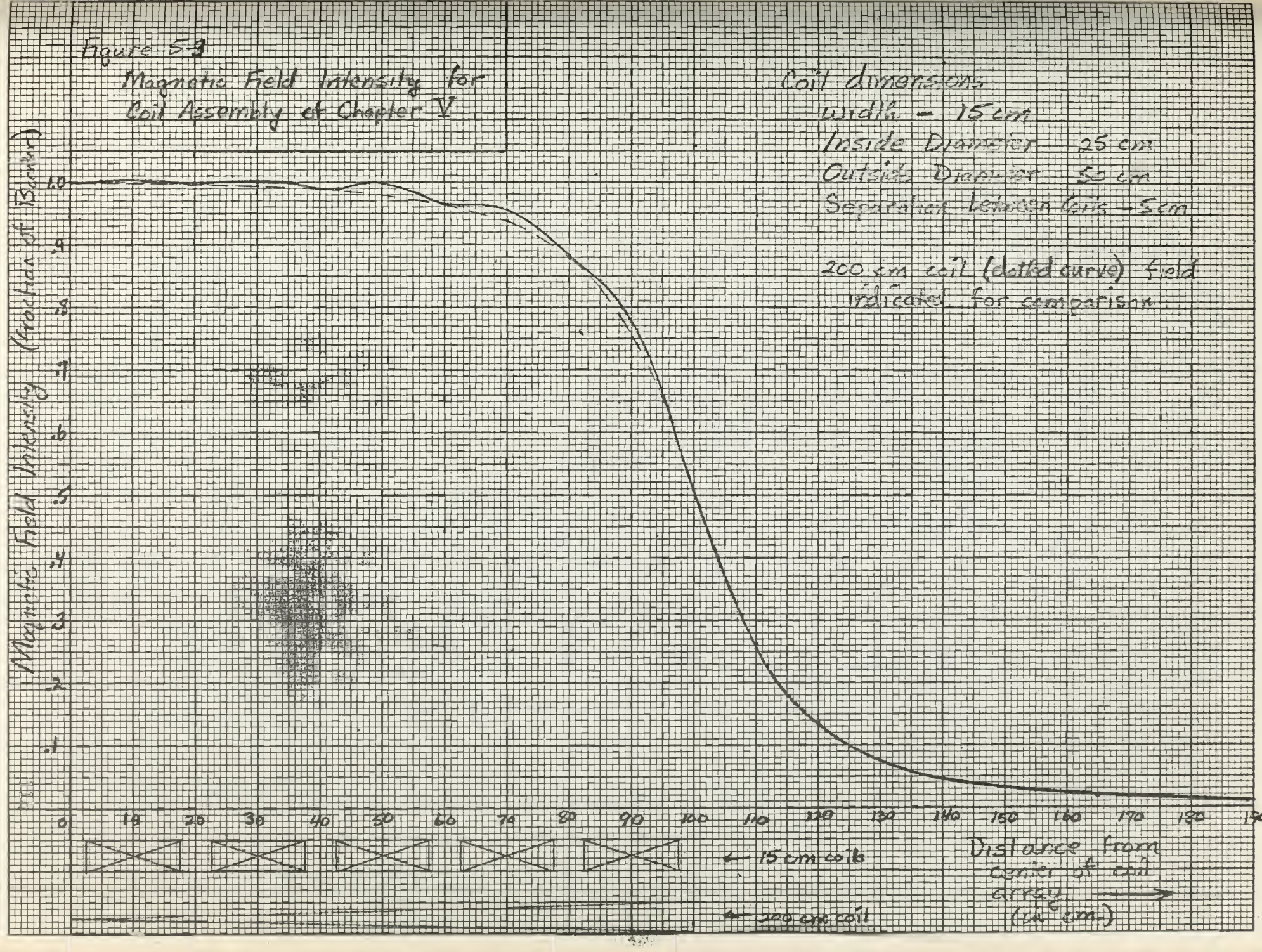

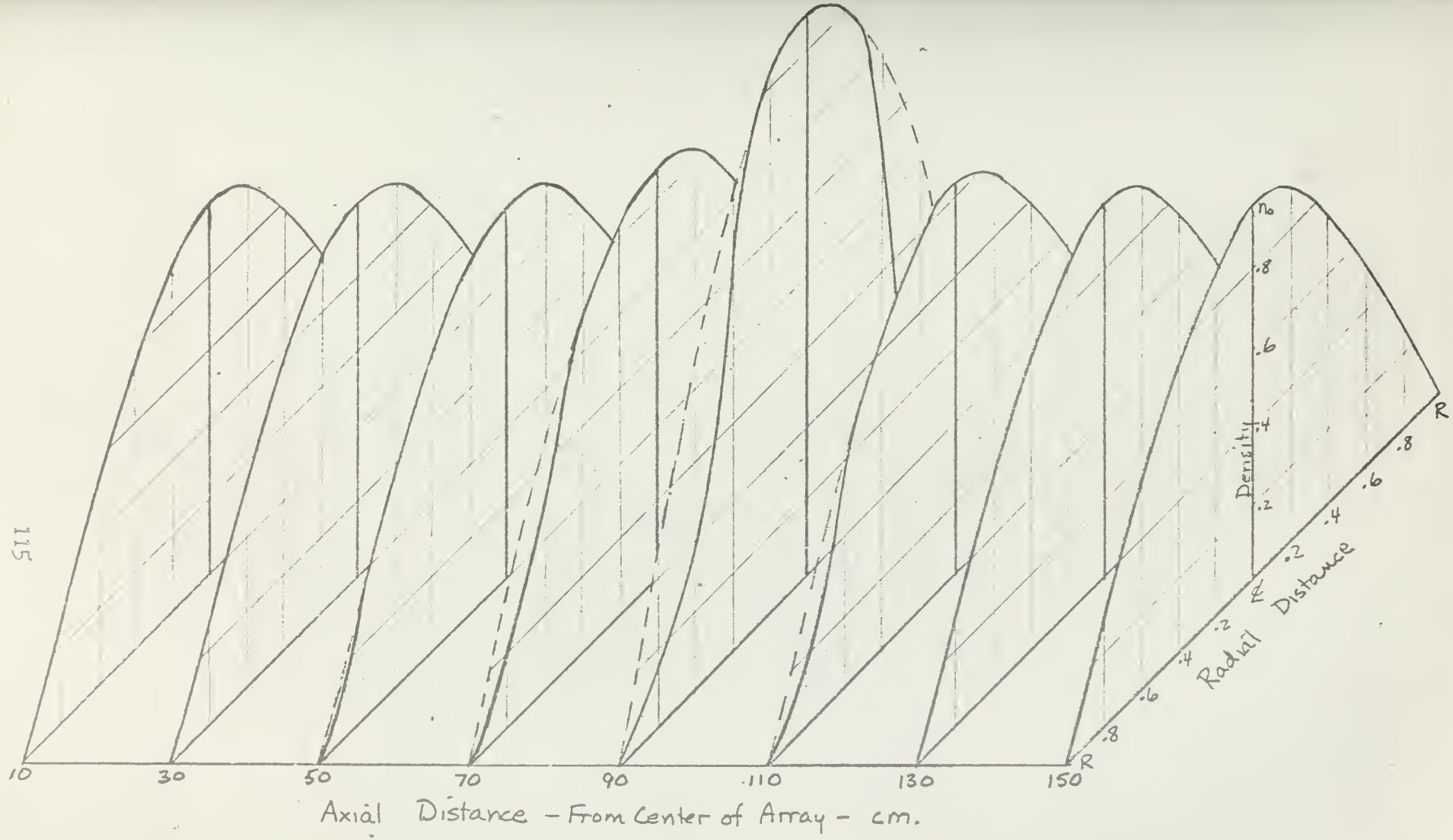

Figure 5-4 Density Profiles, normalized to center of plasma (n_0)
Broken curves are Bessel Functions.

Figure 5-5

Density Distributions

Cross sections from Fig 5-4

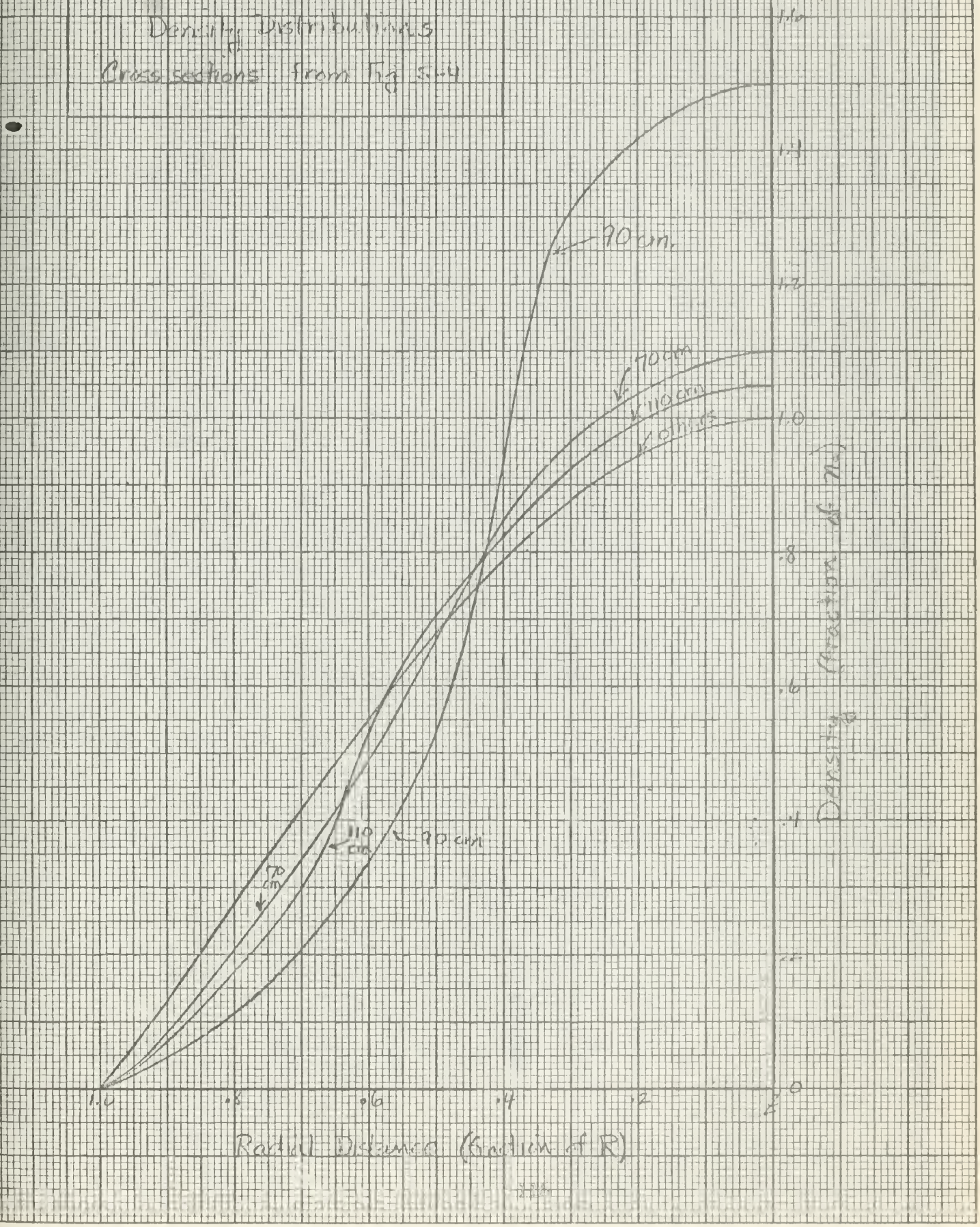

Figure 5-6 – Magnetic Field End Effects: Constant Density Contours for $\Omega = 31.6$

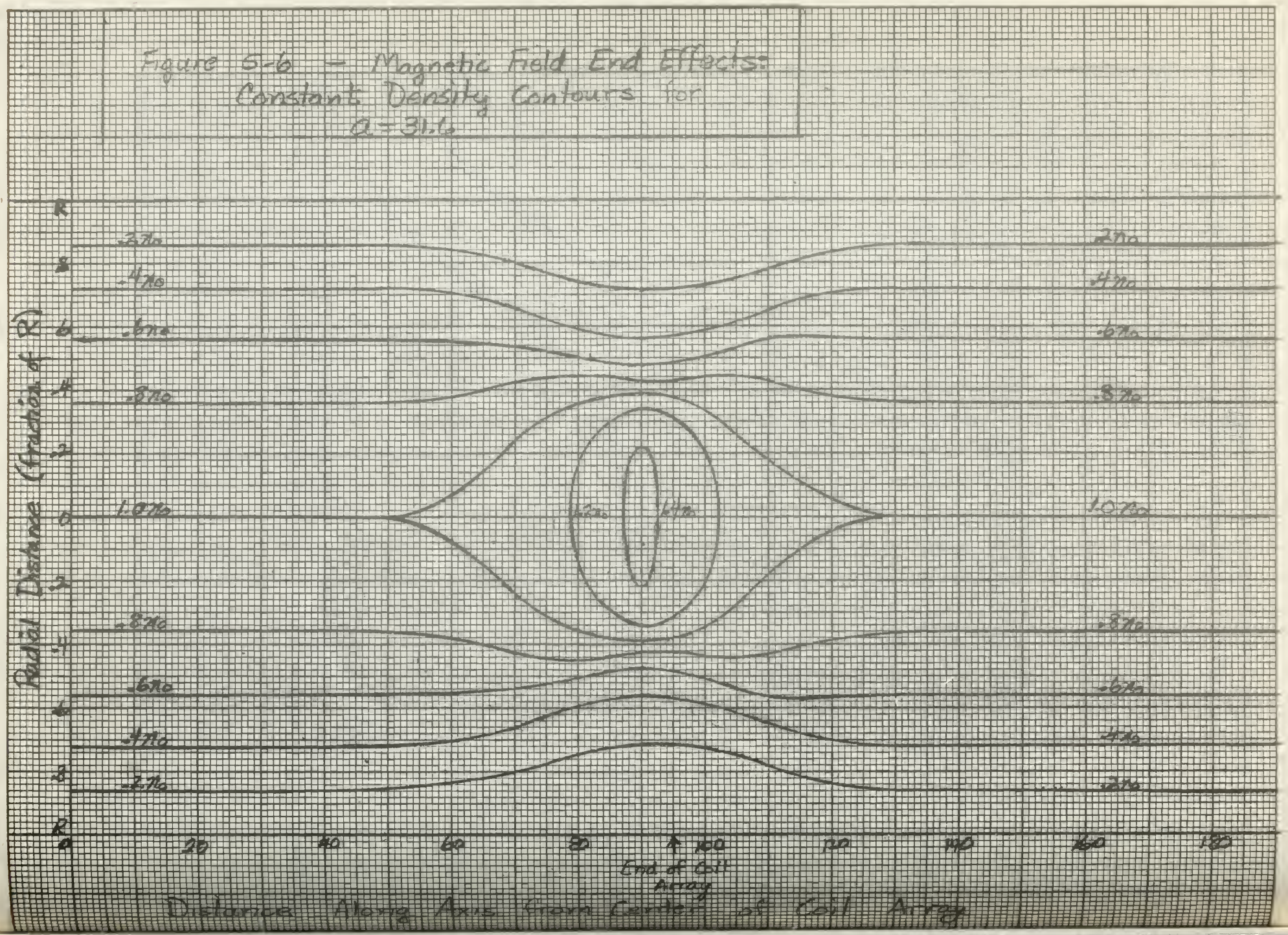

MODEL DATE

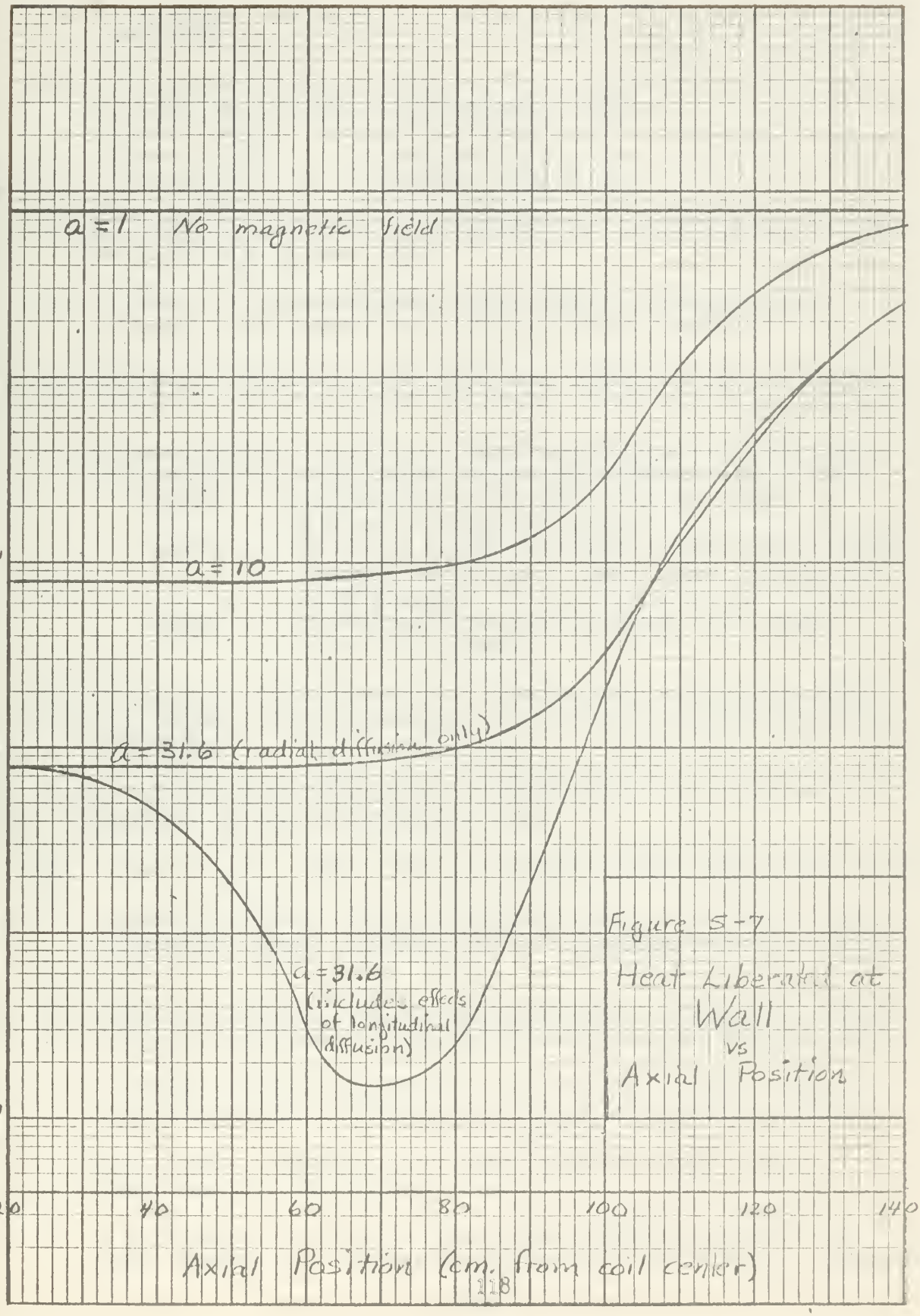

Figure 5-7
Heat Liberated at Wall vs Axial Position

BIBLIOGRAPHY

1. L. Spitzer, Jr., Physics of Ionized Gases, Interscience Publishers, Inc., 1956.

2. W. P. Allis, Motions of Ions and Electrons, Handbuch der Physik, Vol. XXI, pp. 383-444, Springer-Verlag. 1956.

3. G. Ecker, Theory of the Positive Column, Proc. of the Phys. Soc. of London, Vol. 67, pp. 485-491, June 1954.

4. S. C. Brown, Basic Data of Plasma Physics, Technology Press of MIT and John Wiley & Sons, 1959.

5. G. Ecker, Die Raumladungzone an der Grenze des Bogenplasmas, Zeitschrift fur Physik, Vol. 135, pp. 105-118, 1953.

6. C. Flammer, Spheroidal Wave Functions, Staford University Press, 1957.

7. A. Guthrie and R. K. Wakerling, The Characteristics of Electrical Discharges in Magnetic Fields, McGraw-Hill Book Co., Inc., 1949.
   Chapter 1 - Qualitative Description of the Arc Plasma in a Magnetic Field, by D. Bohm
   Chapter 2 - The Use of Probes for Plasma Exploration in Strong Magnetic Fields, by D. Bohm, E. H. S. Dorkop, and S. W. Massey
   Chapter 3 - The Minimum Ionic Kinetic Energy for a Stable Sheath, by D. Bohm.

8. I. Langmuir, The Interaction of Electron and Positive Ion Space Charges in Cathode Sheaths, Physical Review, Vol. 33, pp. 954-989, 1929.

9. W. Magnus and F. Oberhettinger, Special Functions of Mathematical Physics, Chelsea Publishing Co., 1949.

10. E. Jahnke and F. Ende, Table of Functions, Dover Publications, 1945.

11. Mathematical Tables Project, National Bureau of Standards, Tables of Spherical Bessel Functions, Vol. 1, Columbia University Press, 1947.

12. Mathematical Tables Project, National Bureau of Standards, Tables of Associated Legendre Functions, Columbia University Press, 1945.

13. G. Ecker, Enhanced Interaction in the Positive Column, UCRL-9144, University of California, Lawrence Radiation Laboratory, 1960.

14. F. H. Clauser, Symposium of Plasma Dynamics, Addison-Wesley Publishing Co., Inc., 1960.

15. D. R. Whitehouse, Summer Program Notes in Plasma Dynamics, MIT 1959. Section One - Plasma Theory, by W. P. Allis and S. J. Buchsbaum.

16. F. W. Sears, Thermodynamics, Kinetic Theory of Gases and Statistical Mechanics, Addison-Wesley Publishing Co., 1953.

17. A Sommerfeld, Partial Differential Equations in Physics, Academic Press, Inc., 1949.

18. G. Francis, The Flow Pattern at Low Frequency, Handbuch der Physik, Vol. XXII, pp. 53-202, Springer-Verlag, 1956.

19. A. von Engel, Ionized Gases, Oxford at the Clarendon Press, 1955.

20. H. B. Dwight, Electrical Coils and Conductors, McGraw-Hill Book Co., Inc., 1945.

APPENDIX I - Curvilinear Coordinates: Transformation Equations

Because of notation differences between references, the transformation equations for all coordinate systems employed in this thesis are presented below:

1. Cylindrical Coordinates (r,ϕ,z) - Figure I-1

$$\begin{aligned} x &= r\cos\phi \\ y &= r\sin\phi \\ z &= z \end{aligned} \qquad \text{(I-1)}$$

where $r \geq 0$, $0 \leq \phi \leq 2\pi$ $\qquad -\infty < z < \infty$

2. Spherical Coordinates (r,θ,ϕ) - Figure I-2

$$\begin{aligned} x &= r\sin\theta\cos\phi \\ y &= r\sin\theta\cos\phi \\ z &= r\cos\theta \end{aligned} \qquad \text{(I-2)}$$

where $r \geq 0$ $\quad 0 \leq \phi \leq 2\pi$ $\quad 0 \leq \theta \leq \pi$

3. Prolate Spheroidal Coordinates (η, ξ, ϕ) - Figure I-3

$$\begin{aligned} x &= \frac{d}{2}\left[(1-\eta^2)(\xi^2-1)\right]^{1/2}\cos\phi \\ y &= \frac{d}{2}\left[(1-\eta^2)(\xi^2-1)\right]^{1/2}\sin\phi \\ z &= \frac{d}{2}\eta\xi \end{aligned} \qquad \text{(I-3)}$$

where $-1 \leq \eta \leq 1$ $\quad 1 \leq \xi < \infty$ $\quad 0 \leq \phi \leq 2\pi$

In the prolate spheroidal system the surface ξ = constant >1 is an elongated ellipsoid of revolution with major axis of length $d\xi$ and minor axis of length $d\,(\xi^2-1)^{\frac{1}{2}}$. The degenerate surface $\xi = 1$ is the straight line along the z-axis from $z = -\frac{1}{2}d$ to $z = +\frac{1}{2}d$. The surface $|\eta|$ = constant <1 is a hyperboloid of revolution of two sheets with an

asymptotic cone whose generating line passes through the origin and is inclined at the angle $\beta = \cos^{-1}\eta$ to the z-axis. The degenerate surface $|\eta| = 1$ is that part of the z-axis for which $|z| < \frac{1}{2}d$. The surface ϕ = constant is a plane through the z-axis forming the angle ϕ with the x,z-plane.

4. Oblate Spheroidal Coordinates (η, ξ, ϕ) - Figure I-4

$$x = \frac{d}{2}\left[(1-\eta^2)(\xi^2+1)\right]^{1/2}\cos\phi$$
$$y = \frac{d}{2}\left[(1-\eta^2)(\xi^2+1)\right]^{1/2}\sin\phi \qquad (I\text{-}4)$$
$$z = \frac{d}{2}\eta\xi$$

where $-1 \leq \eta \leq 1 \quad 0 \leq \xi < \infty \quad 0 \leq \phi \leq 2\pi$

In the oblate spheroidal system the surface $|\xi|$ = constant > 0 is a flattened ellipsoid of revolution with major axis of length $d(\xi^2+1)^{\frac{1}{2}}$ and minor axis of length $d|\xi|$. The surface $\xi = 0$ is a circular disk of radius $a = \frac{1}{2}d$ which lies in the x,y-plane and is centered at the origin. The surface $|\eta|$ = constant < 1 is a hyperboloid of revolution of one sheet with an asymptotic cone whose generating line passes through the origin and is inclined at the angle $\beta = \cos^{-1}\eta$ to the z-axis. The degenerate surface $|\eta| = 1$ is the z-axis. The surface $\eta = 0$ is the x,y-plane except for the circular disk $\xi = 0$. The surface ϕ = constant is again the plane through the z-axis making the angle ϕ with the x, z-plane. The transformation from prolate to oblate coordinates is made by replacing ξ by $i\xi$ in the prolate equations.

Reference for spheroidal systems: Flammer, Spheroidal Wave Functions 6

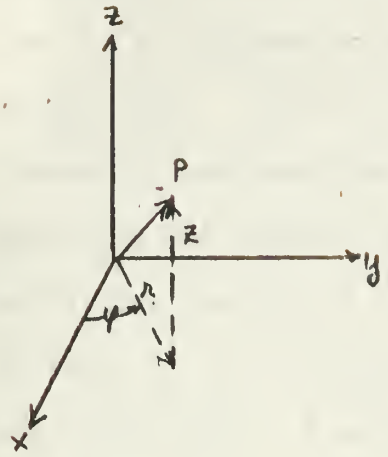

Figure I-1 Cylindrical Coordinates

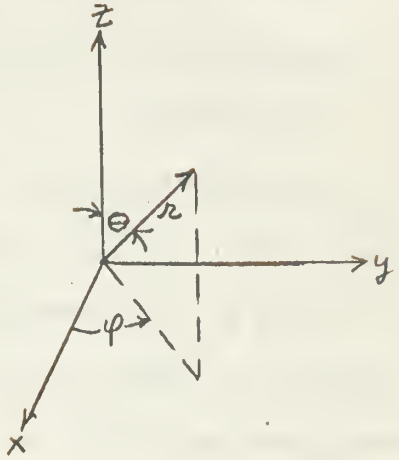

Figure I-2 Spherical Coordinates

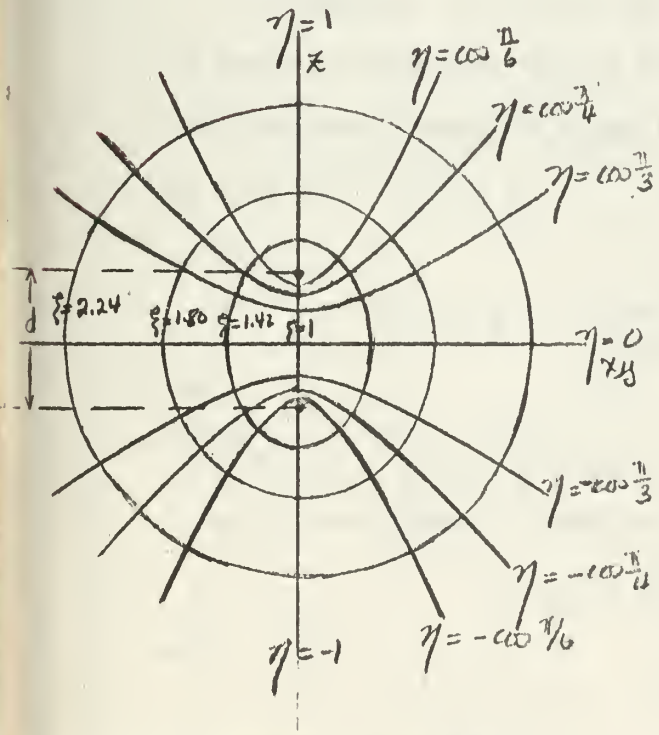

Figure I-3 Prolate Spheroidal Coordinates – axis of revolution is z-axis

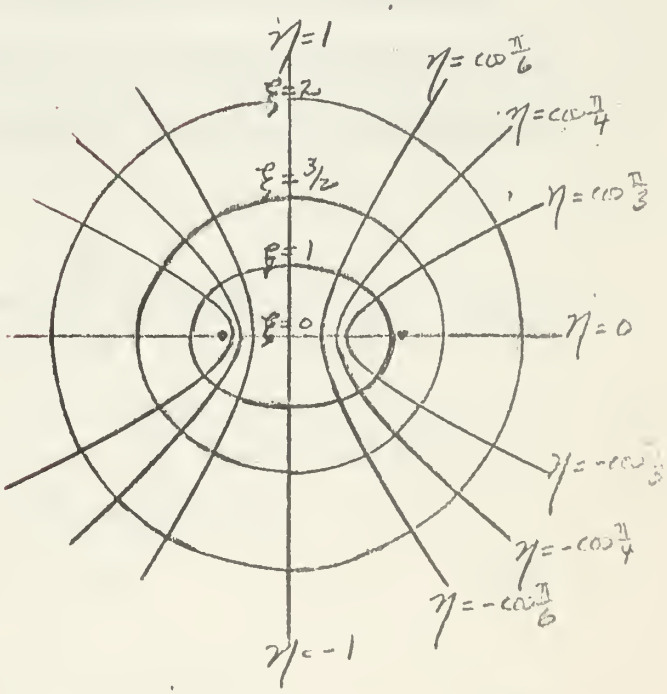

Figure I-4 Oblate Spheroidal Coordinates – axis of revolution is z-axis

APPENDIX II

SPHEROIDAL WAVE FUNCTIONS

The particle density distribution in the vicinity of a prolate spheroid is describable by the prolate angle function of the first kind, $S_{01}^{(1)}(c,\eta)$ and the prolate radial functions of the first and second kinds, $R_{01}^{(1)}(c,\xi)$ and $R_{01}^{(2)}(c,\xi)$, respectively. Flammer [6] has tabulated $S_{01}^{(1)}(c,\eta)$ (See Fig. II-1, which is taken from his data) and the radial functions $R_{01}^{(1)}(c,\xi)$ and $R_{01}^{(2)}(c,\xi)$ for different values of c and the independent variables η and ξ. The range of ξ for the radial functions in his tables is, however, quite restricted (ξ =1.005, 1.020, 1.044, and 1.077) and consequently it was necessary to compute further tables of the radial functions (Table II-1 and II-2).

To compute $R_{01}^{(1)}(c,\xi)$ and $R_{01}^{(2)}(c,\xi)$ the following expansions in terms of spherical Bessel functions and Legendre Polynomials were obtained from Flammer's general equations. (4.1.15) for $R_{mn}^{(1)}(c,\xi)$ and (4.2.6) for $R_{mn}^{(2)}(c,\xi)$

$$R_{01}^{(1)}(c,\xi) = \frac{1}{\sum_{r=1}^{\infty\,\prime} d_r^{01}(c)} \sum_{r=1}^{\infty\,\prime} (\omega)^{r-1} d_r^{01}(c)\, j_r(c\xi) \qquad \text{(II-1)}$$

and

$$R_{01}^{(2)}(c,\xi) = \frac{1}{k_{01}^{(2)}(c)} \left\{ \sum_{r=1}^{\infty\,\prime} d_r^{01}(c)\, Q_{r-1}^{01}(\xi) + \sum_{r=1}^{\infty\,\prime} d_{plr}^{01}(c)\, P_{r-1}^{0}(\xi) \right\} \qquad \text{(II-2)}$$

where from Flammer's equation (4.1.8) and (4.2.5b):

$$j_r(\xi) = \sqrt{\frac{\pi}{2\xi}}\, J_{r+\frac{1}{2}}(\xi) \qquad \text{II-1a}$$

and

$$k_{01}^{(2)}(c) = -\frac{d_1^{01}(c)\, c^2}{3} \sum_{r=1}^{\infty\,\prime} d_r^{01}(c) \qquad \text{II-2a}$$

and where the prime over the summation sign indicates that the summation is over only odd values of r, and where $d_r^{01}(c)$ and $d_{plr}^{01}(c)$

are expansion coefficients. Flammer tabulates these coefficients to five significant figures.

The prolate radial functions of the first kind, $R_{01}^{(1)}(c,\xi)$ (Table II-1), were calculated using a desk calculator and the Mathematical Tables Project Tables of Spherical Bessel Functions [11] . The figures have been spot checked, and are believed correct to plus or minus one in the last digit.

The Prolate Radial Functions of the second kind, $R_{01}^{(2)}(c,\xi)$ (Table II-2) were calculated on the CDC-1604 Computer using equation (II-2). Most of the Legendre Functions required for the expansions were also generated on the computer, using the following equations given by Jahnke and Emde [10] .

$$P_n(\xi) = \frac{1\cdot 3\cdot 5\cdots(2n-1)}{n!}\left[\xi^n - \frac{n(n-1)}{2(2n-1)}\xi^{n-2} + \frac{n(n-1)(n-2)(n-3)}{2\cdot 4\cdot(2n-1)(2n-3)}\xi^{n-4} - \cdots\right] \quad \text{(II-3)}$$

$$Q_n(\xi) = P_n(\xi)Q_0(\xi) - \sum_{m=1}^{n}\frac{1}{m}P_{m-1}(\xi)\,P_{n-m}(\xi) \quad \text{(II-4)}$$

Because of the slow convergence of the equations (II-3) for large values of ξ only those functions for $\xi < 1.2$ were computed. The values for $\xi \geq 1.2$ were taken from Tables of Associated Legendre Functions [12] . The Values of Q_0 for $\xi < 1.2$ were calculated on a desk calculator using the following relation from Jahnke and Emde [10].

$$Q_0(\xi) = \coth^{-1}(\xi) = \frac{1}{2}\ln\frac{\xi+1}{\xi-1} \quad \text{II-5}$$

and tables of logarithms.

The radial functions $R_{01}^{(1)}(c,\xi)$ and $R_{01}^{(2)}(c,\xi)$ are tabulated here for values of c between 0.1 and 2.0 and for values of ξ between 1.0 and3.6 and 1.0 and 2.0 respectively. These functions are graphed in Figures (II-2), (II-3), and (II-4). The tabulated values are correct

to the number of digits shown, except that all five digit results are considered correct to plus or minus one unit in the last digit since Flammer's coefficients are listed to only five significant digits. The decreasing number of significant digits for higher values of c and ζ is a consequence of the decreasing rate of convergence of the series (II-2) for relatively large c and ζ. The number of significant digits was determined by inspection of the terms and generous estimates of the maximum magnitude of the neglected terms. The author has endeavered to err on the conservative side in reporting these values, and believes all digits reported to be correct.

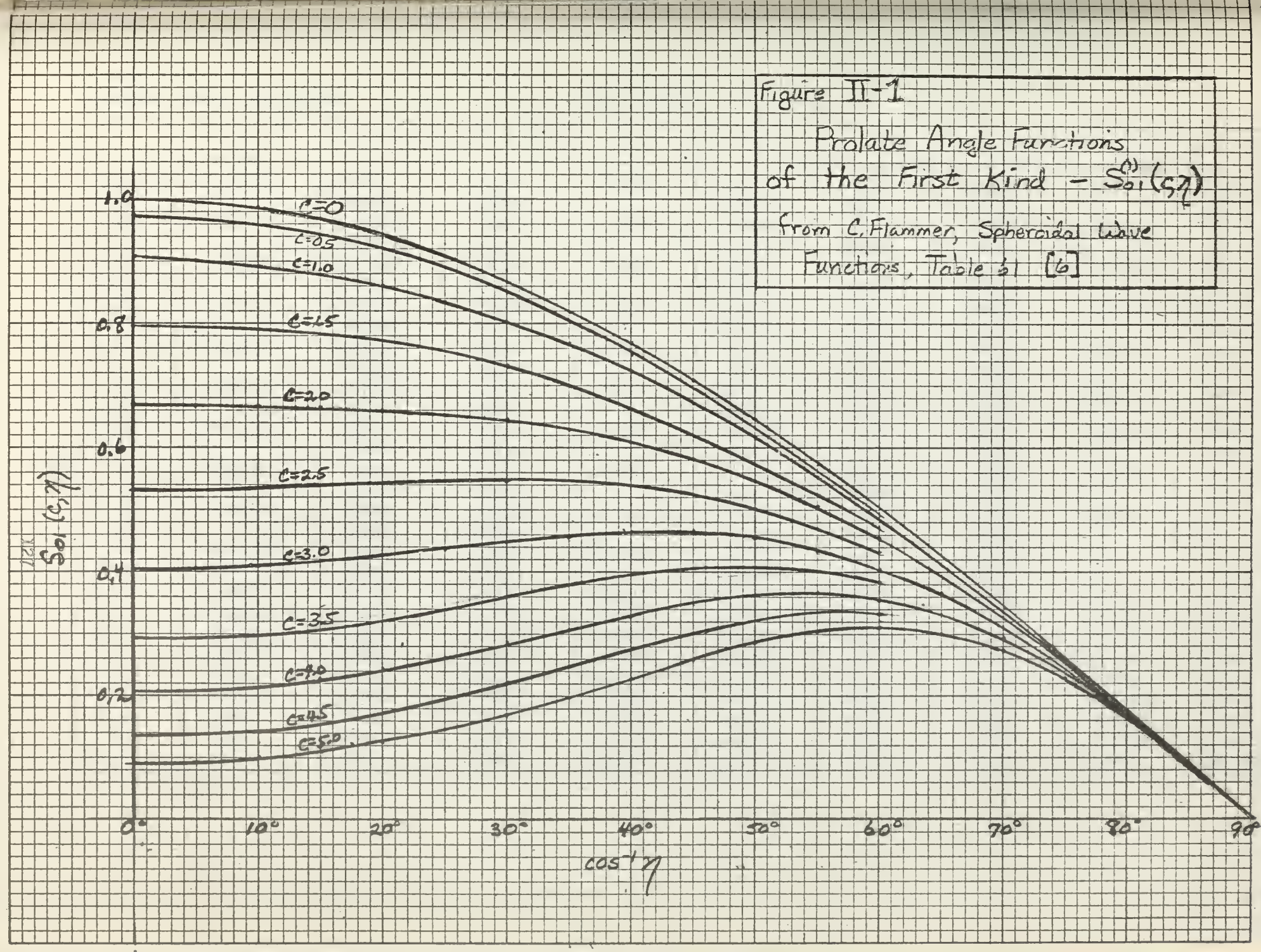
Figure II-1
Prolate Angle Functions of the First Kind – $S_{01}^{(1)}(c,\eta)$
From C. Flammer, Spheroidal Wave Functions, Table 6.1 [6]
1.0
0.8
0.6
0.4
0.2
$S_{01}^{(1)}(c,\eta)$
c=0
c=0.5
c=1.0
c=1.5
c=2.0
c=2.5
c=3.0
c=3.5
c=4.0
c=4.5
c=5.0
0°
10°
20°
30°
40°
50°
60°
70°
80°
90°
$\cos^{-1}\eta$

TABLE II-1
PROLATE RADIAL FUNCTIONS $R_{01}^{(1)}(c,\xi)$

ξ	c = 0.1	c = 0.2	c = 0.4	c = 0.5	c = 0.6	c = 0.8	c = 1.0	c = 1.5	c = 2.0
1.00	.033313	.066507	.13206	.16419	.19574	.25667	.31406	.43787	.52851
1.05		.069803	.13844		.20476	.26772	.32633		.53094
1.10	.036637	.073096	.14478	.17966	.21368	.27851	.33814	.45841	.53126
1.15		.076384	.15109		.22248	.28905	.34945		.52776
1.20	.039958	.079668	.15736	.19486	.23116	.29932	.36027	.47330	.52225
1.25		.082947	.16359		.23972	.30930	.37056		.51422
1.30	.043277	.086221	.16979	.20977	.24815	.31900	.38032	.48244	.50376
1.35		.089489	.17594		.25646	.32840	.38954	.	.49099
1.40	.046594	.092752	.18205	.22437	.26462	.33750	.39820	.48582	.47601
1.45		.096010	.18812		.27264	.34628	.40630		.45897
1.50	.049908	.099262	.19415	.23864	.28052	.35474	.41382	.48351	.44001
1.55		.10251	.20013		.28826	.36287	.42076		.41929
1.60	.053218	.10575	.20606	.25256	.29583	.37067	.42711	.47568	.39697
1.65		.10898	.21194		.30326	.37813	.43285		.37323
1.70	.056526	.11221	.21777	.26610	.31052	.38524	.43800	.46255	.34825
1.75		.11543	.22355		.31762	.39200	.44254		.32221
1.80	.059830	.11864	.22928	.27925	.32455	.39839	.44647	.44445	.29532
1.85		.12185	.23496		.33132	.40443	.44978		.26776
1.90	.063130	.12505	.24056	.29199	.33790	.41010	.45248	.42175	.23972
1.95		.12824	.24612		.34432	.41540	.45457		.21141
2.00	.066427	.13142	.25163	.30430	.35055	.42032	.45604	.39491	.18301
2.2	.073008	.14408	.27302	.32757	.37362	.43620	.45583	.33083	.072294
2.4	.079572	.15660	.29339	.34892	.39359	.44590	.44613	.25670	-.025667
2.6	.086117	.16896	.31266	.36826	.41033	.44939	.42746	.17741	-.10203
2.8	.092641	.18117	.33075	.38546	.42372	.44675	.40057	.097919	-.15113
3.0	.099143	.19320	.34761	.40046	.43370	.43815	.36643	.022950	-.17099
3.2	.10562	.20505	.36317	.41318	.44022	.42388	.32618	-.043341	-.16314
3.4	.11207	.21671	.37739	.42356	.44326	.40432	.28108	-.097598	-.13243
3.6	.11850	.22816	.39045	.43157	.44290	.37992	.23249	-.13746	-.085917

TABLE II-2

PROLATE RADIAL FUNCTIONS $R_o^{(2)}(c, \xi) = R \times 10^P$

	C=0.1		C=0.2		C=0.4		C=0.5		C=0.6		C=0.8		C=1.0		C=1.5		C=2.0	
ξ	R	P	R	P	R	P	R	P	R	P	R	P	R	P	R	P	R	P
1.000288	-.10285	4	-.25803	3	-.65407	2	-.42287	2	-.29723	2	-.17219	2	-.11416	2	-.56282	1	-.35355	1
1.000512	-.94239	3	-.23647	3	-.59978	2	-.38793	2	-.27281	2	-.15822	2	-.10502	2	-.51910	1	-.32635	1
1.00115	-.82163	3	-.20622	3	-.52362	2	-.33892	2	-.23855	2	-.13862	2	-.92200	1	-.45772	1	-.28812	1
1.0018	-.75505	3	-.18955	3	-.48161	2	-.31189	2	-.21965	2	-.12781	2	-.85126	1	-.42381	1	-.26698	1
1.0032	-.66999	3	-.16824	3	-.42796	2	-.27736	2	-.19551	2	-.11399	2	-.76084	1	-.38042	1	-.23985	1
1.00461	-.61641	3	-.15482	3	-.39416	2	-.25561	2	-.18030	2	-.10528	2	-.70382	1	-.35301	1	-.22267	1
1.00722	-.55116	3	-.13848	3	-.35299	2	-.22911	2	-.16176	2	-.94665	1	-.63431	1	-.31952	1	-.20160	1
1.0288	-.35740	3	-.89941	2	-.23066	2	-.15034	2	-.10665	2	-.63061	1	-.42688	1	-.21866	1	-.13716	1
1.0576	-.26799	3	-.67540	2	-.17416	2	-.11393	2	-.81155	1	-.48397	1	-.33018	1	-.17061	1	-.10536	1
1.080	-.22851	3	-.57647	2	-.14919	2	-.97836	1	-.69874	1	-.41891	1	-.28708	1	-.14874	1	-.90417	0
1.109	-.19350	3	-.48875	2	-.12704	2	-.83548	1	-.59852	1	-.36097	1	-.24853	1	-.12879	1	-.76385	0
1.2	-.13224	3	-.33521	2	-.88237	1	-.58492	1	-.42247	1	-.25860	1	-.17974	1	-.91535	0	-.48714	0
1.3	-.97781	2	-.24882	2	-.66370	1	-.44343	1	-.32274	1	-.19991	1	-.13948	1	-.67892	0	-.29808	0
1.4	-.76840	2	-.19631	2	-.53053	1	-.35704	1	-.26157	1	-.16336	1	-.11377	1	-.51458	0	-.1608	0
1.5	-.62681	2	-.16081	2	-.44025	1	-.29829	1	-.21975	1	-.13789	1	-.95318	0	-.38731	0	-.534	-1
1.6	-.52468	2	-.13519	2	-.37493	1	-.25561	1	-.18917	1	-.11884	1	-.81083	0	-.28262	0	+.326	-1
1.7	-.44771	2	-.11588	2	-.32551	1	-.22316	1	-.16573	1	-.10387	1	-.69525	0	-.19346	0	+.101	0
1.8	-.38780	2	-.10084	2	-.28687	1	-.19763	1	-.14712	1	-.9165	0	-.59782	0	-.1161	0	+.155	0
1.9	-.33999	2	-.88835	1	-.25586	1	-.17701	1	-.13192	1	-.8137	0	-.51332	0	-.4830	-1	+.196	0
2.0	-.30108	2	-.79062	1	-.23046	1	-.15998	1	-.11923	1	-.7250	0	-.4384	0	+.111	-1	+.22	0

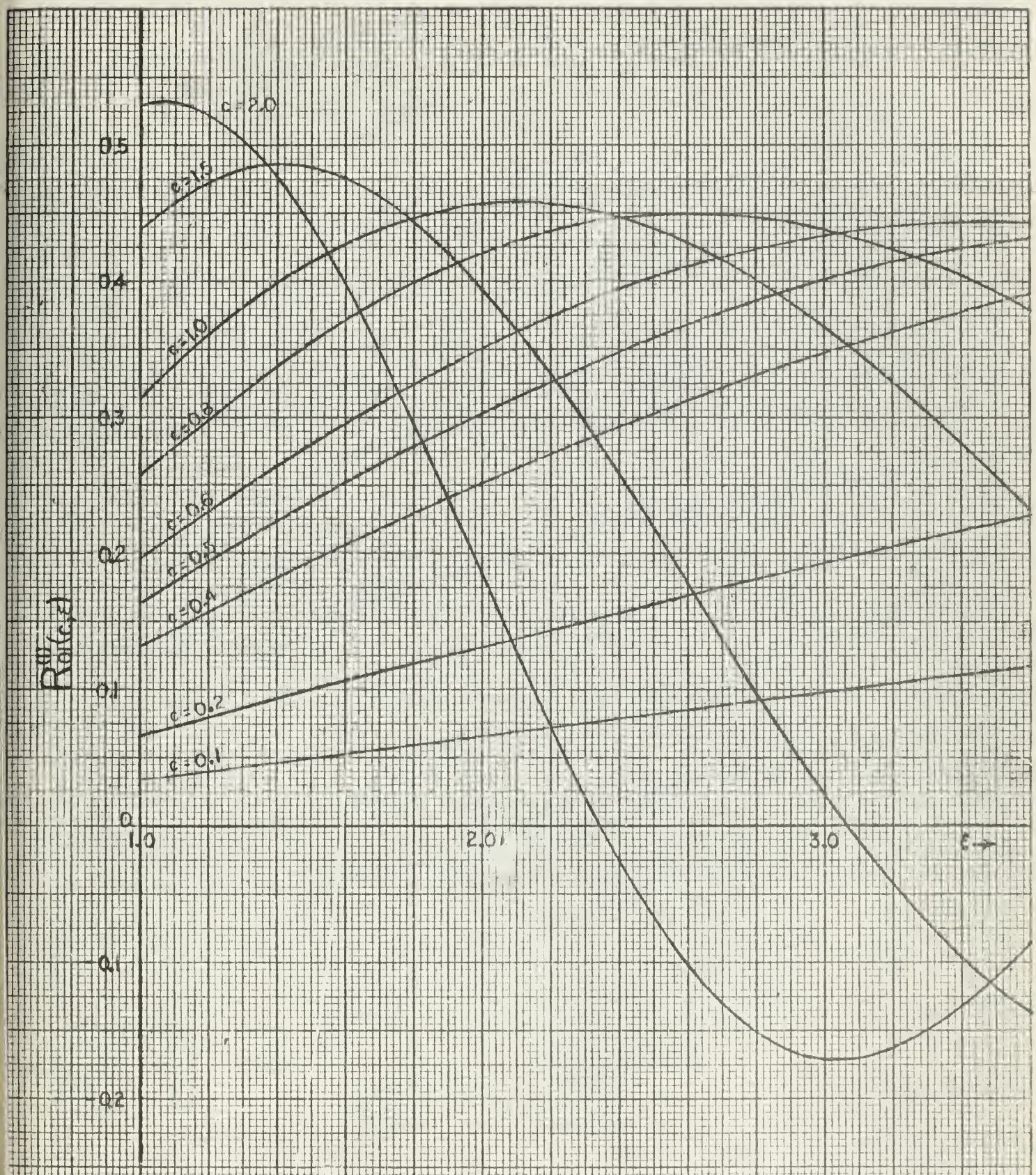

Fig. II-2 Prolate Radial Functions of the First Kind, $R^{(1)}_{01}(c,\xi)$

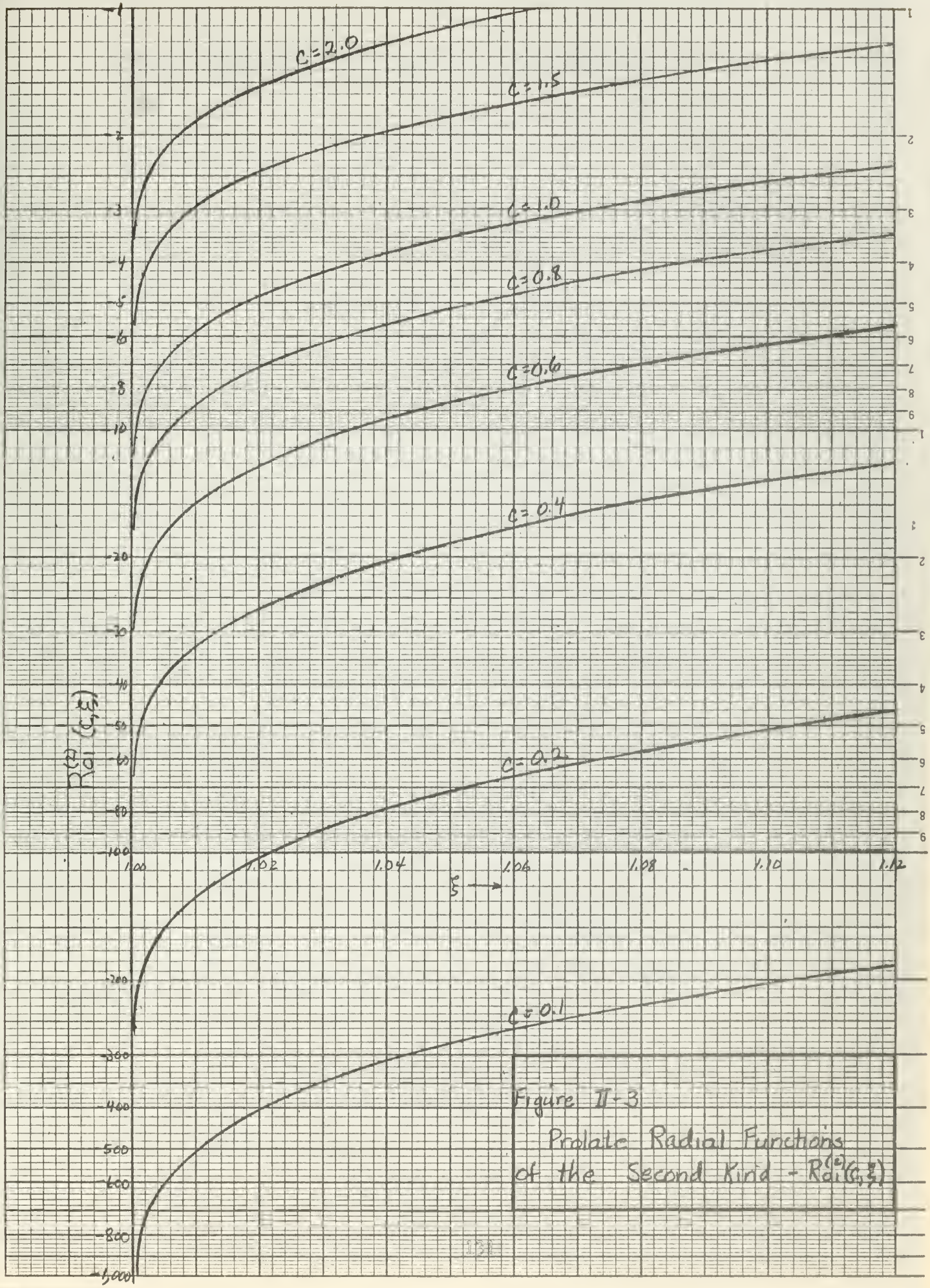

Figure II-3

Prolate Radial Functions of the Second Kind - $R_{01}^{(2)}(c,\xi)$

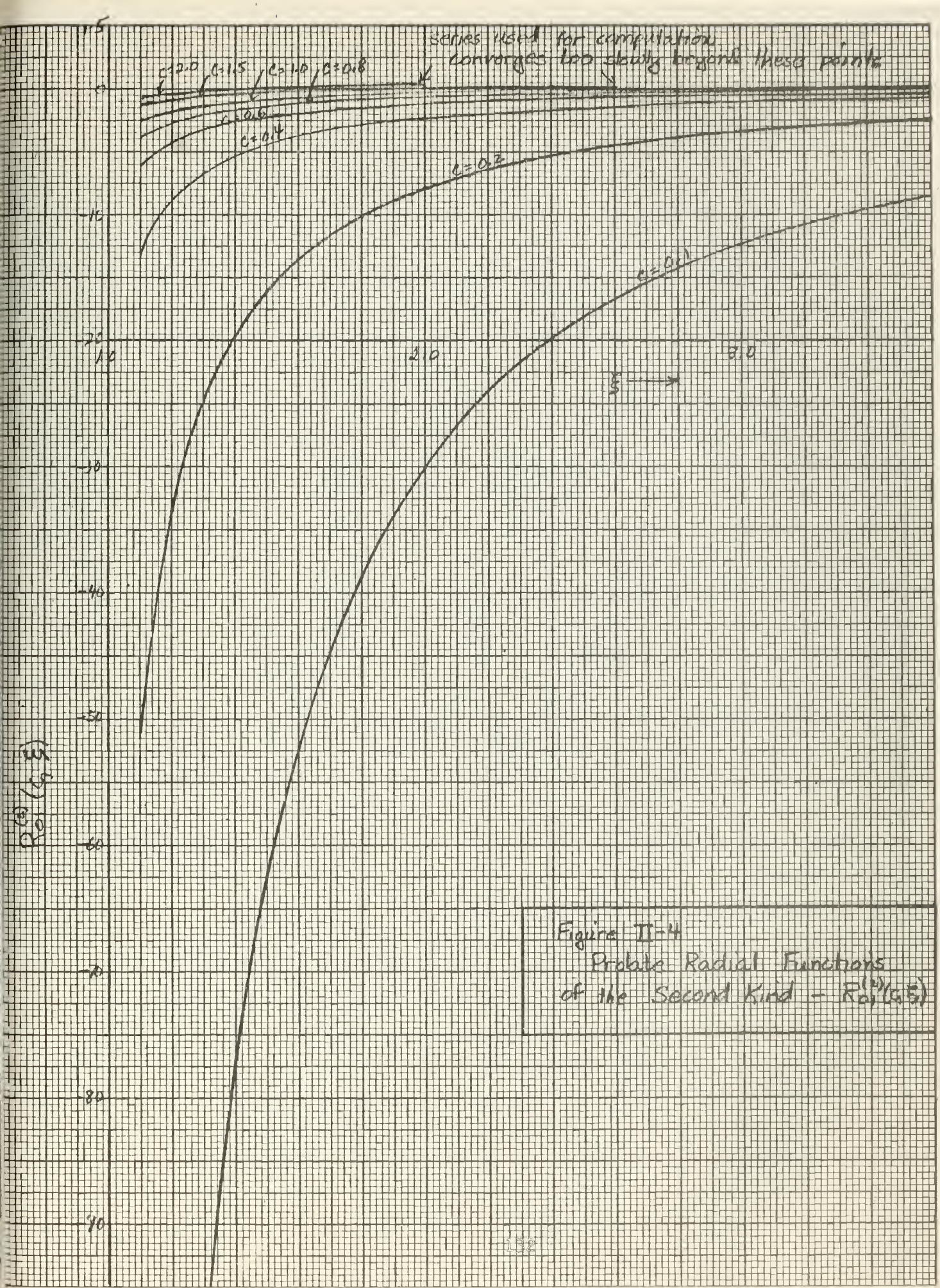

Figure II-4
Prolate Radial Functions of the Second Kind – $R_{01}^{(2)}(c,\xi)$